# USE OF VARIOUS SIGNALS FOR MILLING CUTTER BREAKAGE DETECTION

BY

YEONG-SHIN TARNG

A DISSERTATION PRESENTED TO THE GRADUATE SCHOOL
OF THE UNIVERSITY OF FLORIDA IN PARTIAL FULFILLMENT
OF THE REQUIREMENTS FOR THE DEGREE OF
DOCTOR OF PHILOSOPHY

UNIVERSITY OF FLORIDA

1988

Dedicated to God my Father and
the Lord Jesus Christ

ACKNOWLEDGMENTS

I wish to express my sincere appreciation to Dr. Jiri Tlusty for his advice, encouragement, and guidance during my whole graduate study.

I would like also to thank the members of my Ph.D. Supervisory Committee, Dr. John K. Schueller, Dr. Jose C. Principe, Dr. Donald W. Dareing, and Dr. Carl D. Crane, for their understanding, for reading the manuscript, and for their assistance with this research. Special thanks are due to the staff of the Machine Tool Laboratory for their help during the experimental work. Gratitude is also extended to Robert L. Wells for his valuable suggestions during the editing of the dissertation manuscript.

The financial assistance from National Science Foundation is greatly appreciated.

TABLE OF CONTENTS

page

ACKNOWLEDGMENTS..... iii

LIST OF TABLES..... vii

LIST OF FIGURES..... ix

ABSTRACT..... xvi

CHAPTERS

1 INTRODUCTION..... 1

2 BACKGROUND AND LITERATURE REVIEW..... 5

2.1 Acoustic Emission Approach..... 7

2.2 Cutting Force Approach..... 9

2.2.1 Time Series Method..... 9

2.2.2 Deterministic Method..... 13

3 MODELLING OF THE MILLING PROCESS..... 16

3.1 Description of the Milling Process..... 16

3.2 Milling Force Model..... 18

3.2.1 Straight Toothed Cutter..... 18

3.2.2 Helical Toothed Cutter..... 22

3.3 Regeneration of Waviness..... 25

3.4 Run-out on the Cutter..... 29

4 DETECTION OF TOOL BREAKAGE USING THE CUTTING FORCE SIGNAL..... 36

4.1 Simulation of the Cutting Force Signal With and Without Tool Breakage..... 36

4.1.1 Straight Toothed Cutter..... 36

4.1.2 Helical Toothed Cutter..... 45

4.2 Detection Algorithm for Tool Breakage..... 50

4.3 Experimental Set-up..... 59

4.4 Experimental Verification..... 65

4.5 Limitations of the Cutting Force Signal for Tool Breakage Detection..... 68

5 ANALYSIS AND DETECTION OF TOOL BREAKAGE USING VIBRATION SIGNALS..... 78

5.1 Reconstruction of the Cutting Force Signal Using an Accelerometer..... 78

5.1.1 Inverse Filtering Method..... 80

5.1.2 Analog Computer Method..... 81

5.2 Analysis of Characteristic Changes in Vibration Signals Due to Tool Breakage.... 82

5.3 Detection of Tool Breakage Using Displacement Signal..... 89

5.4 Experimental Set-up..... 100

5.5 Experimental Verification..... 105

5.6 Comparison of Detection of Tool Breakage Using Displacement Signal and Force Signal..... 109

6 DETECTION OF TOOL BREAKAGE USING DISPLACEMENT SIGNAL IN A VARIETY OF CUTTING CONDITIONS..... 117

6.1 Spindle Speed..... 117

6.2 Workpiece Material..... 125

6.3 Axial Depth of Cut..... 128

6.4 Feedrate..... 132

6.5 Radial Immersion of Cut..... 136

6.6 Interrupted Cuttings..... 139

6.6.1 Milling over a Slot..... 142

6.6.2 Milling over a Hole..... 142

6.6.3 Milling over Circular Exit and Entry Boundaries..... 145

6.7 Corner Slotting..... 147

6.8 Different Flutes of Cutters..... 149

6.9 Percentage of Tool Breakage..... 151

7 STRATEGIES FOR DETECTION OF TOOL BREAKAGE UNDER VARYING CUTTING CONDITIONS..... 154

7.1 Pattern Analysis..... 154

7.2 Threshold Setting..... 155

8 CONCLUSIONS AND FUTURE WORK..... 164

APPENDICES

A LISTING OF SUBROUTINES FOR MODELLING OF MILLING PROCESS..... 166

B EXAMPLE PROGRAM FOR SIMULATION OF DISPLACEMENT SIGNAL OF SPINDLE..... 184

REFERENCES..... 188

BIOGRAPHICAL SKETCH..... 195

LIST OF TABLES


| TABLE | | page |
|---|---|---|
| 4.1 | Cutting parameters in the simulation of the cutting force in face milling..... | 39 |
| 4.2 | Simulation parameters for the spindle system..... | 39 |
| 4.3 | Radial throw in the face milling cutter..... | 45 |
| 4.4 | Cutting parameters in the simulation of the cutting force in end milling..... | 47 |
| 4.5 | Cutting parameters with different speeds to verify the dynamometer response..... | 72 |
| 5.1 | Modal parameters for the transfer function of the spindle..... | 96 |
| 5.2 | Cutting parameters in the simulation of the cutting tests using a spindle system with multiple degrees of freedom..... | 99 |
| 5.3 | Cutting parameters in the detection of tool breakage using the displacement signal..... | 105 |
| 5.4 | Cutting parameters in up milling with three consecutive tool breakages..... | 109 |
| 5.5 | Cutting parameters in up milling with force and displacement sensors active..... | 115 |
| 6.1 | Cutting parameters in up milling with different spindle speeds..... | 119 |
| 6.2 | Cutting parameters in down milling with different spindle speeds..... | 122 |
| 6.3 | Cutting parameters in the cutting tests using different workpiece materials..... | 128 |

6.4 Cutting parameters in the cutting tests with different axial depths of cut..... 132

6.5 Cutting parameters in the cutting tests with different feedrates..... 132

6.6 Cutting parameters in the cutting tests with different radial immersions of cut..... 136

6.7 Cutting parameters in the interrupted cuttings..... 142

6.8 Cutting parameters in the corner slotting..... 147

6.9 Cutting parameters in the cutting tests with different flutes of cutters..... 149

6.10 Cutting parameters in the cutting tests with different percentages of broken edge..... 151

LIST OF FIGURES


| FIGURE | | page |
|---|---|---|
| 2.1 | Tool breakage monitoring scheme..... | 6 |
| 3.1 | Type of milling operations. a) face milling; b) peripheral milling..... | 17 |
| 3.2 | Geometry of milling operation. a) tooth path; b) chip thickness..... | 19 |
| 3.3 | Cutting force directions. a) up milling; b) down milling..... | 21 |
| 3.4 | Geometry of a helical toothed cutter. a) incremental cutting force; b) unrolled surface of cut..... | 23 |
| 3.5 | Regeneration of the waviness in milling. a) waviness of workpiece surface; b) simulation model..... | 26 |
| 3.6 | Geometry of chip thickness with radial throw... | 31 |
| 3.7 | Flow chart for simulation of cutting force..... | 35 |
| 4.1 | Cut geometry in the entry, steady, and exit states..... | 37 |
| 4.2 | Simulation of the cutting force in the entry, steady, and exit states in up milling..... | 38 |
| 4.3 | Simulation of the cutting force in the entry, steady, and exit states in down milling..... | 41 |
| 4.4 | Simulation of the cutting force in the 1/8, 1/4, 1/2, and 1/1 immersions of cut..... | 42 |
| 4.5 | Simulation of the cutting force with 4, 6, 8, and 10 teeth on the cutters..... | 43 |
| 4.6 | Simulation of the cutting force with radial throw in the entry, steady, and exit states.... | 44 |

4.7 Simulation of the cutting force in the entry, steady, and exit states using a helical toothed cutter..... 46

4.8 Simulation of the cutting force in the 1/8, 1/4, 1/2, and 1/1 immersions of cut using a helical toothed cutter..... 48

4.9 Simulation of the cutting force using helical toothed cutters with 2, 3, and 4 flutes..... 49

4.10 Spectra of the simulation of the cutting force in the entry, steady, and exit states.... 51

4.11 Simulation of the instantaneous force, average force, and difference of the average force in the steady state..... 54

4.12 Simulation of the instantaneous force, average force, and difference of the average force in the entry state..... 56

4.13 Simulation of the instantaneous force, average force, and difference of the average force in the exit state..... 57

4.14 Simulation of the instantaneous force and its spectrum, average force, and difference of the average force in the steady state with radial throw..... 58

4.15 Series 20 Omnimil Machining Center..... 60

4.16 Assembly of workpiece-angle plate-dynamometer and transfer function of the dynamometer. a) Y direction; b) Z direction..... 61

4.17 Electrical circuit block diagram. a) external sampling and triggering; b) interrupted circuit for feed control..... 63

4.18 Process diagram for the experimental work..... 64

4.19 Instantaneous force, average force, and difference of the average force in the complete cutting cycle..... 66

4.20 Instantaneous force and its spectrum, average force, difference of the average force in the steady state..... 67

4.21 a) Average force and difference of the average force in the 1/8 immersion of cut.
b) Average force and difference of the average force in the 1/4 immersion of cut..... 69

4.22 a) Average force and difference of the average force in the 3/4 immersion of cut.
b) Average force and difference of the average force in the 1/1 immersion of cut..... 70

4.23 a) Cutting force signals in the Y and Z directions at spindle speed, n = 600 rpm.
b) Cutting force signals in the Y and Z directions at spindle speed, n = 1935 rpm... 71

4.24 Spectra of the simulation of the cutting force in the 1/8, 1/4, 1/2, and 1/1 immersions of cut..... 74

4.25 Peak to peak ratios for the different frequency components contributing to the tool breakage feature.
a) force ratios; b) average force ratios;
c) difference of the average force ratios..... 76

5.1 Simulation of the transfer function between the force and the vibrations.
a) acceleration over force;
b) displacement over force..... 84

5.2 Simulation of the force, acceleration, and displacement signals in a 1/2 immersion of cut with different ratios of $f_t/f_n$.
a) $f_t/f_n$ = 1/20; b) $f_t/f_n$ = 1/5..... 86

5.3 Simulation of the force, acceleration, and displacement signals in a 1/2 immersion of cut with different ratios of $f_t/f_n$.
a) $f_t/f_n$ = 1/2; b) $f_t/f_n$ = 1/1..... 87

5.4 Simulation of the force, acceleration, and displacement signals in a 1/1 immersion of cut with different ratios of $f_t/f_n$.
a) $f_t/f_n$ = 1/20; b) $f_t/f_n$ = 1/1..... 88

5.5 Spectra of the simulation of the force, and displacement in the 1/2 immersion of cut with different ratios of $f_t/f_n$.
a) $f_t/f_n$ = 1/20; b) $f_t/f_n$ = 1/5..... 90

5.6 Spectra of the simulation of the force, and displacement in the 1/2 immersion of cut with different ratios of $f_t/f_n$. a) $f_t/f_n = 1/2$; b) $f_t/f_n = 1/1$..... 91

5.7 Simulation of the displacement, average displacement, and difference of the average displacement signals with different ratios of $f_t/f_n$. a) $f_t/f_n = 1/20$; b) $f_t/f_n = 1/5$..... 93

5.8 Simulation of the displacement, average displacement, and difference of the average displacement signals with different ratios of $f_t/f_n$. a) $f_t/f_n = 1/2$; b) $f_t/f_n = 1/1$..... 94

5.9 Simulation of the average displacement and difference of the average displacement signals in the complete cutting cycle with the ratio of $f_t/f_n = 1/1$..... 95

5.10 Spindle system with multiple degrees of freedom. a) transfer function between the force and displacement; b) curve fitted transfer function..... 97

5.11 a) Simulation of the average displacement and difference of the average displacement signals at spindle speed, n = 480 rpm.
b) Simulation of the average displacement and difference of the average displacement signals at spindle speed, n = 3555 rpm..... 98

5.12 Capacitance probe mounting..... 102

5.13 Electrical circuit diagram for an anti-aliasing filter..... 102

5.14 Process diagram for the experimental work..... 103

5.15 Raw displacement signals in the X and Y directions..... 106

5.16 Average displacement and difference of the average displacement signals in the complete cutting cycle..... 107

5.17 Average displacement and difference of the average displacement signals in the entry and steady states..... 108

5.18 Average displacement and difference of the average displacement signals with three consecutive tool breakages..... 110

5.19 Simulation of the average and difference of the average force and displacement signals independent of the tooth frequency changes..... 111

5.20 Average force and displacement signals obtained from different spindle speeds..... 114

5.21 Difference of the average force and displacement signals obtained from different spindle speeds..... 116

6.1 Transfer function between the force on the cutter and displacement of the spindle. a) Y direction; b) X direction..... 118

6.2 Average displacement signal in up milling with different spindle speeds..... 120

6.3 Difference of the average displacement signal in up milling with different spindle speeds.... 121

6.4 Average displacement signal in down milling with different spindle speeds..... 123

6.5 Difference of the average displacement signal in down milling with different spindle speeds.. 124

6.6 Average displacement signal obtained from the three kinds of workpiece material: steel, cast iron, aluminum..... 126

6.7 Difference of the average displacement signal obtained from the three kinds of workpiece material: steel, cast iron, aluminum..... 127

6.8 Cut geometry with the varying axial depths of cut..... 129

6.9 Average displacement signal with the changes of the axial depths of cut..... 130

6.10 Difference of the average displacement with the changes of the axial depths of cut..... 131

6.11 Cut geometry with the varying feedrates..... 133

6.12 Average displacement signal with varying feedrates..... 134

6.13 Difference of the average displacement signal with varying feedrates..... 135

6.14 Average displacement signal in the 1/8, 1/4, 1/2, 3/4, and 1/1 immersions of cut..... 137

6.15 Difference of the average displacement signal in the 1/8, 1/4, 1/2, 3/4, and 1/1 immersions of cut..... 138

6.16 Cut geometry for the gradual change of the radial immersion of cut..... 140

6.17 Average displacement and difference of the average displacement signals with the gradual change of radial immersion of cut..... 141

6.18 Cut geometry of the slot..... 143

6.19 Average displacement and difference of the average displacement signals during milling over a slot..... 143

6.20 Cut geometry of the hole..... 144

6.21 Average displacement and difference of the average displacement signals during milling over a hole..... 144

6.22 Cut geometry with the circular exit and entry boundaries..... 146

6.23 Average displacement and difference of the average displacement signals during milling over circular boundaries..... 146

6.24 Cut geometry of the corner slotting..... 148

6.25 Average displacement and difference of the average displacement signals during slotting the square corner..... 148

6.26 Average displacement and difference of the average displacement signals in the end milling with 4, 3, and 2 flutes of cutters..... 150

6.27 Average displacement and difference of the average displacement signals with different percentages of a broken cutting edge..... 152

7.1 Simulation of the ratio of the difference displacement to the mean displacement..... 159

7.2 Moving average displacement and difference of the average displacement signals with the normalization ratio of the difference of the average displacement signal..... 161

Abstract of Dissertation Presented to the Graduate School of the University of Florida in Partial Fulfillment of the Requirements for the Degree of Doctor of Philosophy

USE OF VARIOUS SIGNALS FOR MILLING CUTTER BREAKAGE DETECTION

BY

YEONG-SHIN TARNG

DECEMBER 1988

Chairman: Dr. Jiri Tlusty
Major Department: Mechanical Engineering

For untended manufacturing operations, in-process monitoring of tool breakage plays a critically important role. A system for sensing milling cutter breakage has been developed using a deterministic approach. It is based on recognizing the changes of cutting force patterns. The regular periodic variation per tooth is filtered out by synchronized sampling, then averaging per tooth. A distinct tool breakage feature is clearly available after differencing the average cutting force per tooth.

Due to practical difficulties for cutting force measurements in milling, the use of vibration signals is explored. It has been found that the displacement signal of the spindle is suitable to replace the cutting force

signal for the purpose of cutter breakage detection using this algorithm.

Numerous cutting tests have been done. It has been shown that the displacement signal of the spindle is effective in the recognition of cutter breakage under varying cutting conditions. Furthermore, this processing method is also useful for high speed milling and can be easily implemented in real-time. Finally, the threshold for cutter breakage detection is further investigated to make it independent of changes in cutting parameters.

# CHAPTER 1
# INTRODUCTION

Unmanned machining centers (UMC) have become a vision for the future of manufacturing technology. This could tremendously save manpower and maximize machine uptimes so as to increase productivity. However, the feasibility of using the unmanned machining centers is greatly dependent on the development of diagnostic systems for machining centers. One of the most important diagnostic systems is the sensor for detection of tool failure. Generally speaking, there are three types of tool diagnosis [1].

The first type is the tool wear sensor. This sensor should be sensitive to the amount of tool wear. Therefore, it would be possible to calculate the rate of tool wear. The cutting tool could be removed from use before it reaches enough wear to produce excessive cutting force or temperature, which would eventually lead to complete failure of the cutting edge.

The second type is the sensor for immediate detection of any tool failure, such as chipping, cracking or massive failure of a cutting edge. This sensor would provide an emergency action quickly stopping the machining operation

in order to avoid further damage to the tool, workpiece, or tool holder.

The third type is the protection device. This device has no direct information about the cutting tool. It is designed to protect the machine or the cutting tool from damage due to the overloads regardless of the cause.

Milling is an extremely important machining operation. However, an efficient and reliable tool diagnostic system for milling is still not available. In milling operations, the development of tool wear is usually gradual, not sudden. Hence, the monitoring of tool wear could be considered using off-line techniques [2]. Vision and pattern recognition systems [3] might be used to repeatedly observe the edges of the milling cutter between cutting operations in order to assess the tool wear width. If the tool wear reaches a certain level, a precautionary action could be taken so as to avoid any further damage.

However, the occurrence of tool failure is unavoidable for milling with heavier chip loads or with workpiece materials, such as steel, that are hard on the cutting edge. If tool breakage or chipping occurs suddenly by any cause, the damaged cutting edge is still in use. The local breakage is accumulated and then spread to the following teeth as a chain reaction because of the overload of the following teeth. As a result, catastrophic consequences for the tool, the workpiece, and the machine might happen. Therefore, tool failure sensing is much more important than

tool wear sensing, especially for high speed high power milling. The task of this research is therefore to attempt to achieve the second type of tool diagnosis as mentioned above, i.e. immediate detection of tool failure in milling.

Under these considerations, the requirements of a tool breakage sensor system [4] can be summarized as following:

1. Reliability, on the safe side:
   100% alarm on tool damage beyond a set level.

2. Robustness:
   High sensitivity to breakage, very low sensitivity to transients (entry, exit, interrupted cuttings), and to variations in cutting parameters (workpiece material, feed, speed, radial immersion, up/down milling).

3. Highly automated threshold setting:
   Adjustable to formulate and set an alarm threshold under varying cutting conditions.

4. Practicality of sensor:
   Easy to locate in the machine.
   Suitable for daily use.

5. Fast response:
   Response time for producing an alarm signal should be short enough to prevent the following teeth being damaged.

This dissertation deals with this task in a deterministic way based on recognizing and analyzing the tool breakage feature in a sensor signal. Then, the tool breakage feature is extracted by a signal processing algorithm in order to do the decision-making. This is different from the stochastic process approach. The contents of this dissertation are summarized below.

In Chapter 2, the basic concepts of detection of tool breakage throughout the work are discussed. Considerable

research has been undertaken on this subject, so a literature review of those works is included.

In Chapter 3, a mechanistic model of the milling process is described and computerized. This model is used to simulate the dynamics of cutting force and vibration in milling operations.

In Chapter 4, a detection algorithm using the cutting force signal is presented. Experimental work to verify this algorithm is also shown. In addition, limitations of cutting force signal for tool breakage detection are discussed.

In Chapter 5, tool breakage features in vibration signals are analyzed. A detection algorithm with experimental work using the displacement signal is shown.

In Chapter 6, detection of tool breakage using the displacement signal under a variety of cutting conditions is shown.

In Chapter 7, the strategies of how to distinguish the transient response signals from tool breakage signals and how to set an alarm threshold are explored and developed.

Finally, Chapter 8 concludes this work and presents some ideas about future research.

# CHAPTER 2
# BACKGROUND AND LITERATURE REVIEW

A system of detection of tool failure requires very sensitive, accurate, and reliable techniques, which may be classified as direct and indirect methods.

Direct methods generally involve measuring the volumetric change in the tool such as using touch trigger probes, optical sensors, radio-active sensors, electrical resistance sensors, etc. They tend to be off-line techniques because measurements are usually taken as the tool moves out of the cut. Indirect methods utilize measurements of cutting parameters during the cutting which may be correlated with the tool wear or breakage. These cutting parameters include temperature, force, torque, vibration, sound, acoustic emission, etc. As a result, indirect methods are generally considered as on-line techniques.

As mentioned in Chapter 1, immediate detection of tool failure in milling should be implemented in real-time. Therefore, direct methods may not be appropriate for this application because they tend to be off-line techniques. Optical sensors are applicable to intermittent cutting

operations [5] [6], such as milling, where cutting edges are periodically exposed to air. Under this consideration, optical sensors may be utilized as an on-line technique in milling. However, the complexity of milling operations and workpiece geometries limits its application as, for example, in die milling. Further, the hostility of the cutting environment, such as dirt and lubrication oil, may lead to attenuation and scatter of light. The problem of poor reliability and repeatability is likely to be encountered under industrial applications. Therefore, the detection of tool breakage in milling should be focused on indirect methods. A general basic scheme for indirect methods is shown in Figure 2.1.

Considerable research has been undertaken using indirect methods [7]. In recent years, two approaches have been considered to be worthy of further investigation and development. One approach is based on the analysis of the acoustic emission signal coinciding with tool breakage; the other approach is based on the analysis of changes in the pattern of the cutting force signal.

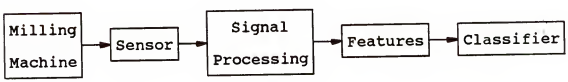


Figure 2.1 Tool breakage monitoring scheme

## 2.1 Acoustic Emission Approach

The acoustic emission signal is obtained from a very high frequency piezoelectric transducer. Kannatey-Asibu and Dornfeld [8] defined the acoustic emission as

> the transient elastic energy spontaneously released in materials undergoing deformation, fracture or both [8, pp. 248].

Therefore, the acoustic emission signal is sensitive to micro- and macro-fractures due to chip formation, chip breaking, tool wear, and tool breakage [9]. Typically, the frequency content of the acoustic emission signal is higher than 100 KHz. It is well beyond the frequency range of machine vibration and noise. Thus, the relatively uncontaminated acoustic emission signal can be obtained by passing the signal through a high-pass filter. However, the choice of a suitable bandwidth of the acoustic emission signal varies significantly from one investigator to the next [10] [11] [12].

It has been shown that a sudden acoustic emission burst is generated at the moment of tool fracture [13]. However, the acoustic emission signal is also sensitive to the variation of cutting parameters [14]. Up to now, no clear relationship has been established between the acoustic emission signal and the cutting parameters [15]. Therefore, it is not easy to determine the proper threshold value to distinguish between the tool breakage and the background noise due to chip formation, chip breaking. Two

recent studies have been proposed to solve this problem in turning where single point machining operations are used. One is a time series analysis technique using an autoregressive filter to model the acoustic emission signal [16]. Experiments indicate that the model parameters could ignore the change of cutting parameters, but show a strong sensitivity to the progress of tool wear. The other is the integration of cutting force and acoustic emission signals via neural networks [17]. The cutting force signal was measured simultaneously and utilized to solve the problem of threshold setting through the neural process networks.

However, in milling operations, a milling cutter with several cutting edges can lead to many different signal interactions. The ambiguous identification of tool breakage occurs because of the signal interactions in multi-tool machining [18]. In addition, entry and exit transients, due to sudden loading and unloading, also produce a large acoustic emission burst which may be higher than that produced by tool breakage, depending on the extent of damage on the tool [19] [20]. A special signal processing strategy using an intelligent insert is being developed in order to prevent the entry and exit spikes from interfering with tool fracture detection [18].

To summarize, the major problems of the acoustic emission approach appear in choosing a suitable bandwidth and in eliminating the noise signals due to chip

formation, chip breakage, multi-tool machining, entry and exit transients, the variation of cutting parameters, etc., so as to set a proper threshold value. In addition, the cost of the required instrumentation is also expensive.

## 2.2 Cutting Force Approach

The cutting force in milling offers very good features for sensing the milling cutter breakage. There are various ways of measuring the cutting force in milling, either directly from a table-type dynamometer, or a dynamometer built into the spindle bearings, or indirectly evaluating the cutting force from the spindle motor current, torque, vibration, or sound. Then, the cutting force signal may be processed in a number of ways to extract features depending on the desired applications. In general, the processing algorithms can be divided into either the time series method (black box type) based on the stochastic process model or the deterministic method based on the analytical understanding of the signal changes.

### 2.2.1 Time Series Method

The use of mathematical models to explain the behavior of physical systems is the foundation of science. If the mathematical model is derived by the physical laws, the model is called a deterministic model. The system

behavior can be determined or calculated accurately. On the other hand, if the mathematical model is derived by the probabilistic laws, the model is called a stochastic model. The future values of the system are predicted by the stochastic model using a sequence of time series data. A general process can be described by the combination of the two models.

In a milling process, the cutting force, f(t) can be represented as [20]

$$f(t) = \frac{\omega_s(B)}{\delta_r(B)}\, u(t) + \frac{\theta_q(B)}{\phi_p(B)}\, a(t) \qquad (2\text{-}1)$$

$$\omega_s = \omega_0 - \omega_1 B - \omega_2 B^2 - \ldots - \omega_s B^s \qquad (2\text{-}2)$$

$$\delta_r = 1 - \delta_1 B - \delta_2 B^2 - \ldots - \delta_r B^r \qquad (2\text{-}3)$$

$$\theta_q = 1 - \theta_1 B - \theta_2 B^2 - \ldots - \theta_q B^q \qquad (2\text{-}4)$$

$$\phi_p = 1 - \phi_1 B - \phi_2 B^2 - \ldots - \phi_p B^p \qquad (2\text{-}5)$$

where

B - backward shift operator

u(t) - cutting process parameters which are assumed to be unknown

a(t) - gaussian white noise

In Equation (2-1), $[\omega_s(B)/\delta_r(B)]\ u(t)$ represents the milling dynamics and $[\theta_q(B)/\phi_p(B)]\ a(t)$ represents the process noise. In order to make the detection of tool breakage independent of cutting process parameters, $[\omega_s(B)/\delta_r(B)]\ u(t)$ should be removed. Thus the cutting force versus time becomes a stationary stochastic process; that is,

$$f(t) = \frac{\theta_q(B)}{\phi_p(B)}\, a(t) \qquad (2\text{-}6)$$

This cutting force model with autoregressive $\phi_p(B)$ and moving average $\theta_q(B)$ components is called an autoregressive moving average model (ARMA) with the order of p and q [21]. The use of a real-time recursive ARMA(p,q) model requires nonlinear, time consuming estimation techniques. However, an autoregressive model (AR) is a linear filter and suitable to monitor physical systems with fast dynamics. Therefore, the cutting force model (AR) with the order p can be expressed as

$$f(t) = \frac{1}{\phi_p(B)}\, a(t) \qquad (2\text{-}7)$$

$$= \frac{1}{1 - \phi_1 B - \phi_2 B^2 - \ldots - \phi_p B^p}\, a(t) \qquad (2\text{-}8)$$

and then

$$f(t) = \phi_1 f(t\text{-}1) + \phi_2 f(t\text{-}2) + \ldots + \phi_p f(t\text{-}p) + a(t) \qquad (2\text{-}9)$$

The value of f(t) can be predicted by using current estimated values of $\phi_1'$, $\phi_2'$, ...., obtained from a recursive parameter adaptation algorithm and past observation f(t-1), f(t-2), ....; that is

$$f'(t) = \phi_1' f(t\text{-}1) + \phi_2' f(t\text{-}2) + \ldots + \phi_p' f(t\text{-}p) \qquad (2\text{-}9)$$

The prediction error, a(t), is the difference between the actual f(t) and predicted f'(t);

$$a(t) = f(t) - f'(t) \qquad (2\text{-}10)$$

If the process is stationary, the prediction error is a white noise with a constant variance. When the process

is suddenly deviated by a tool breakage event, the AR filter is disturbed. A sudden and sharp deviation of prediction error is observed. This is how the time series method can be applied to tool breakage detection.

In [22], a tool breakage detection algorithm has been proposed using spindle motor current. A 28th order autoregressive filter was applied to detect tool breakage. The spindle motor current is known to be proportional to the motor torque generated in the cutting process. Therefore, the changes in the cutting process, for instance tool breakage, can be monitored by using the spindle motor current. However, experiments demonstrated that the spindle motor current is proportional to the cutting torque only up to about 20 Hz. Thus, this algorithm can only be applied at low spindle speeds.

The same approach was also implemented using feed force in end milling [23] instead of spindle motor current. Although the cutter had only two flutes, a 15th order of autoregressive filter was still required. High order time series filters requiring long computation time windows might not be adequate for real-time applications. Moreover, this approach still could not distinguish properly between the transient cuttings (i.e. entry, exit, interrupted cuttings, etc.) and tool breakage event.

### 2.2.2 Deterministic Method

It seems that the stochastic process approach leads to a very high order time series modelling. The robustness of detection of tool breakage is still not satisfactory with these high orders. On the other hand, the mechanics concerning the cutting force have been well modelled with regard to the cutting parameters such as feedrate, speed, depth of cut, radial immersion, and run-out. Therefore, the analytical understanding of the cutting force needs to be studied. Once the basic features of the cutting force are recognized, a more robust processing algorithm for detection of tool breakage is possible.

A scheme for monitoring tool and cutting conditions combining five features extracted from the cutting force has been proposed [24]. The scheme uses these five basic features and is able to separate tool breakage from other changes in the cutting process. However, the scheme works well only if there is only one flute actively cutting. With an increasing number of flutes on the cutter, it becomes difficult to extract these five features from the cutting force.

In [25], two types of tool breakage detection methods using vibration analysis techniques have been proposed. One is based on cepstrum and the other on auto-correlation coefficients. These processing techniques require a long finite-duration time window with a certain time delay. For

the transients and slotting, a reliable threshold setting is still difficult.

A tool breakage monitoring method using the fluctuation signal of the spindle rotational speed has also been proposed [26]. The fluctuation signal could represent the variation of the cutting torque in milling. The detection algorithm is based on a cutting state vector extracted from the speed fluctuation pattern during one revolution. Then, the cutting state vector is compared with a reference vector to recognize tool breakage. The disadvantages of this proposed method are the inherent one revolution delay in detecting tool breakage and the reference vector required.

An alternative way, using the average force per tooth method, has been developed by Altintas et al. [27] [28]. The algorithm is based on synchronous sampling of the cutting force with the spindle speed and it will be further developed in this dissertation. By means of a simple pattern analysis [29], tool breakage can easily be distinguished from transients like entry, exit, cornering, and interrupted cuttings.

The signal used as the basis of this detection method is cutting force signal. In reality, it is difficult to accurately measure the cutting force in milling. In the experimental work, the cutting force signal is measured using a table-type dynamometer, but it distorts the cutting force signal at high frequencies and restricts the working

space during milling operations. Therefore, compensation and replacement of the table-type dynamometer have been presented in order to improve these problems [30]. Alternative signals, like an accelerometer signal on the headstock and a displacement signal of the spindle, have been considered to detect tool breakage directly. It has been shown that the displacement signal correctly indicates the characteristic changes due to tool breakage [31]. Thus, a very promising way for the detection of tool breakage in high speed milling has been proposed by measuring the displacement of the spindle, using for example a capacitance probe [4].

In addition, a knowledge-based approach using the average displacement signal has also been considered [32]. It is expected that this research, adopting the knowledge-based processing with AI (artificial Intelligence) technologies, may enhance the detection system which has been developed.

# CHAPTER 3
# MODELLING OF THE MILLING PROCESS

## 3.1 Description of the Milling Process

Milling is an universal machining process for removing material from a workpiece by the relative motion between the workpiece and a rotating cutter having multiple cutting edges. In milling operations, the surfaces generating by the cutter may be classified into two general categories, face and peripheral millings.

In face milling, the cutter rotates about an axis which is perpendicular to the machined surface (see Figure 3.1.a). In peripheral milling, the cutter rotates about an axis which is parallel to the machined surface (see Figure 3.1.b).

The analysis of the milling process has been well studied [33-38]. Therefore, a mechanistic model of the milling process has been developed [39-41].

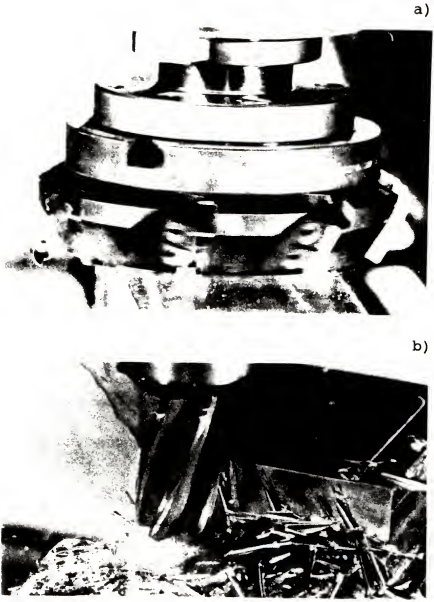


Figure 3.1 Types of milling operations [42, pp. 148].
a) face milling; b) peripheral milling.

## 3.2 Milling Force Model

In a milling operation, the tooth path resulting from the rotation and translation of the cutter is a cycloid. However, the tooth path can be considered as circular arcs with good approximation under the assumption that the feed per tooth, $f_t$, is much smaller than the cutter radius (see Figure 3.2). The feed per tooth is

$$f_t = f / Nm \tag{3-1}$$

where

f - feedrate

N - spindle speed

m - number of the teeth on the cutter

In Figure 3.2.b, the mean chip thickness, $h_m$, at the cutter rotation $\theta$ may be calculated as

$$h_m = f_t * \sin\theta \tag{3-2}$$

### 3.2.1 Straight Toothed Cutter

The instantaneous tangential force acting on the cutting edge is the product of the specific cutting force and the area of the chip cut.

$$\begin{aligned} f_T &= k_s * a_a * h_m \\ &= k_s * a_a * f_t * \sin\theta \end{aligned} \tag{3-3}$$

where

$f_T$ - instantaneous tangential force on the cutting edge

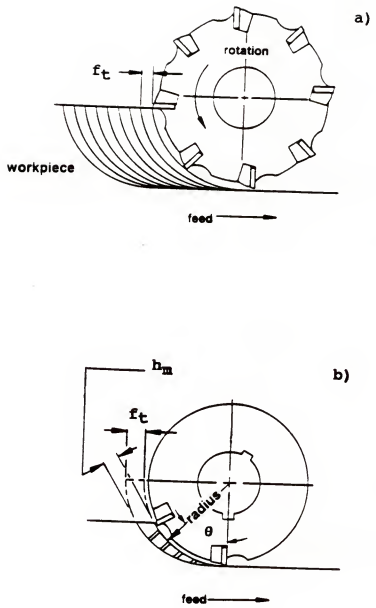


Figure 3.2 Geometry of milling operation.
a) tooth path; b) chip thickness.

$k_s$ - specific cutting force

$a_a$ - axial depth of cut

The corresponding instantaneous radial force is the instantaneous tangential force multiplying by a constant, c.

$$f_R = c * f_T = c * k_s * a_a * f_t * \sin\theta \qquad (3\text{-}4)$$

To decompose the cutting forces $f_T$ and $f_R$ into the X and Y directions, two different methods of generating surfaces by the milling operation need to be considered. They may be called up milling (see Figure 3.3.a) and down milling (see Figure 3.3.b).

The instantaneous cutting forces in the X and Y directions can be represented as

$$f_X = f_T * \cos\theta + f_R * \sin\theta \qquad (3\text{-}5)$$

$$f_Y = -f_T * \sin\theta + f_R * \cos\theta \qquad (3\text{-}6)$$

In multi-tooth milling, there may be more than one tooth active in the cutting. Therefore, the instantaneous cutting forces in the X and Y directions corresponding to a particular angular cutter position are the summation of their force components acting on each tooth engaged with the workpiece.

$$F_X = \sum_{i=1}^{m} \delta(i) * f_{X(i,\theta)} \qquad (3\text{-}7)$$

$$F_Y = \sum_{i=1}^{m} \delta(i) * f_{Y(i,\theta)} \qquad (3\text{-}8)$$

and

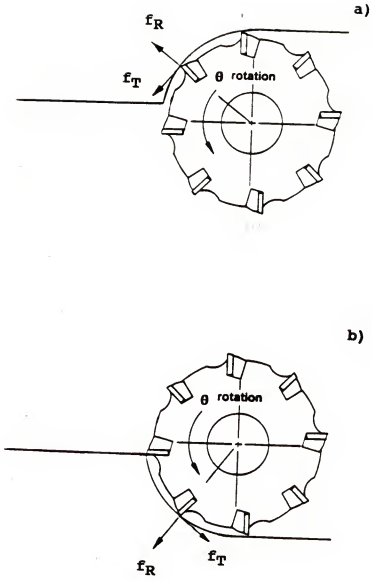


Figure 3.3 Cutting force directions.
a) up milling; b) down milling.

$$\delta(i) = 1 \quad \text{if} \quad \theta_s < \theta_i < \theta_e$$
$$= 0 \quad \text{otherwise}$$

where

m - number of the teeth on the cutter

$\theta_s$ - starting angle of cut

$\theta_e$ - exit angle of cut

### 3.2.2 Helical Toothed Cutter

Figure 3.4.a shows a three dimensional helical toothed cutter and the incremental cutting force along the cutting edges of the cutter with the axial depth of cut, $a_a$. The unrolled circumference of the cutter is shown in Figure 3.4.b. Every helical cutting edge becomes a straight line under the helix angle, $\beta$. All the cutting edges move with the same peripheral cutting speed. The engagement angle, $\psi$, for every cutting edge is

$$\psi = \frac{a_a * \tan\beta}{r} \tag{3-9}$$

Thus, the tooth, $T_1$, moves through the range from the position $\theta = \theta_a$ to the position $\theta = \theta_a + \psi$. Accordingly, the teeth, $T_2$ and $T_3$, move by $\psi$ and $2\psi$ ahead, respectively. Although the tool may have the several teeth cutting simultaneously, the actual cutting edges exist only $\theta_s < \theta_i < \theta_e$.

In order to calculate the instantaneous cutting force, every cutting edge is considered incrementally by

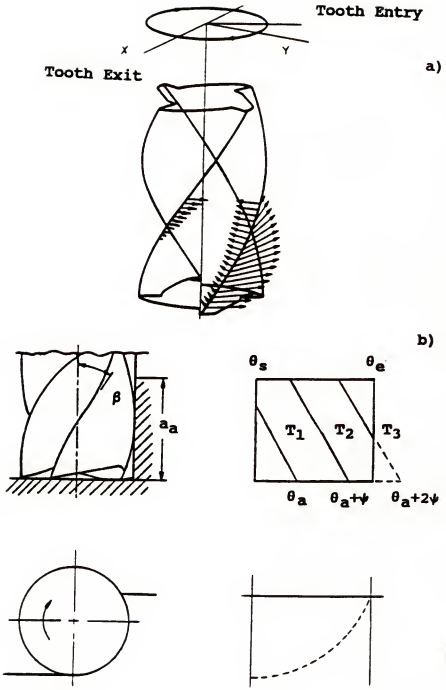


Figure 3.4 Geometry of a helical toothed cutter.
a) incremental cutting force;
b) unrolled surface of cut.

$\Delta\psi$, corresponding to the increment of the axial depth of cut, $\Delta a_a$. Therefore, the element of tangential force, $\Delta f_T$, is the product of the specific cutting force and the corresponding elemental chip cut.

$$\Delta f_T = k_s * \Delta a_a * h_m$$
$$= k_s * \Delta a_a * f_t * \sin\theta \qquad (3\text{-}10)$$

The radial component of force is

$$\Delta f_R = c * \Delta f_T = c * k_s * \Delta a_a * f_t * \sin\theta \qquad (3\text{-}11)$$

Again, these elemental forces may be decomposed into the X and Y directions. The elemental forces in the X and Y directions can be represented as

$$\Delta f_X = \Delta f_T * \cos\theta + \Delta f_R * \sin\theta \qquad (3\text{-}12)$$

$$\Delta f_Y = -\Delta f_T * \sin\theta + \Delta f_R * \cos\theta \qquad (3\text{-}13)$$

To obtain the instantaneous force acting on the cutter at any angular position, it is necessary to sum the elemental forces acting along the engaged ranges of all the cutting edges.

$$F_X = \sum_{i=1}^{m} \sum_{j=1}^{n} \delta(i,j) * \Delta f_{X(i,j)} \qquad (3\text{-}14)$$

$$F_Y = \sum_{i=1}^{m} \sum_{j=1}^{n} \delta(i,j) * \Delta f_{Y(i,j)} \qquad (3\text{-}15)$$

and

$$\delta(i,j) = 1 \quad \text{if} \quad \theta_s < \theta_{(i,j)} < \theta_e$$
$$= 0 \quad \text{otherwise}$$

where

n - total incremental elements in the direction of the axial depth of cut

m - number of the teeth on the cutter

In the foregoing discussion, it has been assumed that the cutting force is obtained from a cutter designed with equally spaced cutting edges, with no consideration of the regeneration of waviness and the run-out on the cutter. In reality, both of them not only exist but also vary the cutting force. Therefore, they should be taken into account in the cutting force model.

## 3.3 Regeneration of Waviness

Because of the inherent insufficient stiffness of the spindle system, there is a cutter vibration at the time that the workpiece surface is produced. As a result, a waviness is generated on the workpiece surface [38] (see Figure 3.5.a). A variable component of chip thickness, $h_v$, is obtained due to the regeneration of the waviness. This is because each tooth removes the chip from the surface produced by the preceding teeth. If any vibration exists during the cut, a variable thickness is generated.

$$h_v = z - z_b \tag{3-16}$$

where

$z$ - current vibration of the cutter normal to the cut

$z_b$ - undulation of the surface produced by the preceding teeth at current position of cut

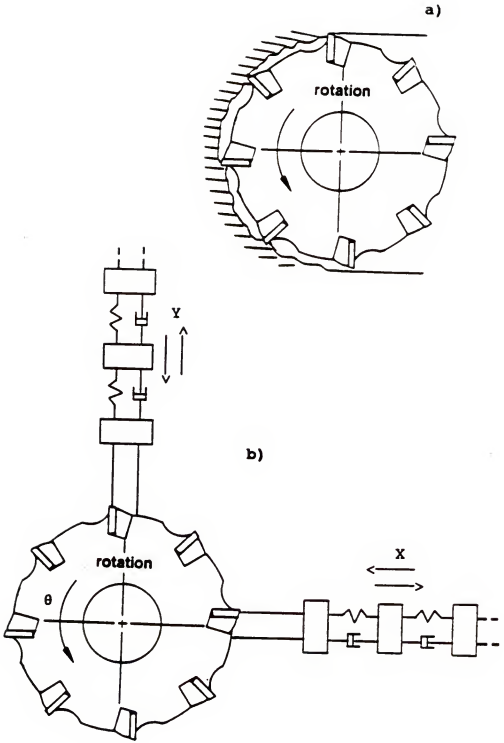


Figure 3.5 Regeneration of the waviness in milling.
a) waviness of workpiece surface;
b) simulation model.

A milling cutter model may be established by using modal analysis on the transfer function of the spindle system (see Figure 3.5.b). The vibration of the cutting edge may be expressed as

$$z = x * \sin\theta + y * \cos\theta \tag{3-17}$$

where

x - displacement of the cutter in the X direction

y - displacement of the cutter in the Y direction

Once the instantaneous cutting force has been calculated, the vibrations of $x_i$ and $y_i$ in each mode can also be solved by Euler's equations.

$$\ddot{x}_i = \frac{F_X - C_{Xi} * \dot{x}_i - K_{Xi} * x_i}{M_{Xi}} \tag{3-18}$$

$$\ddot{y}_j = \frac{F_Y - C_{Yj} * \dot{y}_j - K_{Yj} * y_j}{M_{Yi}} \tag{3-19}$$

and

$$\dot{x}_i(t+\Delta t) = \dot{x}_i(t) + \ddot{x}_i(t) * \Delta t \tag{3-20}$$

$$\dot{y}_j(t+\Delta t) = \dot{y}_j(t) + \ddot{y}_j(t) * \Delta t \tag{3-21}$$

and

$$x_i(t+\Delta t) = x_i(t) + \dot{x}_i(t+\Delta t) * \Delta t \tag{3-22}$$

$$y_j(t+\Delta t) = y_j(t) + \dot{y}_j(t+\Delta t) * \Delta t \tag{3-23}$$

where

$\ddot{x}_i$, $\ddot{y}_j$ - acceleration of the X or Y direction in i or j mode

$\dot{x}_i$, $\dot{y}_j$ - velocity of the X or Y direction in i or j mode

$x_i$, $y_j$ - displacement of the X or Y direction in i or j mode

$M_{Xi}$, $M_{Yj}$ - mass coefficients

$C_{Xi}$, $C_{Yj}$ - damping coefficients

$K_{Xi}$, $K_{Yj}$ - spring coefficients

$\Delta t$ - integration time interval

Finally, the vibrations of cutter in the X and Y directions can be obtained by the superposition of the vibration in each mode.

$$x = \sum_{i=1}^{nx} x_i \tag{3-24}$$

$$y = \sum_{j=1}^{ny} y_j \tag{3-25}$$

where

nx - number of modes in the X direction

ny - number of modes in the Y direction

Substituting Equations (3-24) and (3-25) into (3-17), the actual chip thickness, h, can be expressed as the summation of the mean and variable components of chip thickness. That is

$$h = h_m + h_v = f_t * \sin\theta + z - z_b \tag{3-26}$$

This is only true when $(f_t * \sin\theta + z) > z_b$. If the vibration between the cutter and workpiece becomes so big that the cutting edge may jump out and loose contact with the workpiece surface, i.e. $(f_t * \sin\theta + z) < z_b$, the actual chip thickness, h, is equal to zero.

Now, Equations (3-3) and (3-10) may be modified to incorporate the effect of the regeneration of waviness and become

$$f_T = k_s * a_a * (f_t * \sin\theta + z - z_b) \quad \text{if } f_t * \sin\theta + z > z_b$$
$$= 0 \quad \text{if } ft * \sin\theta + z < z_b \tag{3-27}$$

and

$$f_T = k_s * \Delta a_a * (f_t * \sin\theta + z - z_b) \quad \text{if } f_t * \sin\theta + z > z_b$$
$$= 0 \quad \text{if } ft * \sin\theta + z < z_b \tag{3-28}$$

Finally, it has been shown that the influence of the regeneration of waviness on the cutting force may be neglected as long as milling is in the stable cut without chattering [43].

### 3.4 Run-out on the Cutter

Cutter run-out is a common phenomenon affecting the performance of milling operations. In general, run-out may be referred to as radial and axial throws which may arise from eccentricities when the cutter is held in the spindle. When indexable insert type cutters are used, run-out is more likely due to insert size variation, spindle out-of-roundness, and setting of inserts [44]. For the non-indexable, regrindable type cutters, run-out commonly

results from the cutter offset with respect to the spindle rotation [41].

Usually, the axial throw is small relative to the axial depth of cut, so its effect on the cutting force may be neglected. However, the magnitude of radial throw is the same order as that of feed per tooth. It may cause each tooth to experience a different chip thickness. Therefore, the cutting force analysis becomes much more complicated due to the presence of the radial throw.

The chip thickness with radial throw can be derived by using the circular tooth path approximation [41], see Figure 3.6. The actual mean chip thickness, $h_{mc}$, can be expressed as

$$h_{mc} = r_i - r_b \tag{3-29}$$

where

$r_i$ - radius of the ith tooth in the cut

$r_b$ - distance from the ith tooth center to surface left by the preceding cut

Using the law of sines, $r_b$, can be calculated as

$$\frac{r_{i-1}}{\sin(\pi/2 + \theta)} = \frac{r_b}{\sin(\pi/2 - \phi)} \tag{3-30}$$

then

$$r_b = r_{i-1} \frac{\cos\phi}{\cos\theta} \tag{3-31}$$

and

$$\phi = \theta + \epsilon \tag{3-32}$$

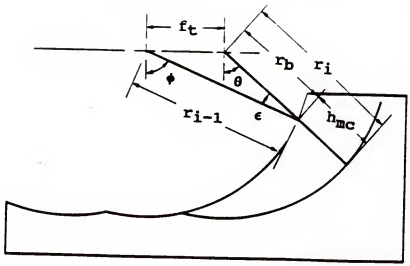


Figure 3.6 Geometry of chip thickness with radial throw.

Substituting Equation (3-32) into (3-31),

$$r_b = r_{i-1} * (\cos\epsilon - \frac{\sin\theta * \sin\epsilon}{\cos\theta}) \qquad (3\text{-}33)$$

Again, using the law of sines, $\cos\epsilon$ and $\sin\epsilon$ can be calculated as

$$\frac{r_{i-1}}{\sin(\pi/2 + \theta)} = \frac{f_t}{\sin\epsilon} \qquad (3\text{-}34)$$

then

$$\sin\epsilon = \frac{f_t * \cos\theta}{r_{i-1}} \qquad (3\text{-}35)$$

and

$$\cos\epsilon = (1 - \sin^2\epsilon)^{1/2} = \frac{(r_{i-1} - f_t^2 * \cos^2\theta)^{1/2}}{r_{i-1}} \qquad (3\text{-}36)$$

Substituting Equations (3-35) and (3-36) into Equation (3-33), $r_b$ can be expressed as

$$r_b = (r^2_{i-1} - f_t^2 * \cos^2\theta)^{1/2} - f_t * \sin\theta \qquad (3\text{-}37)$$

Finally, substituting Equation (3-37) into (3-29), $h_{mc}$ can be expressed as

$$h_{mc} = r_i - (r^2_{i-1} - f_t^2 * \cos^2\theta)^{1/2} + f_t * \sin\theta \qquad (3\text{-}38)$$

The term, $(f_t^2 * \cos^2\theta)$, may be neglected in Equation (3-38), since the feed per tooth, $f_t$, is much smaller than the cutter radius, i.e. $(r^2_{i-1} >> f_t^2 * \cos^2\theta)$. Therefore, the actual mean chip thickness is

$$h_{mc} = (r_i - r_{i-1}) + f_t * \sin\theta \qquad (3\text{-}39)$$

This result shows that radial throw introduces another term to the chip thickness. It also needs to be considered that the radial throw may be severe in

comparison to the term, ($f_t$ * sinθ), especially at entry and exit positions where θ is small. As a result, $r_{i-1}$ may be greater than ($r_i$ + $f_t$ * sinθ) which results in negative chip thickness value in Equation (3-39). What is really happening is that some teeth experience no chip load or partial chip load and a particular tooth removes the workpiece surface left two or more teeth ago.

Therefore, Equation (3-39) needs a further modification to include these conditions.

$$h_{mc} = (r_i - r_{i-k}) + k * f_t * \sin\theta \qquad (3\text{-}40)$$

where tooth i removes the surface left by tooth i-k.

However, the determination of the coefficient, k, is not straightforward. Hence, a special calculation algorithm has been developed [39]. It checks the previous chip thickness consecutively until the constant, k, is found. That is

$$h_i = \sum_{j=1}^{k} f_t * \sin\theta + r_{i-j} - r_{i-j-1}$$

$$\text{if } f_t * \sin\theta + r_{i-k} - r_{i-k-1} < 0 \qquad (3\text{-}41)$$

where $h_i$ is a non-positive constant. $h_i$ may also be called the chip thickness of over cut due to the radial throw.

Hence, the modified actual mean chip thickness may be expressed as

$$h_{mc} = f_t * \sin\theta + (r_i - r_{i-1}) + h_i$$

$$\text{if } f_t * \sin\theta + r_i > r_{i-1}$$

$$= 0$$

$$\text{if } f_t * \sin\theta + r_i < r_{i-1} \qquad (3\text{-}42)$$

Again, Equations (3-3) and (3-10) may be modified to incorporate the effect of radial throw and become

$$f_T = k_s * a_a * (f_t * \sin\theta + r_i - r_{i-1} + h_i)$$
$$\text{if} \quad f_t * \sin\theta + r_i > r_{i-1}$$
$$f_T = 0$$
$$\text{if} \quad f_t * \sin\theta + r_i < r_{i-1} \qquad (3\text{-}43)$$

and

$$f_T = k_s * \Delta a_a * (f_t * \sin\theta + r_i - r_{i-1} + h_i)$$
$$\text{if} \quad f_t * \sin\theta + r_i > r_{i-1}$$
$$f_T = 0$$
$$\text{if} \quad f_t * \sin\theta + r_i > r_{i-1} \qquad (3\text{-}44)$$

Finally, Figure 3.7 shows a flow chart of modelling the dynamics of cutting force in milling. A mechanistic force model with straight and helical toothed cutters including the effects of regeneration of waviness and radial throw has been computerized, see Appendix [A]. In the following chapters, this model will be utilized as a useful tool for the simulation and analysis of the cutting force signal in milling operations.

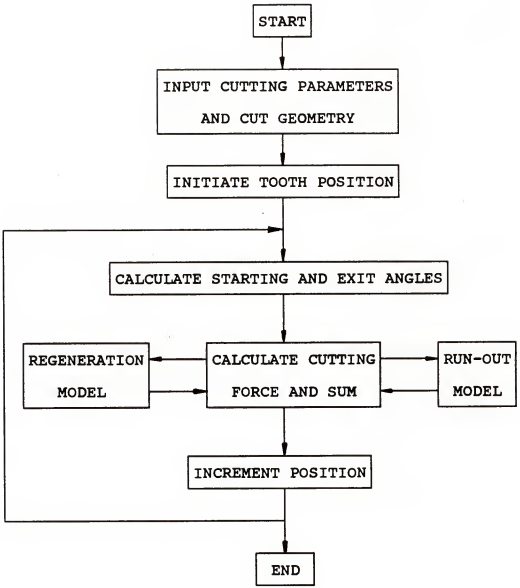


Figure 3.7 Flow chart for simulation of cutting force

# CHAPTER 4
# DETECTION OF TOOL BREAKAGE USING THE CUTTING FORCE SIGNAL

## 4.1 Simulation of the Cutting Force Signal With and Without Tool Breakage

### 4.1.1 Straight Toothed Cutter

The cutting force signal in face milling is periodic with tooth frequency, $f_t$. As one of the teeth is chipped or broken, the tooth following the chipped or broken one will have a bigger chip load in order to remove the material left by the chipped or broken one. Therefore, the characteristics of the cutting force signal are changed because of the existence of tool breakage.

Figure 4.1 shows a face milling cutter (diameter = 101.6 mm) without run-out milling over the most common geometry of workpiece. The cutting parameters are shown in Table 4.1. Based on the transfer functions measured [45], the model of the spindle system at the end of tool is shown in Table 4.2. Figure 4.2 shows the simulation of the cutting force signal in the entry, steady, and exit states with and without tool breakage. The simulation results show

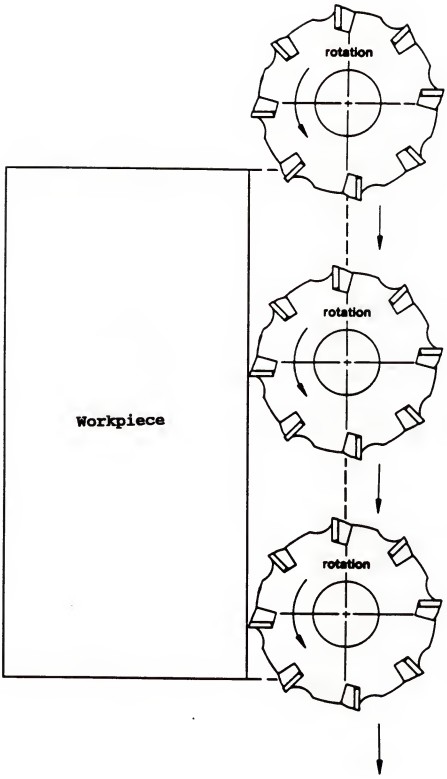


Figure 4.1 Cut geometry in the entry, steady, and exit states.

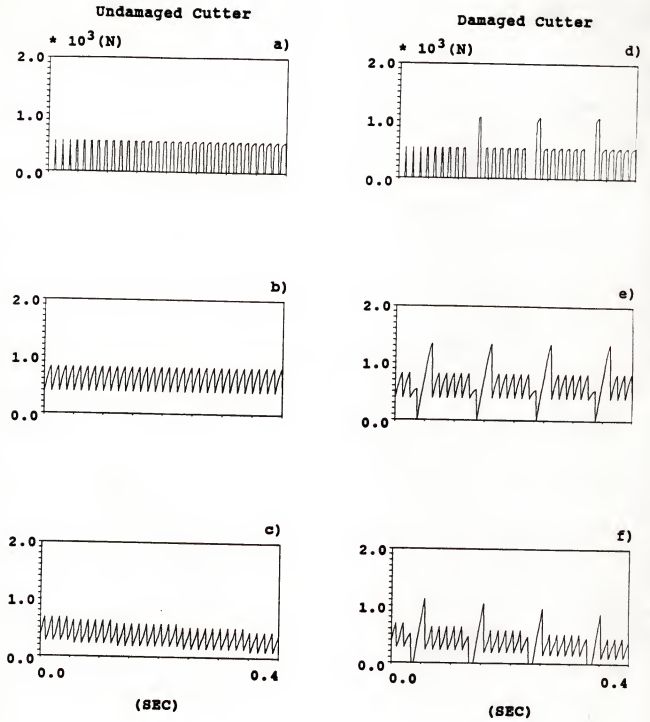


Figure 4.2 Simulation of the cutting force in the entry, steady, and exit states in up milling.

the effect of regeneration of waviness on the cutting force is slight and can be neglected because the cut is stable.

By experiments, it was seen that the broken tooth breaking off the whole cutting area was common. Therefore, it was assumed that the cutting area of a broken tooth was totally broken in the simulation.

Table 4.1 Cutting parameters in the simulation of cutting force in face milling

| spindle speed | depth of cut | feed per tooth | radial immersion | workpiece material |
|---|---|---|---|---|
| rpm | mm | mm | | |
| 600 | 1.27 | 0.254 | 1/2 | cast iron |

Table 4.2 Simulation parameters for the spindle system

| direction | mass (kg) | damping ratio | natural frequency |
|---|---|---|---|
| X | 18.6 | 0.04 | 468 Hz |
| Y | 19.2 | 0.04 | 515 Hz |

In the entry transient, the cutter gradually enters the workpiece and the width of the cutting force signal increases. As to the steady state, the cutting force signal is periodic per tooth period because of the invariant cutting geometry. In the exit transient, both the magnitude

and the width of the cutting force signal decrease. However, for the damaged cutter with a broken tooth, the cutting force signal which decreases, then increases, forms a special tool breakage feature shown in all of the states. It is also true for the case of down milling, see Figure 4.3.

Analogous results were also obtained from the other immersions. Figure 4.4 shows the cutting force signal in the steady state with 1/8, 1/4, 1/2, and 1/1 immersions of cut (where 1/1 immersion represents slotting). In addition, Figure 4.5 shows the cutting force signal in the steady state using the cutter with 4, 6, 8, and 10 teeth in the 1/2 immersion. The clear tool breakage feature is available in all of the cases.

Run-out is an unavoidable phenomenon in milling. In experiments, the best radial throw on the cutting edges was found to be within 0.025 mm (0.001"). An example of radial throw on each tooth is listed in Table 4.3.

As mentioned in Chapter 3, the existence of run-out produces the variation of chip load for each tooth. Therefore, the variable chip load affects the characteristics of the cutting force signal. A simulation of the cutting force signal in entry, steady, and exit states with these radial throws is shown in Figure 4.6. The cutting parameters are the same as those in Figure 4.2. It can be seen that the periodicity of the cutting force signal per tooth is disturbed by the radial throws.

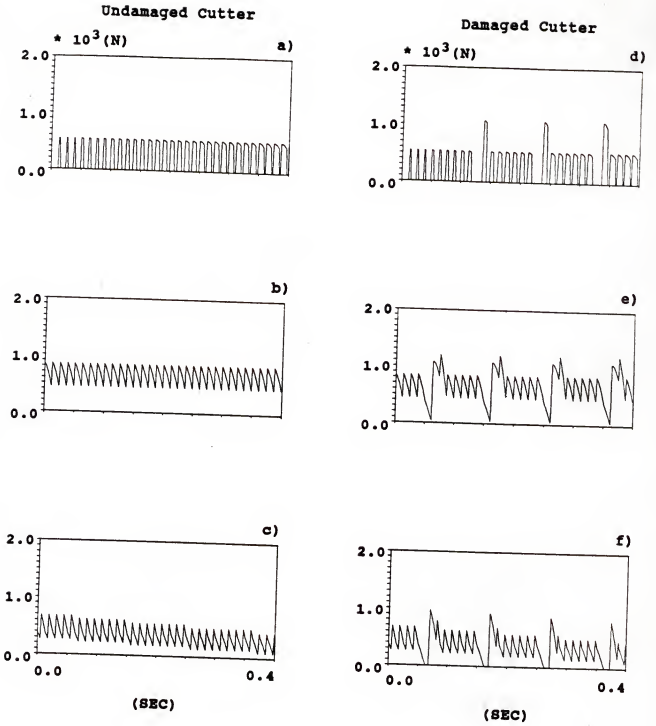


Figure 4.3 Simulation of the cutting force in the entry, steady, and exit states in down milling.

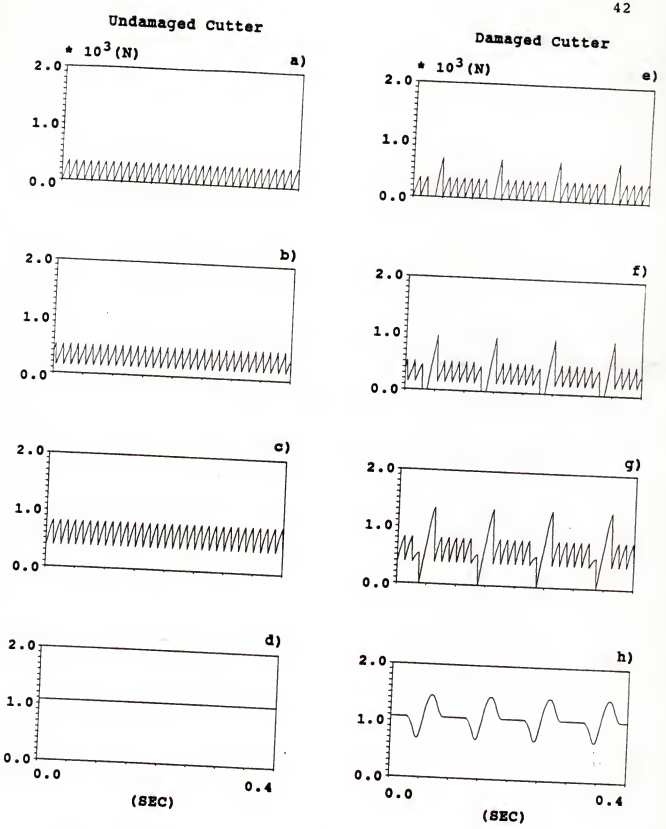


Figure 4.4 Simulation of the cutting force in the 1/8, 1/4, 1/2, and 1/1 immersions of cut.

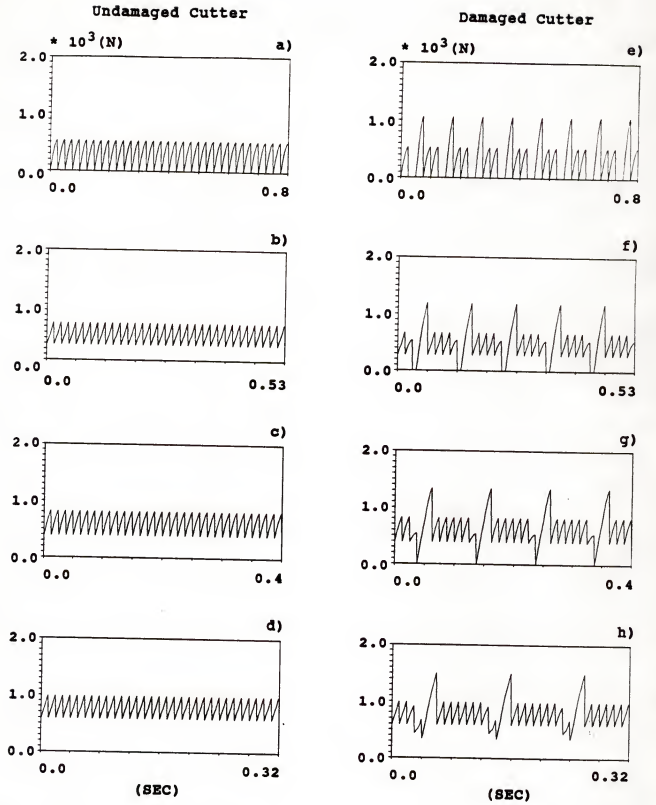


Figure 4.5 Simulation of the cutting force with 4, 6, 8, and 10 teeth on the cutters.

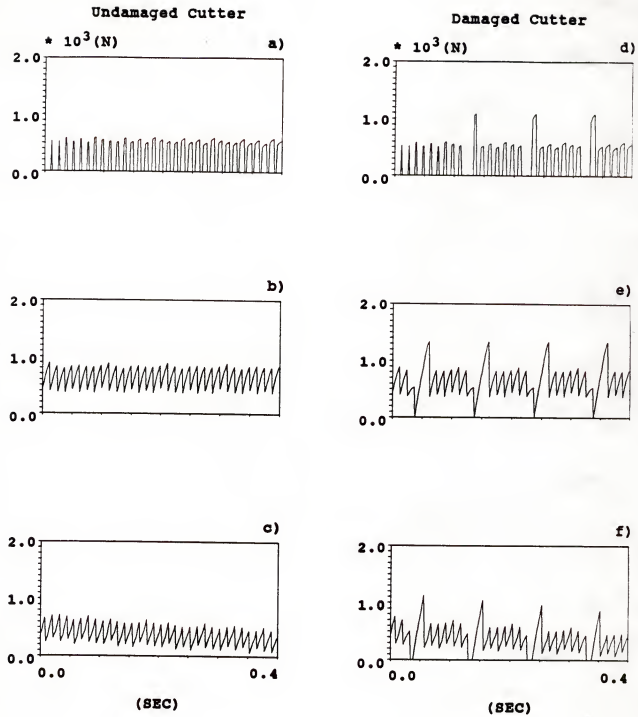


Figure 4.6 Simulation of the cutting force with radial throw in the entry, steady, and exit states.

However, much bigger variation due to tool breakage still remains.

Table 4.3 Radial throw in the face milling cutter

| tooth number | radial throw (mm) | tooth number | radial throw (mm) |
|---|---|---|---|
| 1 | -0.0203 | 5 | -0.0252 |
| 2 | -0.0042 | 6 | -0.0029 |
| 3 | -0.0160 | 7 | 0.0 |
| 4 | -0.0080 | 8 | -0.0069 |

### 4.1.2 Helical Toothed Cutter

In peripheral milling, one of the most common types is end milling. Figure 4.7 shows the simulation of the cutting force signal without run-out in the 1/2 immersion up milling by using a 4-flute end mill cutter (diameter = 25.4 mm) with a helix angle of 30°. The cutting parameters are listed in Table 4.4.

Even though the cutting edges are helical, the variation of the cutting force signal is still periodic with the tooth frequency. The uniform periodicity is disturbed when one of the cutting edges is broken. As a result, much bigger variation of the cutting force signal,

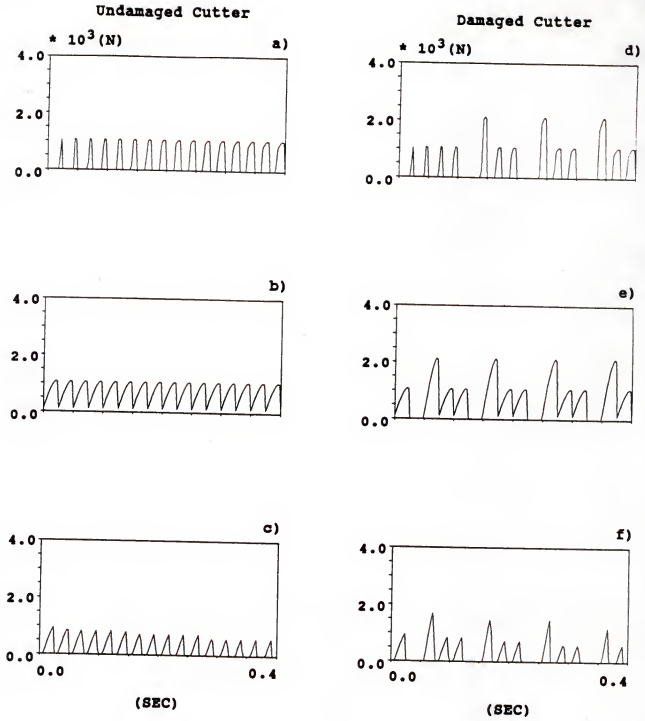


Figure 4.7 Simulation of the cutting force in the entry, steady, and exit states using a helical toothed cutter.

which decreases, then increases, is generated because of the broken edge.

Table 4.4 Cutting parameters in the simulation of the cutting force in end milling

| spindle speed | depth of cut | feed per tooth | radial immersion | workpiece material |
|---|---|---|---|---|
| rpm | mm | mm | | |
| 600 | 2.54 | 0.254 | 1/2 | cast iron |

This is also true for the different immersions of cut. Figure 4.8 shows the cutting force signal in the 1/8, 1/4, 1/2, and 1/1 immersions of cut. Figure 4.9 shows the cutting force signal with 2, 3, and 4 flutes of the end mill cutter in the steady state. It is shown that the distinction between the undamaged and damaged cutters is stronger when a less number of flutes on the cutter is used.

In the foregoing discussion, it is clearly seen that the tool breakage feature in the cutting force signal is available in all kinds of milling operations. Therefore, processing the cutting force signal is recognized as one of the most feasible way to detect tool breakage in milling.

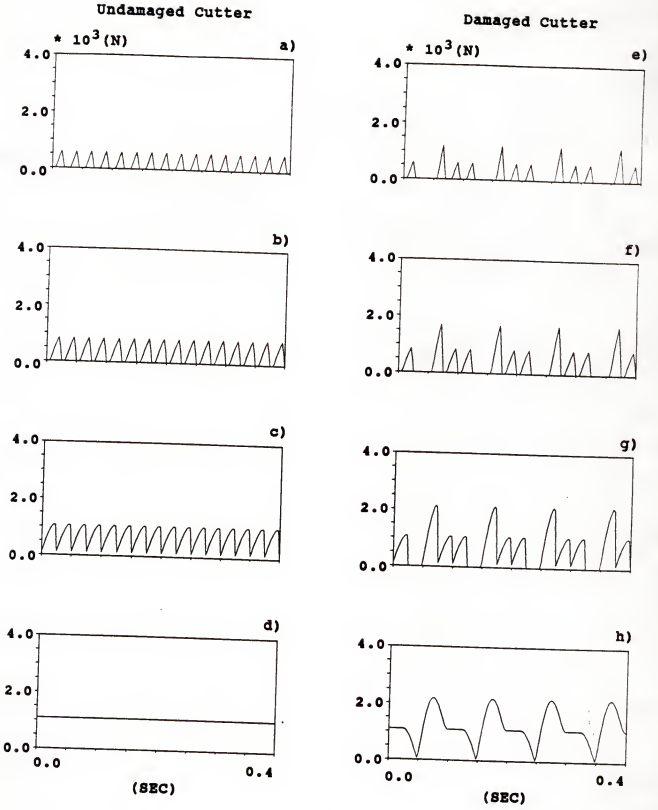


Figure 4.8 Simulation of the cutting force in the 1/8, 1/4, 1/2, and 1/1 immersions of cut using a helical toothed cutter.

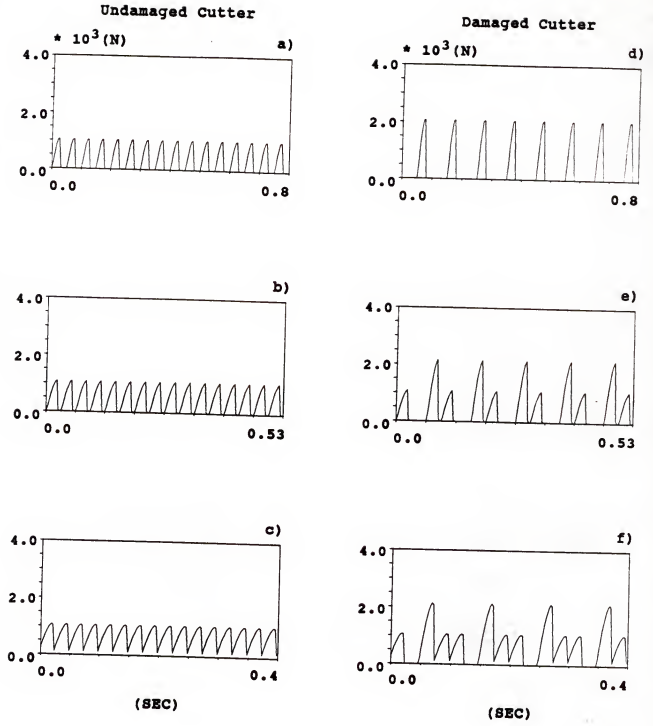


Figure 4.9 Simulation of the cutting force using helical toothed cutters with 2, 3, and 4 flutes.

## 4.2 Detection Algorithm for Tool Breakage

In Section 4.1, it has been shown that the characteristics of the cutting force signal are obviously changed due to tool breakage. Hence, the cutting force signal is available for recognizing tool breakage. However, it is difficult to detect tool breakage using the instantaneous cutting force signal directly. This is because cut geometry, run-out, and the difficulties of force measurement (Section 4.5) change and distort the cutting force signal. Therefore, it is necessary to develop a detection algorithm, and extract the tool breakage feature from the instantaneous cutting force signal.

In order to understand the tool breakage feature in the cutting force signal, the spectrum of the cutting force signal is utilized. Figure 4.10 shows the cutting force spectra corresponding to the signal in Figure 4.2. The DC component of the spectrum is omitted because the tool breakage feature belongs to the AC components in the cutting force spectrum. For the undamaged cutter, the prominent components are not only the component of tooth frequency, $f_t$, but also its harmonics. Both are needed to represent the periodic change of the cutting force signal exactly. For the damaged cutter with a broken tooth, the component of once per revolution, $f_r$, and its harmonics show up. In comparing the spectra between the undamaged and damaged cutters, it is clearly shown that the frequency

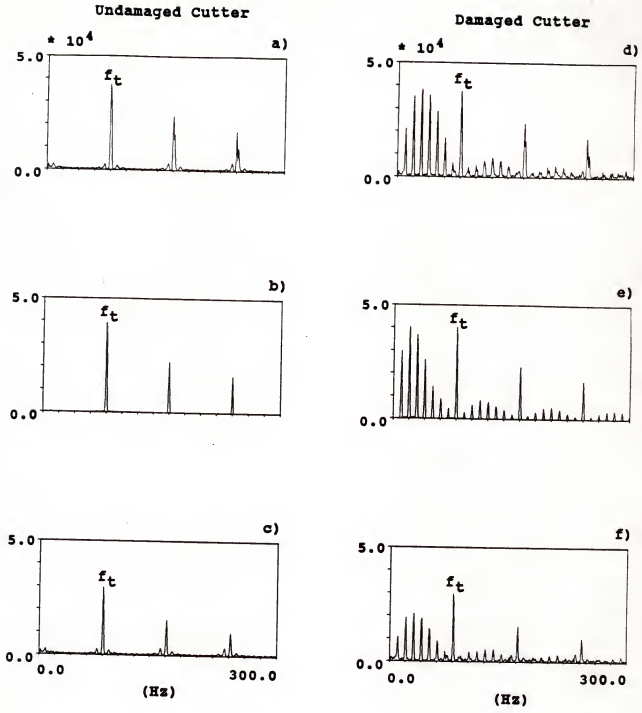


Figure 4.10 Spectra of the simulation of the cutting force in the entry, steady, and exit states.

components of tool breakage are $f_r$ and its harmonics, depending on the number of teeth on the cutter. This frequency area may be called a "tool breakage zone".

Now, the task is how to process the cutting force signal and make the components inside the tool breakage zone stand out, or suppress the components outside this zone. Several methods have been under investigation, such as the time series method, the power method [46], and the difference per tooth average method. So far, it seems that the difference per tooth average method is the best one. The main advantage of this method is that it is simple, quick, and reliable. The difference per tooth average method is illustrated in the following text:

The average force per tooth is calculated as

$$F_{xavg}(j) = \frac{\sum_{i=1}^{n} F_x(i)}{n} \tag{4.1}$$

$$F_{yavg}(j) = \frac{\sum_{i=1}^{n} F_y(i)}{n} \tag{4.2}$$

where

$F_{xavg}$ - average force per tooth in the X direction

$F_{yavg}$ - average force per tooth in the Y direction

$j$ - index for time increment per tooth period

$n$ - number of samples per tooth period

In reality, machining operations may involve contours and corners. Hence, both the X and Y directions of the

cutting force should be taken into account and calculated as the resultant average force per tooth, $F_{avg}$.

$$F_{avg}(j) = (F_{xavg}^2(j) + F_{yavg}^2(j))^{1/2} \quad (4.3)$$

Finally, the difference of the resultant average force per tooth, $\Delta F_{avg}$ is obtained by

$$\Delta F_{avg}(j) = F_{avg}(j) - F_{avg}(j-1) \quad (4.4)$$

Applying the difference per tooth average method, Figure 4.11 shows the simulation results for the cutting force signal in the steady state as shown in Figure 4.2. The first row displays the cutting force signal. For calculation of the average force, nine samples were taken in each tooth period. Averaging the cutting force signal per tooth, see Equations 4.1 and 4.2, filters out the tooth frequency and its harmonic components. Then, the resultant average cutting force signal per tooth, see Equation 4.3, is displayed in the second row. It is shown that the periodic variation per tooth is removed. However, the DC component of the cutting force and the variation due to the broken tooth still remain. The variation due to the broken tooth stands out, once the average of the cutting force per tooth is differenced, see Equation 4.4. The difference of the average cutting force signal is displayed in the third row. It is shown that there is an extremely clear distinction of the difference of the average cutting force between the undamaged and damaged cutters. Therefore, this processing method is a very

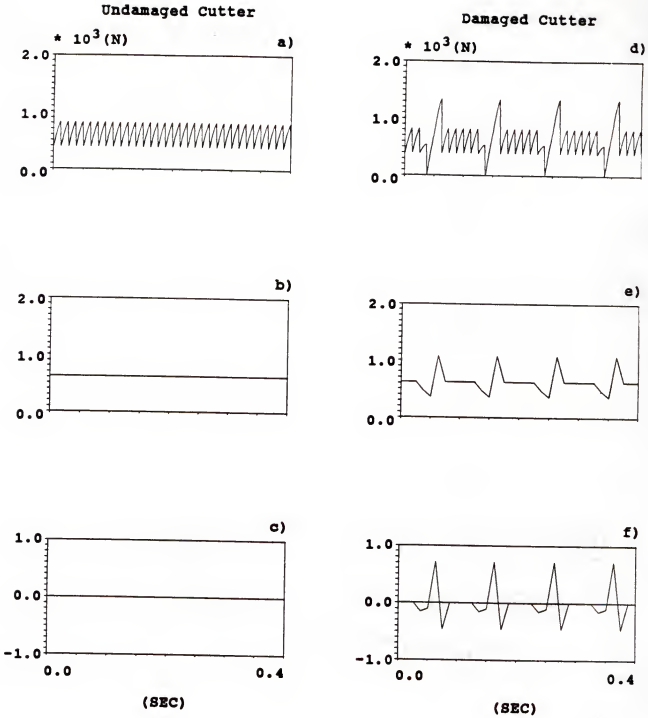


Figure 4.11 Simulation of the instantaneous force, average force, and difference of the average force in the steady state.

efficient way of extracting the tool breakage feature from the cutting force signal.

This is true not only in the steady state, but also in the transient states. Figure 4.12 and Figure 4.13 show the simulation results in the entry and exit transients. A staircase of the average force signal is obtained due to the finite sampling. However, the staircase will disappear when a higher sampling rate is used [27] [29].

Run-out in the form of radial throw also produces another kind of once per revolution signal, see Figure 4.14. Figure 4.14.b and 4.14.f show the spectra of the cutting force data with radial throw in the steady state portion of cut indicated in Figure 4.6. Unfortunately, the frequency components of the radial throw are also located inside the tool breakage zone. Therefore, it affects the difference of the average force. Figure 4.14.c shows the average force signal with the radial throw. Even for the undamaged cutter, a certain level of the difference of the average cutting force signal exists (see Figure 4.14.d). However, a clear distinction of the difference of the average signals is still available between the undamaged and damaged cutters.

To summarize, processing the cutting force signal with the difference per tooth average method through simulation is recognized as a very feasible way to detect tool breakage in milling. Thus, an experimental verification of this method is necessary.

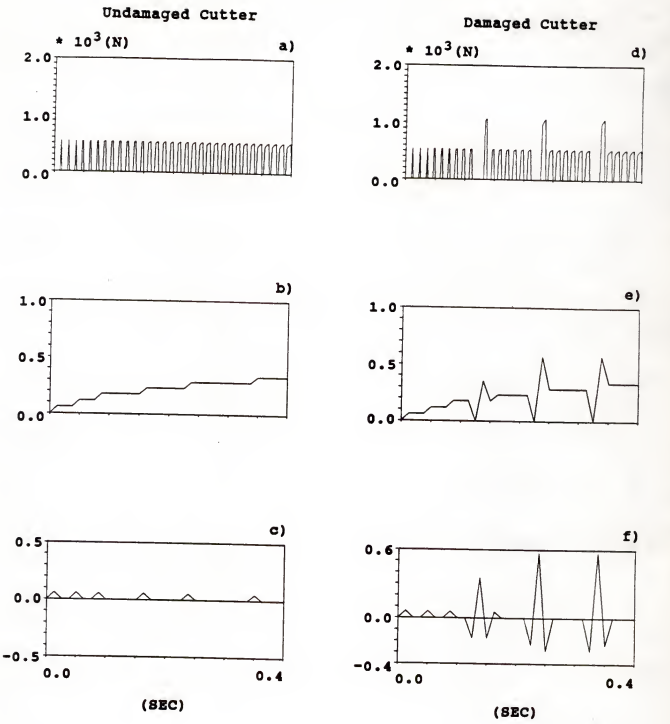


Figure 4.12 Simulation of the instantaneous force, average force, and difference of the average force in the entry state.

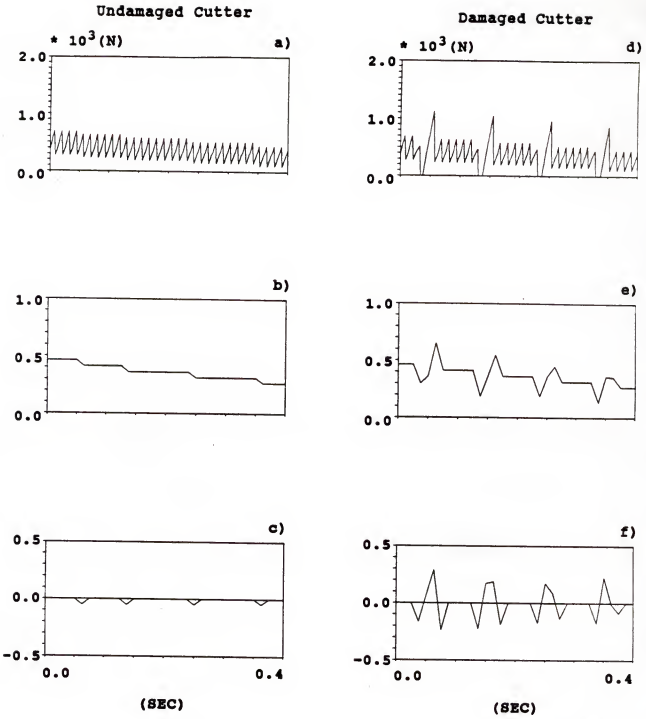


Figure 4.13 Simulation of the instantaneous force, average force, and difference of the average force in the exit state.

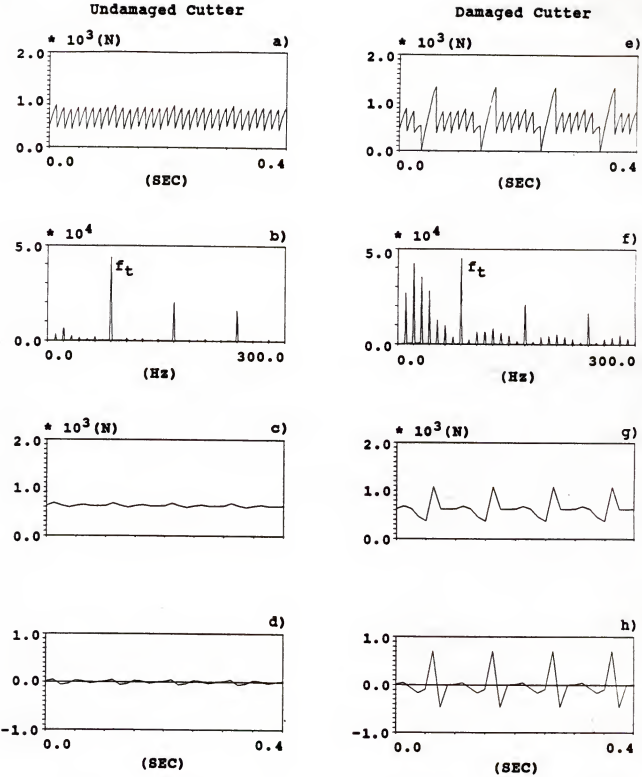


Figure 4.14 Simulation of the instantaneous force and its spectrum, average force, and difference of the average force in the steady state with radial throw.

## 4.3 Experimental Set-up

A Sundstrand Omnimil 20 machining center (White Sundstrand Machine Tool Co.) shown in Figure 4.15, with a maximum rated spindle speed of 5500 rpm and a rated horse power of 25 at 1200 rpm was used in the experiments. It is a horizontal spindle machine with three linear axes,a 360 discrete degree rotary index table, and a 30 position automatic tool exchanger [46].

All of the face milling tests were done by using a 4-inch diameter double-negative ZN3M Carbaloy milling cutter (GE Co.). The catalog number of the inserts is SNG634 or SNG632 (silicon nitride). The maximum run-out among these inserts on the cutter was 0.0254 mm (0.001"). The workpiece material was an ingot of GM-241 cast iron in the form of a flat 12" long, 6" wide and 3.5" thick. The workpiece was bolted to an angle plate so that a large surface was available for milling.

The cutting force signal was obtained by using a table type of dynamometer under the workpiece and the angle plate, see Figure 4.16. The dynamometer was constructed with three directional Kistler load cells (Model 9067). The output signals of the load cells travel through wires to Kistler charge amplifiers (Type 5007). The charge amplifiers convert the signals yielded by the load cells into the proportional cutting force signals in three perpendicular directions. The transfer function of the

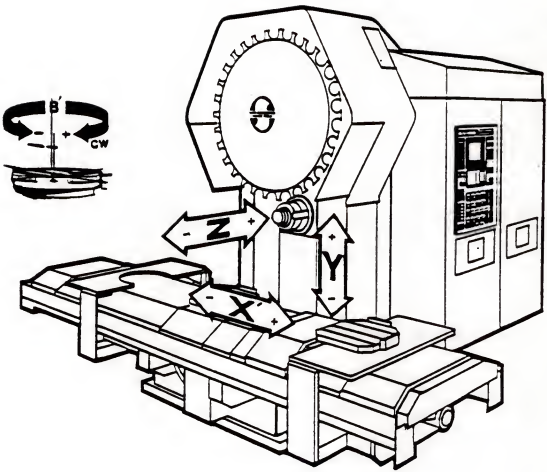


Figure 4.15 Series 20 Omnimil Machining Center.

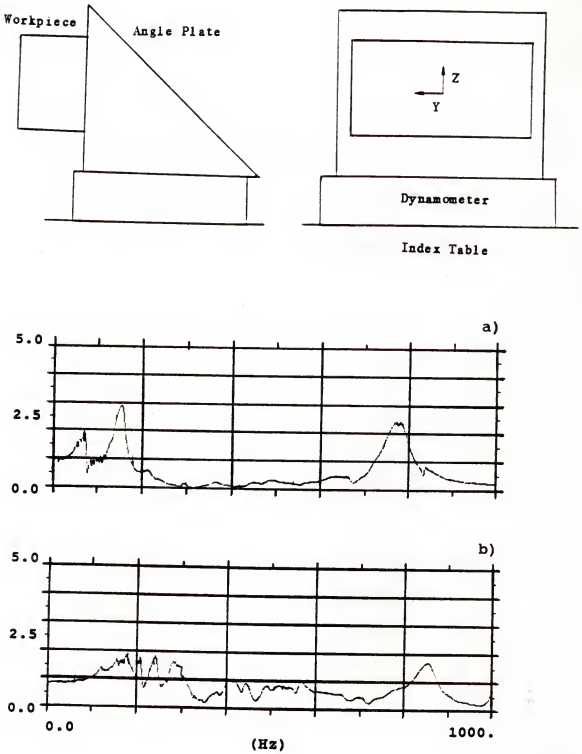


Figure 4.16 Assembly of workpiece-angle plate-dynamometer and transfer function of the dynamometer. a) Y direction; b) Z direction.

dynamometer in the Y and Z directions is shown in Figure 4.16.a and 4.16.b. This transfer function indicates the accuracy with which the dynamometer signal represents the actual cutting force signal (see Section 4.5). The cutting force signals were recorded on an IBM PC-AT microcomputer using a data acquisition board (Data Translation DT2818). The data acquisition system provides four A/D converters with a maximum simultaneous sampling rate of 27.5 KHz and two D/A converters with a maximum sampling rate of 33.0 KHz. The voltage resolution of this board is +/- 10 VDC with 12 bits.

In order to sample the cutting force signal synchronized with the spindle rotation, external sampling and triggering were used. A magnetic pick-up sensed the distance between itself and a steel gear with 72 teeth mounted on the spindle. When the spindle rotated, the distance was converted into an analog signal. This analog signal was transmitted through a comparator, a Schmitt trigger, and a counter from which the external sampling and triggering signals were obtained. Figure 4.17.a shows the electrical circuit block diagram for generating the external sampling and triggering signals. Figure 4.17.b shows the interrupt circuit for feed control of the machining center when tool breakage is detected. Finally the schematic diagram for the experimental work is shown in Figure 4.18.

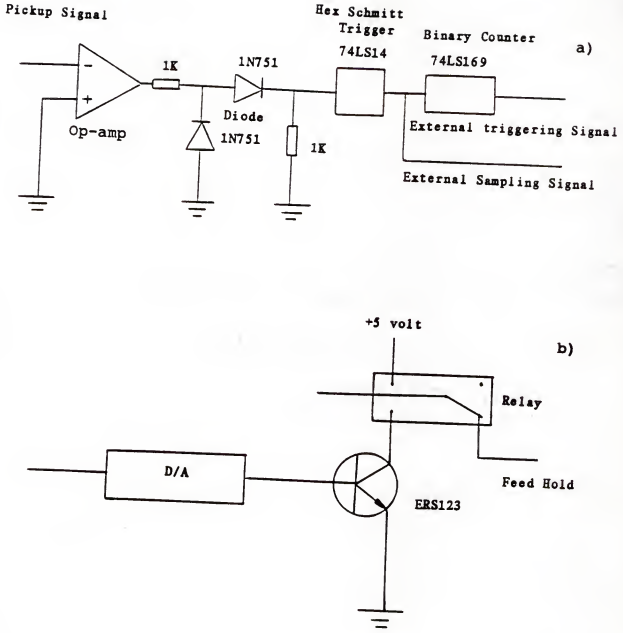


Figure 4.17 Electrical circuit block diagram.
a) external sampling and triggering;
b) interrupted circuit for feed control.

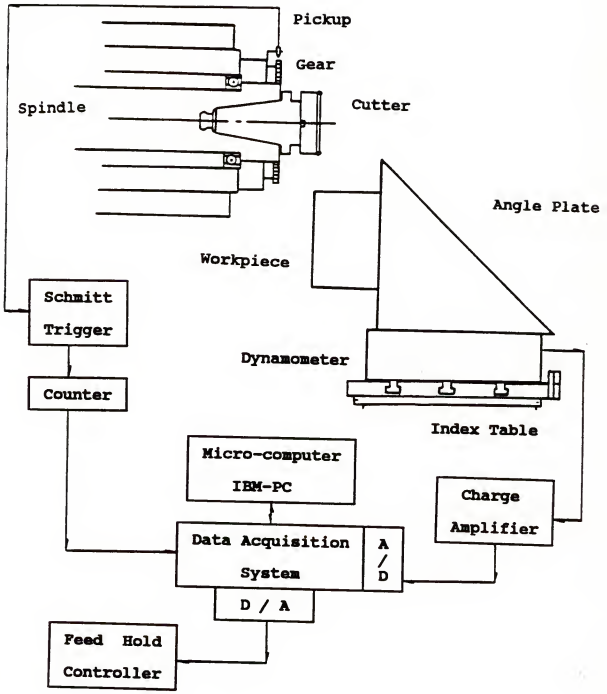


Figure 4.18 Process diagram for the experimental work

## 4.4 Experimental Verification

Using the experimental set-up described in Section 4.3, a series of cutting tests was carried out. They correspond to the simulation results shown in Sections 4.1 and 4.2.

Figure 4.19 shows a 1/2 immersion up milling case. The cutting parameters are the same as listed in Table 4.1. A insert with a broken cutting edge was used to obtain the tool breakage signal in the whole cycle of cutting tests. The first row displays the instantaneous cutting force signal in the whole cycle. The average force signal is displayed in the second row and the difference of the average force signal, in the third row. A clear distinction is available between the undamaged and damaged cutters. In the transient states, the staircase shape of the simulation of the average force disappears. It is smoothed not only by the existence of run-out but also further by the characteristics of the transfer function of the dynamometer. Figure 4.20 is an expanded view of Figure 4.19 during the steady state portion of the cut. The first row displays the instantaneous cutting force signal. The second row displays the corresponding spectra of the cutting force signal. The third row displays the average force signal; the fourth row, the difference of the average force signal. The feature distinguishing tool breakage is clearly observed in the time domain and also in frequency

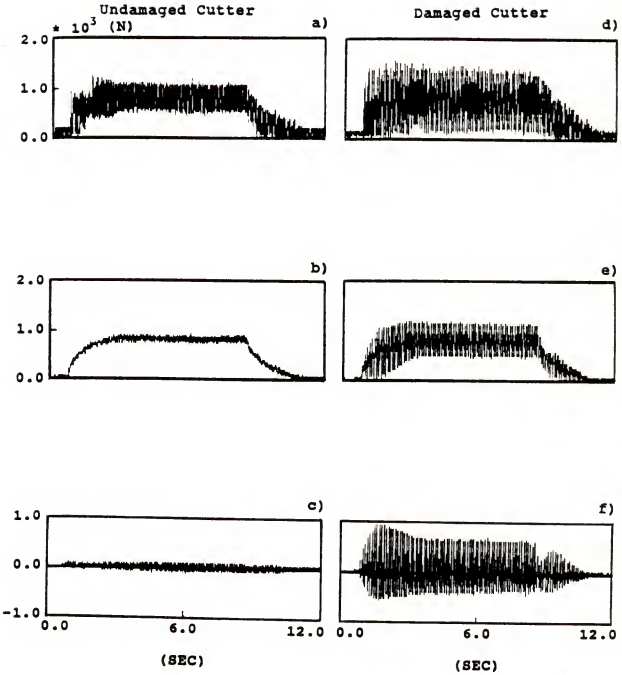


Figure 4.19 Instantaneous force, average force, and difference of the average force in the complete cutting cycle.

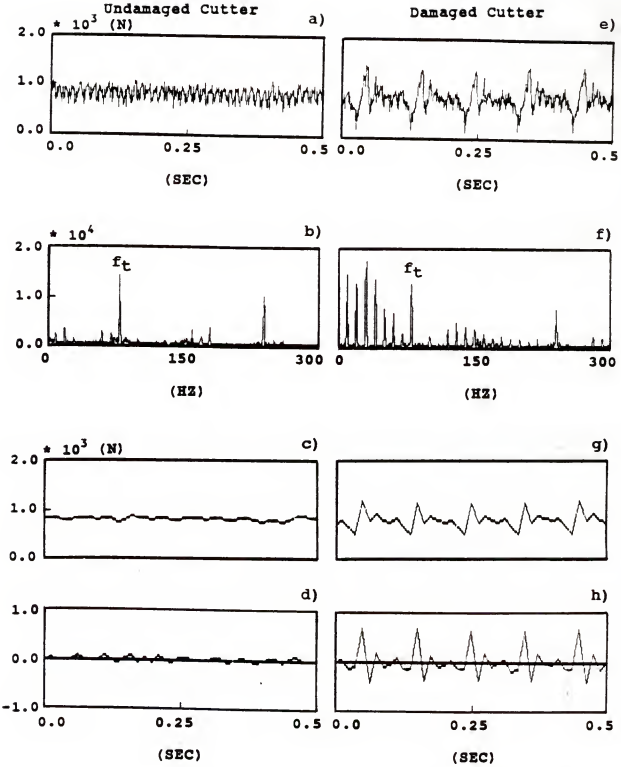


Figure 4.20 Instantaneous force and its spectrum, average force, difference of the average force in the steady state.

domain of the tool breakage zone. The average force and the difference of the average force signal for the 1/8, 1/4, 3/4 and 1/1 are also shown in Figure 4.21 and Figure 4.22.

By experiments, it is shown that applying the difference per tooth average method to process the milling force signal is a very efficient and reliable way for detection of tool breakage.

## 4.5 Limitations of the Cutting Force Signal for Tool Breakage Detection

Although the difference per tooth average method works well for the detection of tool breakage, measurement of the cutting force signal is difficult in milling. In the experimental set-up, an unsatisfactory transfer function between the measured force and the actual force is obtained, see Figure 4.16. Ideally, the magnitude of transfer function at all frequencies is equal to one. Obviously, the dynamometer distorts the cutting force signal, and does so even worse at high frequencies. It is seen that the dynamometer works well only under 100 Hz. This is because the dynamometer with the workpiece and with the angle plate acts as a system with several flexible vibratory modes.

In order to verify the distortion of the cutting force signal, two up milling cutting tests are shown in Figure 4.23. The cutting parameters are listed in Table 4.5.

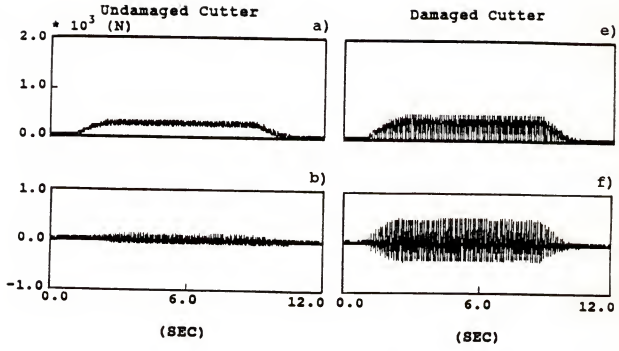


Figure 4.21.a) Average force and difference of the average force in the 1/8 immersion of cut

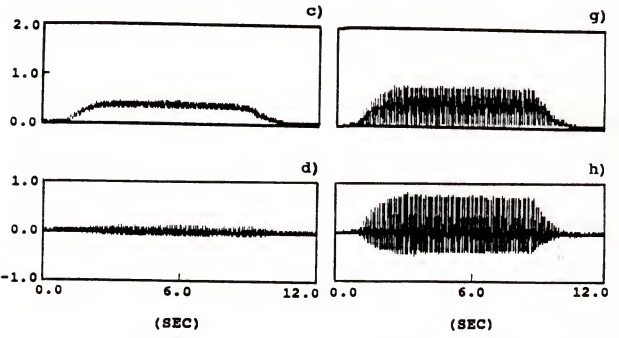


Figure 4.21.b) Average force and difference of the average force in the 1/4 immersion of cut

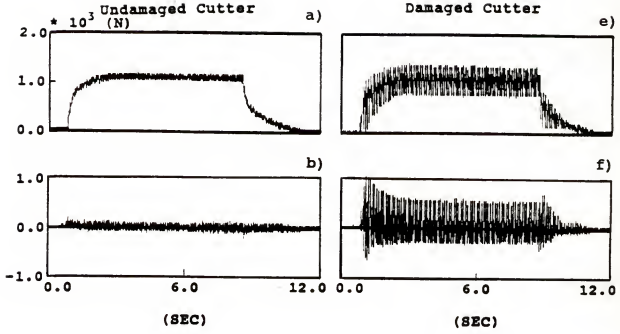


Figure 4.22.a) Average force and difference of the average force in the 3/4 immersion of cut.

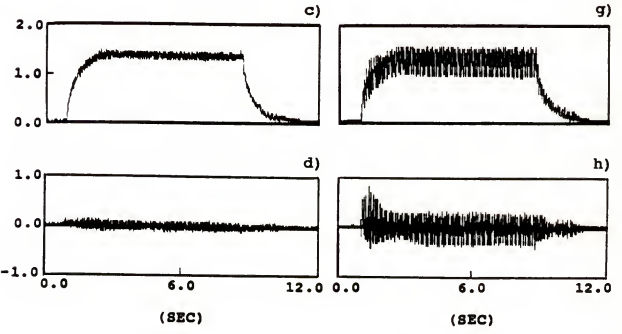


Figure 4.22.b) Average force and difference of the average force in the 1/1 immersion of cut.

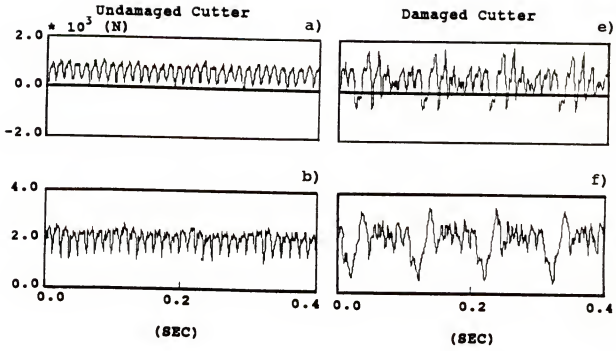


Figure 4.23.a) Cutting force signals in the Y and Z directions at spindle speed, n = 600 rpm.

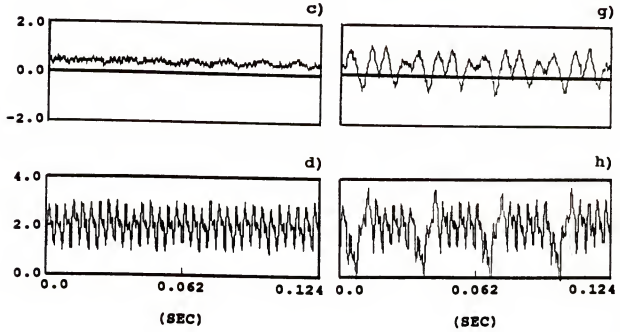


Figure 4.23.b) Cutting force signals in the Y and Z directions at spindle speed, n = 1935 rpm.

Table 4.5 Cutting parameters with different speeds to verify the dynamometer response

| No | spindle speed | depth of cut | feed per tooth | radial immersion | workpiece material |
|---|---|---|---|---|---|
| | rpm | mm | mm | | |
| 1 | 600 | 2.54 | 0.254 | 1/2 | cast iron |
| 2 | 1935 | " | " | " | " |

The first case shows the cutting test data in the steady state corresponding to the spindle speed n = 600 rpm, tooth frequency $f_t$ = 80 Hz. The first row displays the cutting force signal in the Y direction and the second row, in the Z direction. For the undamaged cutter, the periodic variation per tooth is shown in Figure 4.23.a and Figure 4.23.b. For the damaged cutter, the tool breakage variation per revolution is shown in Figure 4.23.e and Figure 4.23.f. It is shown that the response of the dynamometer is still acceptable at this tooth frequency.

Increasing the spindle speed, the second case shows the cutting test done at spindle speed n = 1935 rpm, tooth frequency $f_t$ = 258 Hz. It becomes very hard to identify the periodic variation in the Y direction for the undamaged cutter (see Figure 4.23.c). This is because the signal of the tooth frequency of 258 Hz is not passed by the low frequency response of dynamometer. Moreover, the tool breakage feature is also changed (see Figure 4.23.g).

Fortunately, the cutting force signal in the Z direction (see Figure 4.23.d and Figure 4.23.h) still truly illustrates the characteristic changes due to the tool breakage because of the better frequency response of the dynamometer in the Z direction. Since the cutting force signal is the basis of the detection algorithm, how the distorted cutting force signal affects the detection algorithm needs to be investigated.

Figure 4.24 shows the simulation of spectra of the resultant cutting force signal in the 1/8, 1/4, 1/2, and 1/1 immersions of cut during the steady state portion of the cut. For the undamaged cutter, these spectra are similar except that the variable component of the cutting force signal is zero in the 1/1 immersion case without run-out (see Figure 4.24.d). For the damaged cutter, the components in the tool breakage zone, located at less than $f_t$ and higher than the DC component, clearly stand out.

As mentioned in Section 4.2, sudden and large deviations in the difference of the average cutting force signal are attributed to the components in the tool breakage zone. For the damaged cutter in the 1/8 and 1/4 immersions, the frequency components inside the tool breakage zone spread about the point $f_t/2$ similar to a discrete normal distribution function. In fact, the total of eight components including the component of tooth frequency stands out because there are eight teeth on the cutter. With increasing the radial immersion, the peaks of

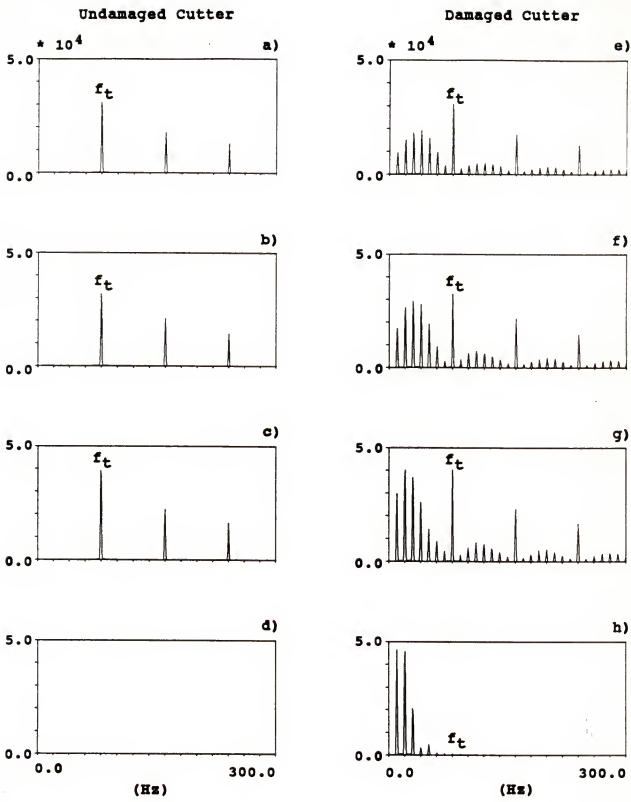


Figure 4.24 Spectra of simulation of the cutting force in the 1/8, 1/4, 1/2, and 1/1 immersions of cut.

the tool breakage components gradually shift close to $f_r$. For the 1/1 immersion case, only $f_t/8$, $2f_t/8$, and $3f_t/8$ components clearly stand out in the tool breakage zone due to the smoother variation of the tool breakage signal, see Figure 4.4.

In reality, a certain degree of magnitude change for each tool breakage component is due to the cutting force signal filtered through the unsatisfactory transfer function of dynamometer. Now the question is which components are more important in their contributions to the tool breakage feature, i.e. the large variation of the difference of average force. Figure 4.25.b and Figure 4.25.c show the peak to peak ratios of individual harmonic tool breakage component (see Fig 4.25.a), contributing to the average and the difference of the average forces. Multiplying the ratios as shown in Figure 4.25.c with the corresponding components in the tool breakage zone in Fig 4.24, it is seen that the tool breakage components of $f_t/8$, $2f_t/8$, $3f_t/8$, $4f_t/8$, and $5f_t/8$ are much more valuable in producing the difference of the average force.

To summarize, a reasonably undistorted frequency response of the cutting force signal up to half of the tooth frequency is necessary for successful detection of milling cutter breakage using the difference per tooth average method.

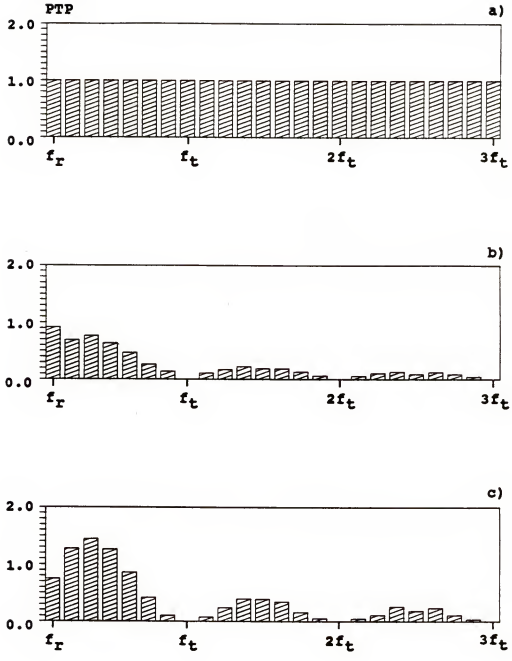


Figure 4.25 Peak to peak ratios for the different frequency components contributing to the tool breakage feature.
a) force ratios; b) average force ratios;
c) difference of the average force ratios.

In the high speed milling, high tooth frequencies are common. In [48], it has been shown that the optimal stable speed for a high metal remove rate is when the tooth frequency, $f_t$, is equal to the natural frequency, $f_n$. The natural frequency of the spindle for the most significant mode is usually in the range of 500 - 600 Hz. However, it is very difficult to achieve a reasonably flat response of a dynamometer with the experimental set-up at these frequencies or even half of them [30].

In addition to this, the dynamometer also inhibits a considerable portion of useful working space for milling operations, and its cost also makes it not suitable for every milling machine. Owing to these disadvantages, the use of an alternative signal instead of the cutting force signal should be explored.

# CHAPTER 5
# ANALYSIS AND DETECTION OF TOOL BREAKAGE USING VIBRATION SIGNALS

## 5.1 Reconstruction of the Cutting Force Signal by Using an Accelerometer

In Chapter 4, an efficient detection algorithm for tool breakage has been developed. However, the difficulties of using a dynamometer to measure the cutting force signal become a major obstacle for the practical use of this method. This is especially true for high speed milling where the tooth frequencies are the order of 600 Hz. Another way of obtaining the cutting force signal must be sought, so that the dynamometer might be excluded.

It was proposed to locate two accelerometers in the X and Y directions on the headstock of milling machine, since they are not expensive, readily available, and easy to use. Although the cutting force acting on the cutter will excite the vibration on the headstock, the accelerometer signal does not resemble the cutting force signal at all. The task becomes, then, how to reconstruct the cutting force signal from the accelerometer signal.

The characteristics of the accelerometer signal can be determined by the transfer function between the cutting force on the cutter and the vibrational acceleration on the headstock. The transfer function, $G(\omega)$ can be expressed as

$$G(\omega) = \frac{A(\omega)}{F(\omega)} \tag{5.1}$$

where

$A(\omega)$ - frequency response of the excited vibrational acceleration on the headstock

$F(\omega)$ - frequency response of the impulse force on the cutter

Considering the system to be linear, the transfer function may be mathematically defined as a unique transformation which maps the input of cutting force, f(n) into the output of vibrational acceleration, a(n) in the discrete time domain. This is denoted as

$$a(n) = G[f(n)] \tag{5.2}$$

and is also expressed as

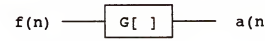


In other words, the input signal, f(n) has been filtered by a linear system that results in the distorted signal, a(n). Now the problem is to recover the original force signal, f(n) by the transfer function, G[ ] and the vibrational acceleration, a(n). This technique is generally referred to as the inverse filtering method.

5.1.1 Inverse Filtering Method

Using Equation (5.1), the cutting force in the frequency domain can be determined by

$$F(\omega) = G^{-1}(\omega) * A(\omega)$$
$$= H(\omega) * A(\omega) \quad (5.3)$$

where

$H(\omega)$ - frequency impulse response for the inverse filter

Then, the cutting force signal, f(n), in the time domain can be calculated by taking the inverse Fourier transform of $F(\omega)$. That is

$$f(n) = F^{-1}[H(\omega) * A(\omega)]$$
$$= h(n) \ (*) \ a(n) \quad (5.4)$$

where

(*) - notation of convolution

h(n) - impulse response of the inverse filter in the discrete time domain

In digital signal processing, h(n) has a finite length of data, but a(n) has an extremely large amount of data obtained by a data acquisition system. A partitioning technique is required to convolve this kind of data since the cutting force signal, f(n), should be obtained in real-time for the purpose of tool breakage detection. With the development of the Fast Fourier Transform (FFT), two partitioning techniques could be applied to solve this

problem. They are the over-and-add and over-and-save methods [49].

Although this method could be implemented in real-time, a certain time delay still exists in waiting for each section of the finite length of data input. In addition to this, nonlinearities in the spindle bearings [50] and the spindle motion of the Z direction affect the characteristics of the transfer function. Adaptivity for the identification of the transfer function during the cutting operations may be required, and therefore this is not a straightforward way to recover the cutting force signal.

### 5.1.2 Analog Computer Method

Another way to reconstruct the cutting force can be realized directly in the time domain using an analog computer method instead of the inverse filtering method. It is assumed that the transfer function between the cutting force and the vibrational acceleration is due to a prominent single degree of freedom system with mass M, damping C, and stiffness K. The reconstruction of the cutting force signal is simply to do the integration of the vibrational acceleration and velocity signals. That is

$$\dot{x} = \dot{x} + \ddot{x} * \Delta t \tag{5.5}$$

$$x = x + \dot{x} * \Delta t \tag{5.6}$$

$$M * \ddot{x} + C * \dot{x} + K * x = F \tag{5.7}$$

where

$\ddot{x}$ - vibrational acceleration signal

$\dot{x}$ - vibrational velocity signal

x - vibrational displacement signal

In reality, the integration must be made as a low-pass filter to avoid the DC component built up. This means that only the AC component of the cutting force signal could be recovered. Furthermore, an inevitable phase distortion is introduced in both the digital and analog integrations. This may lead to considerable errors in the reconstruction of the cutting force. Actually the transfer function of the spindle contains several degrees of freedom, therefore how closely the actual transfer function can be replaced by a prominent single degree of freedom for the successful tool breakage detection needs to be further considered.

In the foregoing discussion, reconstruction of the cutting force signal from the accelerometer signal on the headstock meets considerable practical difficulties. A more promising way using vibration signals to detect tool breakage without the need to reconstruct the cutting force signal has been studied.

## 5.2 Analysis of Characteristic Changes in Vibration Signals Due to Tool Breakage

It has been shown that the cutting force signal offers a very good feature for detecting milling cutter breakage. Unfortunately, practical difficulties in obtaining the

undistorted cutting force signal limit its applications. Therefore, it is worthwhile to search for another signal with a tool breakage feature as good as the cutting force signal.

In this section, the use of vibration signals for finding tool breakage features is explored. Two suitable signals, vibrational acceleration on the headstock and vibrational displacement of the spindle, have been investigated. Both of them are easy to obtain in milling machines.

Theoretically, it is assumed here that the transfer function between the cutting force on the cutter and the vibration on the headstock or the vibration of the spindle is linear and has a single degree of freedom with mass M = 1 kg, damping ratio $\zeta$ = 0.04, natural frequency $f_n$ = 600 Hz, see Figure 5.1. In the next section, a more complicated transfer function with several degrees of freedom will be discussed.

In this simplified spindle system with a single degree of freedom, the vibrational acceleration, $\ddot{x}$ and displacement, x may be expressed as

$$\ddot{x} = ( F - C * \dot{x} - K * x ) / M \qquad (5.8)$$

$$\dot{x} = \dot{x} + \ddot{x} * \Delta t \qquad (5.9)$$

$$x = x + \dot{x} * \Delta t \qquad (5.10)$$

In order to understand the influence of the tooth frequency on the vibration signals with a broken tooth, a sequence of spindle speeds, 225, 900, 2250, 4500 rpm with

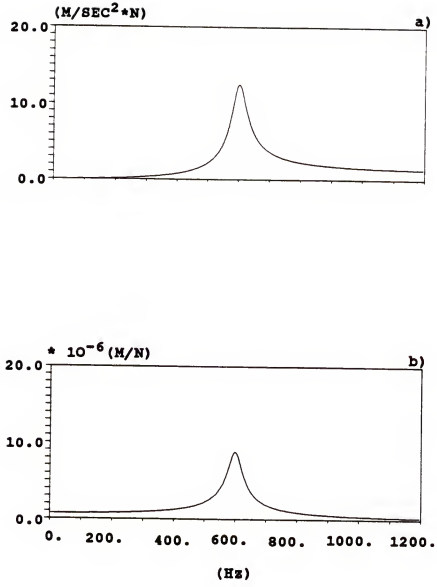


Figure 5.1 Simulation of the transfer function between the force and the vibrations.
a) acceleration over force;
b) displacement over force.

1/2 immersion in the steady state milling has been chosen for investigation. This corresponds to a sequence of ratios of the natural frequencies, $f_n/20$, $f_n/5$, $f_n/2$, $f_n$, see Figure 5.2 and Figure 5.3. The first row displays the force signal, the second row the acceleration signal, and the third row, the displacement signal.

For the case of the tooth frequency far away from the natural frequency, both the acceleration and displacement signals have distinct features available for the detection of a broken tooth (see Figure 5.2.a). It is seen that the force signal is proportionately reproduced by the displacement signal. On the other hand, the acceleration signal produces AC bursts of the natural frequency component excited by the each tooth and loses the DC component. As a result, increasing the tooth frequency close to the natural frequency, the acceleration signal dissipates the characteristic changes due to the broken tooth. In contrast, the displacement signal still retains the characteristic changes (see Figure 5.3.b).

For 1/1 immersion milling, the cases of $f_t$ equal to $f_n/20$ and $f_n$ are shown in Figure 5.4. It is shown that the magnitude of the acceleration signal decays quickly in the steady state in comparison with the 1/2 immersion case. In other words, the magnitude of the acceleration signal attenuates dramatically from the transient states to the steady state in the 1/1 immersion of cut. This is because the acceleration signal cannot pass low frequency

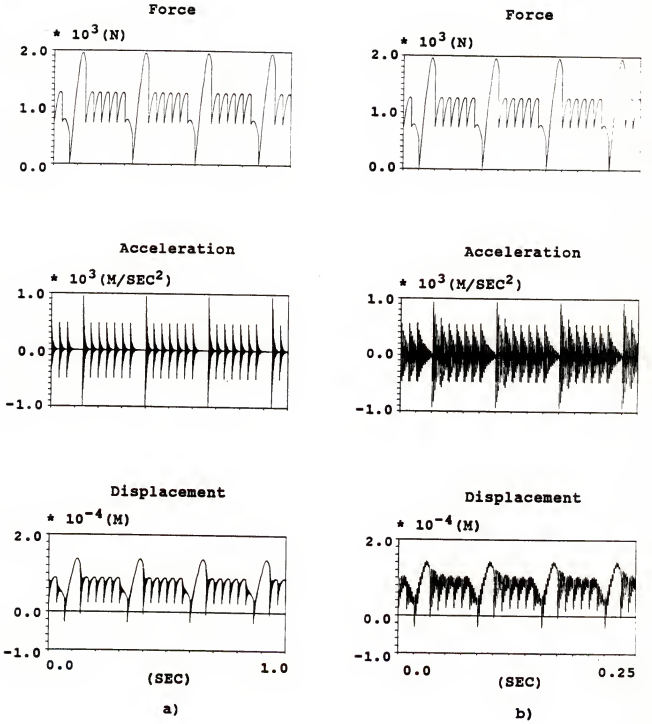


Figure 5.2 Simulation of the force, acceleration, and displacement signals in a 1/2 immersion of cut with different ratios of $f_t/f_n$.
a) $f_t/f_n = 1/20$; b) $f_t/f_n = 1/5$.

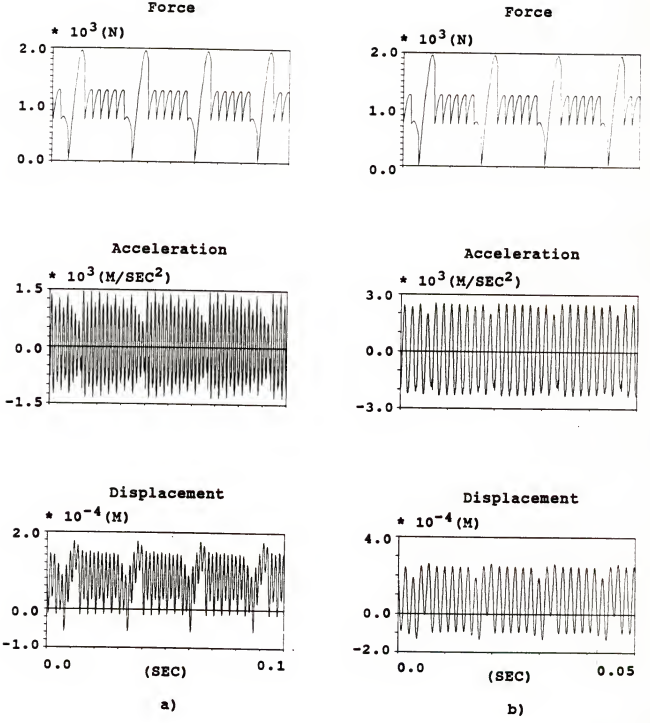


Figure 5.3 Simulation of the force, acceleration, and displacement signals in a 1/2 immersion of cut with different ratios of $f_t/f_n$.
a) $f_t/f_n = 1/2$; b) $f_t/f_n = 1/1$.

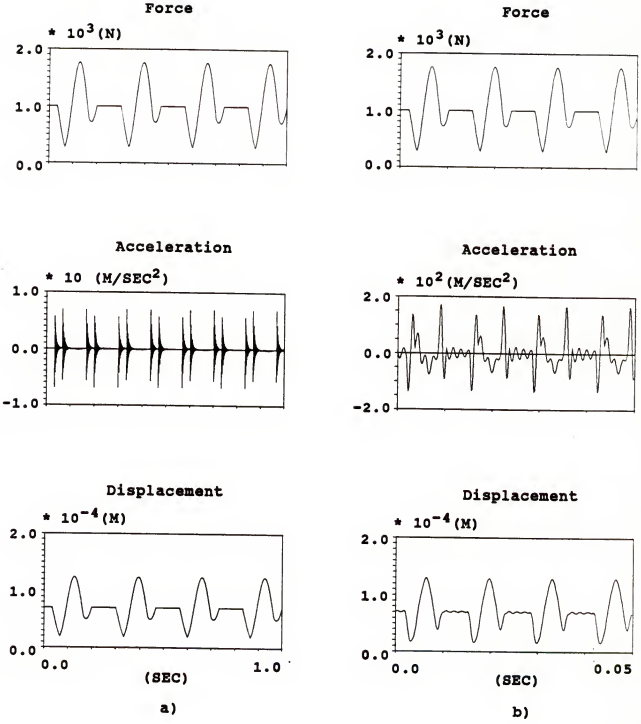


Figure 5.4 Simulation of the force, acceleration, and displacement signals in a 1/1 immersion of cut with different ratios of $f_t/f_n$.
a) $f_t/f_n = 1/20$; b) $f_t/f_n = 1/1$.

components from the force signal in the steady state, see Figure 5.1. This makes the detection of tool breakage using the acceleration signal more difficult. However, this problem does not exist in the displacement signal.

In conclusion, the displacement signal is more useful for the purpose of tool breakage detection. This is because the distinct tool breakage feature is available in the displacement signal at the range of the tooth frequency below or equal to the natural frequency of the spindle.

## 5.3 Detection of Tool Breakage Using Displacement Signal

Although the displacement signal has distinct tool breakage features, it is still difficult to detect tool breakage using the displacement signal directly. This is because not only cut geometry and run-out change the displacement, but also different tooth frequencies corresponding to the transfer function result in different magnification ratios for the displacement signal. Therefore, similar to the cutting force signal, it is necessary to develop a detection algorithm in order to extract the tool breakage feature from the displacement signal.

Again, spectrum analysis is used to understand the tool breakage feature in the displacement signal. Figure 5.5 and Figure 5.6 show the spectra of the simulation data in Figure 5.2 and Figure 5.3. The first row displays the

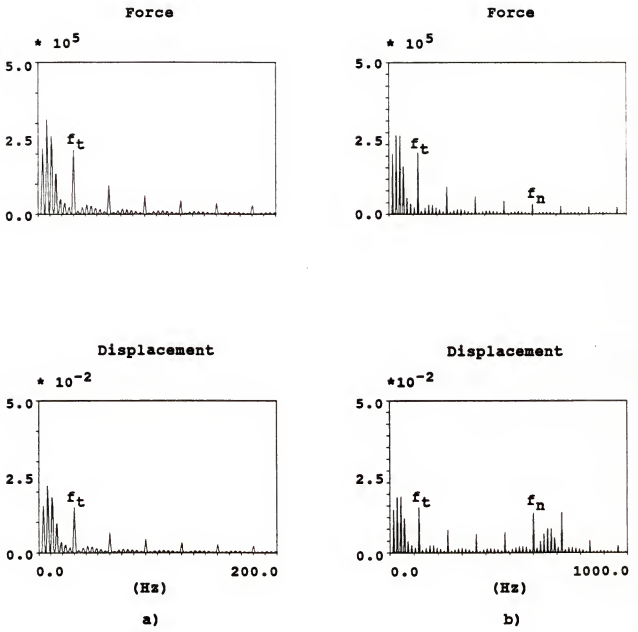


Figure 5.5 Spectra of the simulation of force and displacement in the 1/2 immersion of cut with different ratios of $f_t/f_n$.
a) $f_t/f_n = 1/20$; b) $f_t/f_n = 1/5$.

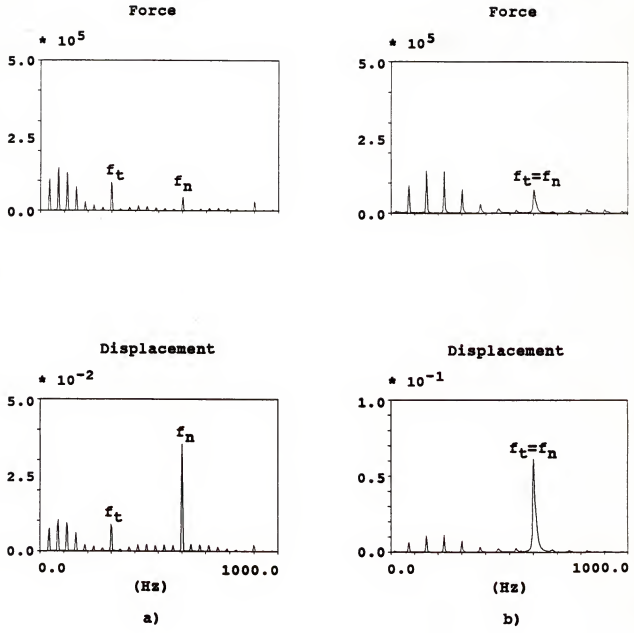


Figure 5.6 Spectra of the simulation of force and displacement in the 1/2 immersion of cut with different ratios of $f_t/f_n$.
a) $f_t/f_n = 1/2$; b) $f_t/f_n = 1/1$.

force spectrum and the second row displays the displacement spectrum. It is seen that the tooth frequency component in the displacement spectrum is equal to the magnification ratio of the transfer function multiplying the corresponding force spectrum component. However, the components inside the tool breakage zone at frequencies less than $f_t$ in the force spectrum are reproduced in the displacement spectrum without regard to the changes of tooth frequency.

Therefore, it is clearly seen that simply applying the difference per tooth average method developed in Chapter 4 can extract the tool breakage feature in the displacement signal. Figure 5.7 and Figure 5.8 show simulation results of the average and the difference of the average displacement signals which correspond to the displacement signal in Figure 5.2 and Figure 5.3. A clear distinction between the undamaged and damaged cutters is observed and is also independent of the tooth frequency changes. Figure 5.9 shows the complete cutting cycle of the average and the difference of the average displacement signals for the tooth frequency equal to $f_n$. Again, the feature of tool breakage is very clear not only in the steady state but also in the transient states.

It was shown by simulation that the detection of tool breakage by means of the displacement signal of the spindle in the single degree of freedom model is very successful. In reality, however, the spindle system may contain several

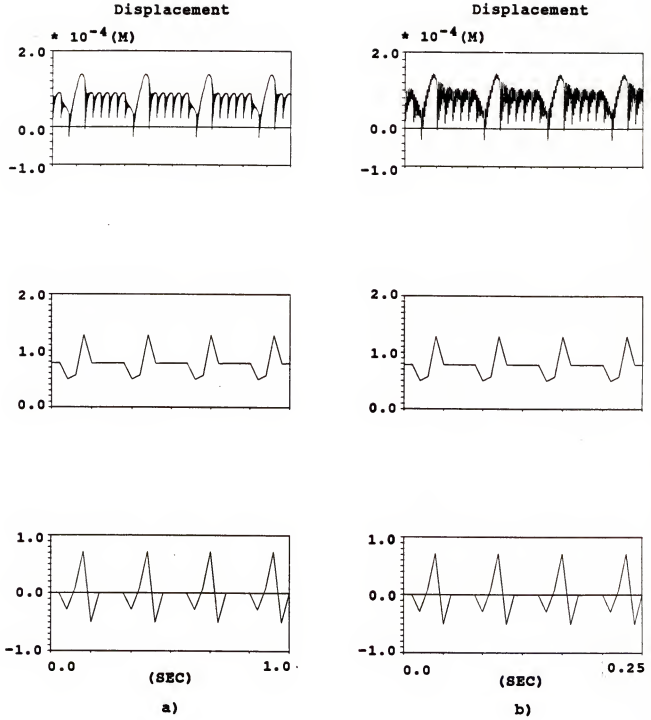


Figure 5.7 Simulation of the displacement, average displacement, and difference of the average displacement signals with different ratios of $f_t/f_n$. a) $f_t/f_n = 1/20$; b) $f_t/f_n = 1/5$.

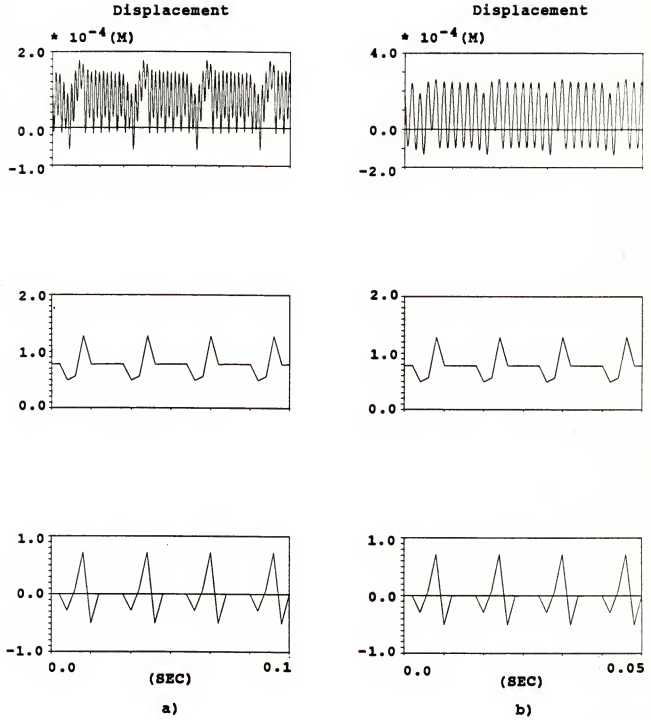


Figure 5.8 Simulation of the displacement, average displacement, and difference of the average displacement signals with different ratios of $f_t/f_n$. a) $f_t/f_n = 1/2$; b) $f_t/f_n = 1/1$.

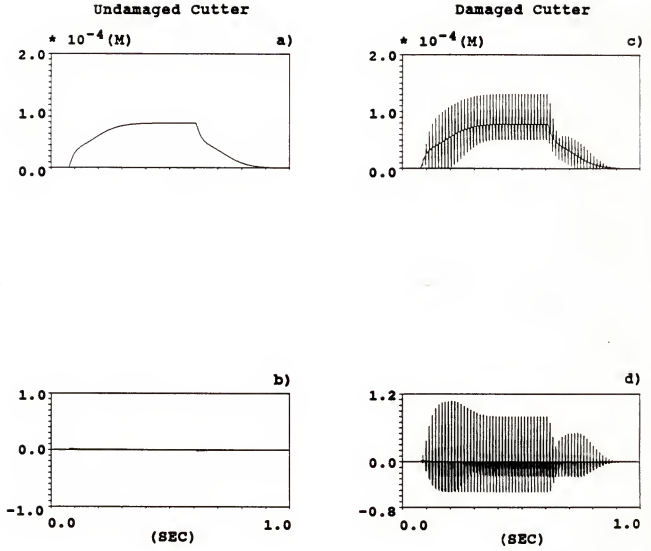


Figure 5.9 Simulation of the average displacement and difference of the average displacement signals in the complete cutting cycle with the ratio of $f_t/f_n$ = 1/1.

degrees of freedom. Figure 5.10 shows an example of a transfer function of the spindle is shown in Fig 5.10.a. Figure 5.10.b shows a "curve fitted" transfer function used to obtain the modal parameters of the spindle system. The identified modal parameters of this transfer function are listed in Table 5.1.

Table 5.1 Modal parameters for the transfer function of the spindle

| mode no | mass (kg) | damping ratio | natural frequency (Hz) |
|---|---|---|---|
| 1 | 680.0 | 0.047 | 274 |
| 2 | 90.9 | 0.140 | 396 |
| 3 | 80.3 | 0.027 | 474 |
| 4 | 260.6 | 0.037 | 633 |
| 5 | 40.5 | 0.028 | 855 |

In order to investigate the detection algorithm applied to this spindle system, Figure 5.11 shows the two simulation results in up milling. One is at the low spindle speed n = 480 rpm, tooth frequency $f_t$ = 64 Hz; the other is at the high spindle speed, n = 3555 rpm, tooth frequency, $f_t$ = 474. The tooth frequency of the second case is exactly equal to the natural frequency of the most dominant mode. The cutting parameters are listed in Table 5.2. In the first case, the average displacement signal is

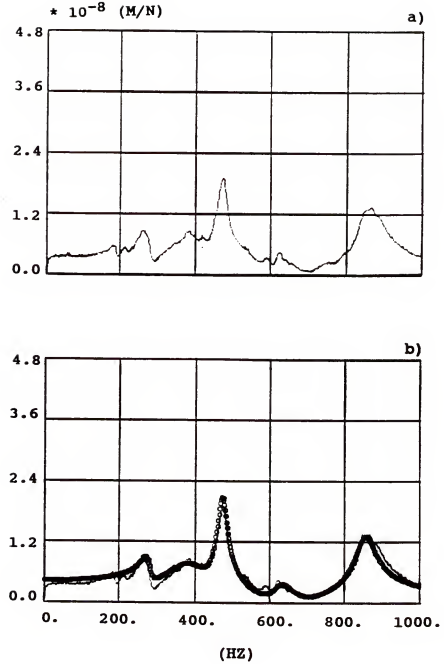


Figure 5.10 Spindle system with multiple degrees of freedom. a) transfer function between the force and displacement; b) curve fitted transfer function.

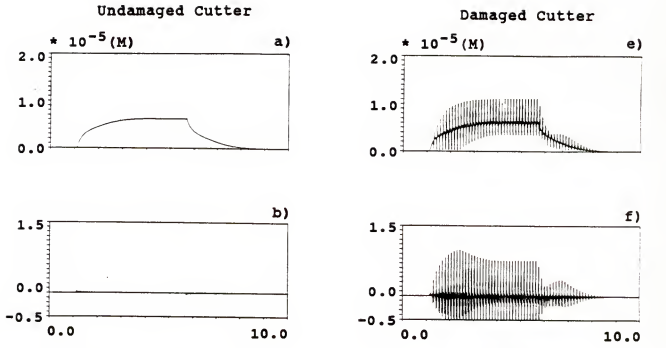


Figure 5.11.a) Simulation of the average displacement and difference of the average displacement signals at spindle speed, n = 480 rpm.

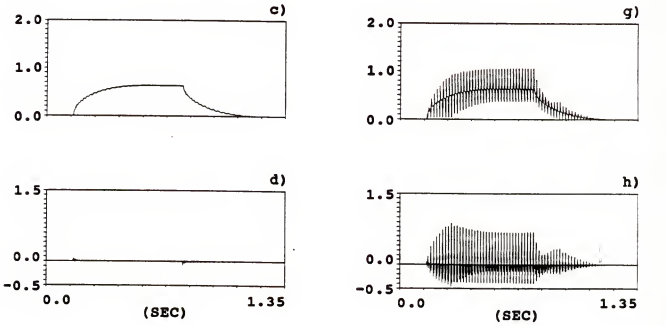


Figure 5.11.b) Simulation of the average displacement and difference of the average displacement signals at spindle speed, n = 3555 rpm.

shown in the first row. The corresponding difference of the average displacement is shown in the second row. The clear distinction between the undamaged and damaged cutters is shown. As to the second case, the average and difference of the average displacement signals are shown in the third and fourth rows respectively. The distinct tool breakage feature, independent of the tooth frequency changes, is still available in the damaged cutter signal. This tells us that the detection algorithm can also be applied to the spindle system with several degrees of freedom.

Table 5.2 Cutting parameters in the simulation of the cutting tests using a spindle system with multiple degrees of freedom

| No | spindle speed | depth of cut | feed per tooth | radial immersion | workpiece material |
|---|---|---|---|---|---|
| | rpm | mm | mm | | |
| 1 | 480 | 2.54 | 0.254 | 1/2 | cast iron |
| 2 | 3555 | " | " | " | " |

To summarize, processing of the displacement signal, through simulation, has been proven to be feasible for tool breakage detection. In addition to this, it was shown that a single degree of freedom model is enough to illustrate and represent the tool breakage feature in the real spindle system with multiple degrees of freedom. Thus, an experimental verification is necessary.

## 5.4 Experimental Set-up

The description of the machining center and the data recording system was given in Section 4.3. For the face milling, the ZN3M Carbaloy milling cutter was still used with three kinds of inserts, depending on the workpiece material and axial depth of cut. The catalog numbers of the inserts are SNG634 (silicon nitride), SNG632 (silicon nitride), and SNE633 (carbide). The run-out on the face milling cutter was adjusted within 0.0254 mm (0.001"). For the end milling, 19.05 mm (0.75") diameter carbide end mill cutters (Robb Jack Co.) with 2, 3, and 4 flutes of 30° helix angle was used. In addition to this, three kinds of workpiece material, GM-241 cast iron, aluminum 7075-T7351, and steel 4330 were available for cutting tests.

The displacement signal was obtained by a multi-channel non-contact measurement device, Accumeasure system 1000 (MTI Co.). This system determines the capacitance between a capacitance probe with a sensing electrode and a ground target. Then, the capacitance is transmitted to a probe amplifier module (AS-1023PA) with a -3 dB corner frequency at 5 KHz. An analog signal proportional to the probe-to-target gap is generated in the circuit when a resultant variable capacitance appears.

Two capacitance probes were located in the X and Y directions between the housing and spindle, close to its flanges (see Figure 5.12). In the design of the lubrication

system for the front bearings of the spindle, an automatic mist oil spray system is provided in the machining center. However, the lubrication oil flows through the gap between the probe and the spindle when the spindle rotates. This may cause a slight measurement error in the displacement signal.

By experiments, some high frequency components were generated in the displacement signal, especially at high spindle speeds close to the natural frequency of the spindle. The sampling frequency controlled by the external clock might be lower than twice these high frequency contents in the displacement signal. This leads to the phenomenon of signal aliasing which shifts the high frequency components into the low frequency domain, such as the tool breakage zone, after the signal is digitized. Therefore, an anti-aliasing low-pass filter is necessary for high spindle speeds. In these experiments, a 2nd order Butterworth analog low-pass filter was designed to reduce the aliasing error. Its cutoff frequency is at 1 KHz. The circuit diagram is shown in Figure 5.13. Figure 5.14 is a schematic of the experimental set-up for the displacement measurements.

The spindle run-out was not taken into account in Section 5.3 for the simulation of the average displacement signal. In fact, a strong periodic displacement signal per revolution is generated when the spindle is free run. Therefore, the difference per tooth average method as

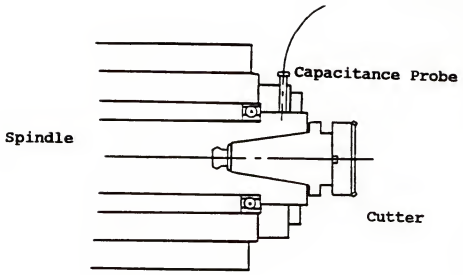


Figure 5.12 Capacitance probe mounting.

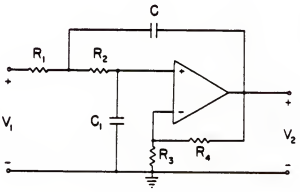


Figure 5.13 Electrical circuit diagram for an anti-aliasing filter.

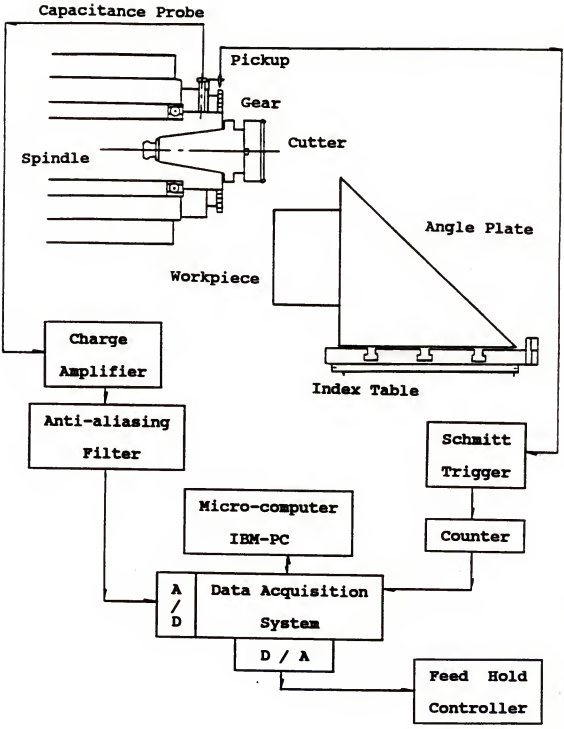


Figure 5.14 Process diagram for the experimental work.

applied to the displacement signal needs a little modification.

Assuming that the vibrational response of the spindle is a linear system, the actual average displacement per tooth can be calculated by subtracting the run-out pattern before cutting from the measured average displacement per tooth. That is

$$D_{xavg}(j) = \frac{\sum_{i=1}^{n} D_x(i)}{n} - D_{xr}(j) \qquad (5.11)$$

$$D_{yavg}(j) = \frac{\sum_{i=1}^{n} D_y(i)}{n} - D_{yr}(j) \qquad (5.12)$$

where

$D_{xavg}$ - actual average displacement in the X direction

$D_{yavg}$ - actual average displacement in the Y direction

$D_x$ - displacement in the X direction

$D_y$ - displacement in the Y direction

$D_{xr}$ - average run-out displacement pattern in the X direction when the spindle is free run

$D_{yr}$ - average run-out displacement pattern in the Y direction when the spindle is free run

$j$ - index for time increment per tooth period

$n$ - number of samples per tooth period

The average resultant displacement per tooth, $D_{avg}$ can be calculated as

$$D_{avg}(j) = (D_{xavg}^2(j) + D_{yavg}^2(j))^{1/2} \qquad (5.13)$$

Then, the difference of the average displacement per tooth, $\Delta D_{avg}$ is given by

$$\Delta D_{avg}(j) = D_{avg}(j) - D_{avg}(j-1) \qquad (5.14)$$

## 5.5 Experimental Verification

Figure 5.15 shows the raw displacement signal in up milling with the spindle run-out. The first row displays the displacement signals in the X direction and the second row, in the Y direction. The cutting parameters are listed in Table 5.3. It is not easy to identify which column corresponds to the damaged cutter and which tooth was broken due to the strong component of the spindle run-out. However, applying the difference per tooth average method to the raw data, the average and the difference of the average displacement signals are shown in Figure 5.16. A clear distinction is available between the undamaged and damaged cutters. The expanded views for the entry and steady states are shown in Figure 5.17.

Table 5.3 Cutting parameters in the detection of tool breakage using displacement signal

| spindle speed | depth of cut | feed per tooth | radial immersion | workpiece material |
|---|---|---|---|---|
| rpm | mm | mm | | |
| 600 | 2.54 | 0.254 | 1/2 | cast iron |

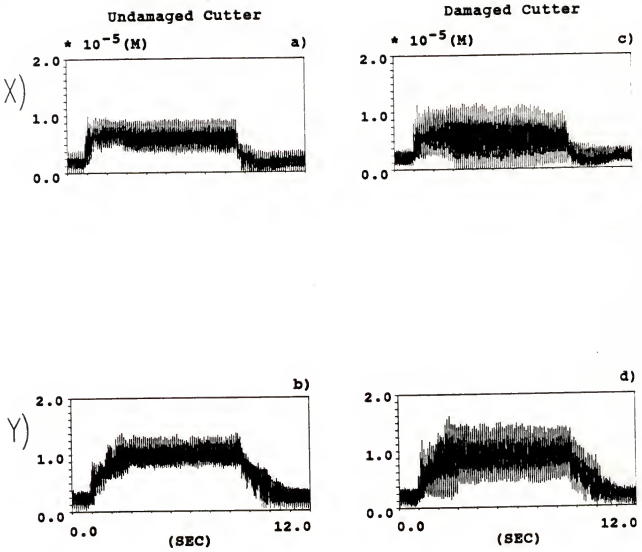


Figure 5.15 Raw displacement signals in the X and Y directions.

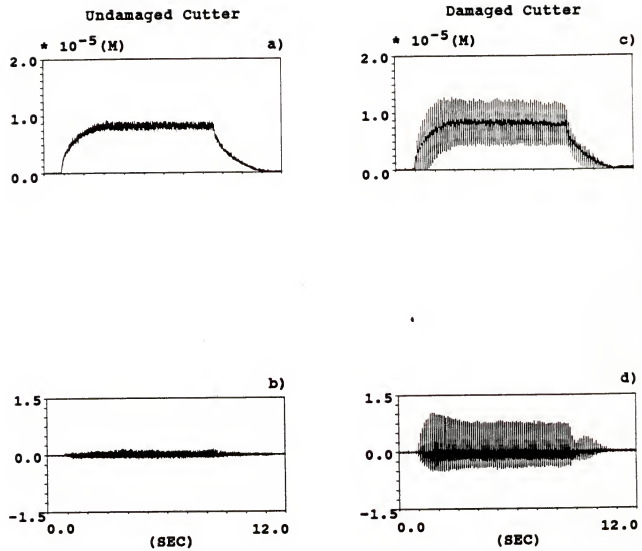


Figure 5.16 Average displacement and difference of the average displacement signals in the complete cutting cycle.

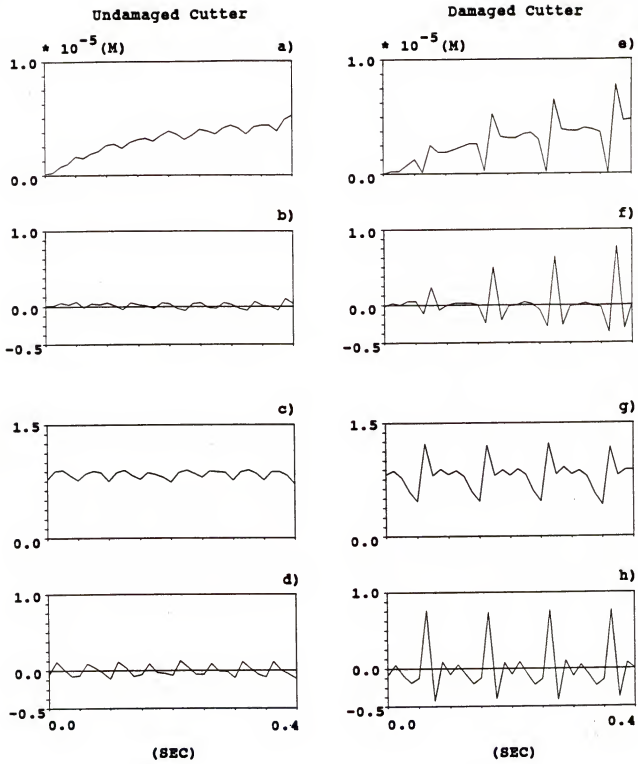


Figure 5.17 Average displacement and difference of the average displacement signals in the entry and steady states.

Figure 5.18 shows an experimental result of three consecutive tool breakages during milling of the steel workpiece. The cutting parameters are listed in Table 5.4. This is a very good example of how important it is to detect tool breakage immediately.

The first chipped tooth suddenly happened at 1.02 sec, then the next one, at 2.48 sec, and finally the third one, at 3.98 sec. If this damaged cutter was still in use, a catastrophic tool failure would occur very soon. It is shown that the difference of the average displacement signal clearly indicates where tool breakage occurs. Once the first chipped tooth is detected, the damage spreading to the other teeth could be prevented.

Table 5.4 Cutting parameters in up milling with three consecutive tool breakages

| spindle speed | depth of cut | feed per tooth | radial immersion | workpiece material |
|---|---|---|---|---|
| rpm | mm | mm | | |
| 600 | 2.54 | 0.381 | 1/2 | steel |

## 5.6 Comparison of Detection of Tool Breakage Using Displacement Signal and Force Signal

It seems that the average and the difference of the average displacement signals are very similar to those of force signals. Figure 5.19 shows the average and the

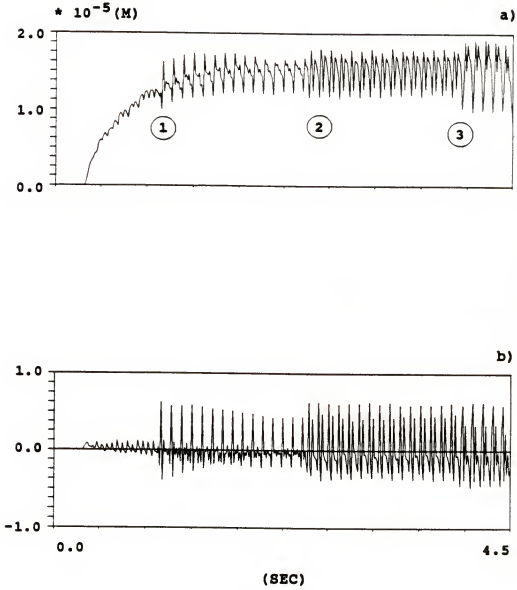


Figure 5.18 Average displacement and difference of the average displacement signals with three consecutive tool breakages.

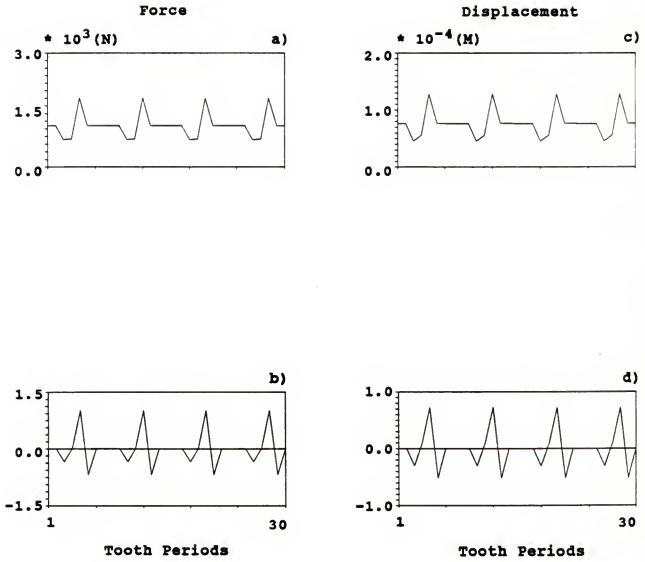


Figure 5.19 Simulation of the average and difference of the average force and displacement signals independent of the tooth frequency changes.

difference of the average force and displacement signals in Figure 5.2 and Figure 5.3. Although the instantaneous displacement signal changes depending on the ratio of $f_t/f_n$, it is shown that after averaging and differencing per tooth, the displacement signal is proportional to the force signal independent of the tooth frequency changes. According to the transfer function shown in Figure 5.1, the ratio between the average displacement and force is approximately equal to the DC component of the transfer function, 1/K, where K is the stiffness parameter.

$$K = M * (2\pi * f_n)^2$$
$$= 1 * (2\pi * 600)^2 = 1.421 * 10^7$$

Actually, the relationship between the average force and displacement may also be expressed using the equations developed in Chapter 3. For the face milling with run-out free cutter, the instantaneous forces in the X and Y directions may be expressed as

$$f_X = f_T * \cos\theta + f_R * \sin\theta$$
$$= k_s * a_a * f_t * (\sin\theta * \cos\theta + c * \sin^2\theta) \qquad (5.15)$$

and

$$f_Y = -f_T * \sin\theta + f_R * \cos\theta$$
$$= k_s * a_a * f_t * (-\sin^2\theta + c * \sin\theta * \cos\theta) \qquad (5.16)$$

where

$k_s$ - specific cutting force

$a_a$ - axial depth of cut

$f_t$ - feed per tooth

c - ratio of $f_T/f_R$, constant

The corresponding average forces in the X and Y directions are given by

$$F_{xavg} = \frac{m}{2\pi} \int_{\theta_e}^{\theta_s} k_s * a_a * f_t * (\sin\theta * \cos\theta + c * \sin^2\theta) d\theta \qquad (5.17)$$

$$F_{yavg} = \frac{m}{2\pi} \int_{\theta_e}^{\theta_s} k_s * a_a * f_t * (-\sin^2\theta + c * \sin\theta * \cos\theta) d\theta \qquad (5.18)$$

where

$m$ - number of the teeth on the cutter

$\theta_s$ - starting angle of cut

$\theta_e$ - exit angle of cut

Then, the resultant average force may be expressed in the form,

$$F_{avg} = (F_{xavg}^2 + F_{yavg}^2)^{1/2}$$

$$= \frac{m * k_s * a_a * f_t}{2\pi} F(\theta_s, \theta_e, c) \qquad (5.19)$$

$$= \frac{m * k_s * a_a * f_t}{2\pi} F(\phi_s, c) \qquad (5.20)$$

where

$F(\theta_s, \theta_e, c)$ - function of $\theta_s$, $\theta_e$, $c$

$F(\phi_s, c)$ - function of $\phi_s$, $c$

$\phi_s$ - swept angle of cut, i.e. $\theta_e - \theta_s$

Finally, the resultant average displacement may also be expressed in the form,

$$D_{avg} = \frac{m * k_s * a_a * f_t}{2\pi K} F(\phi_s, c) \qquad (5.21)$$

Figure 5.20 shows the experimental comparison between the average force and displacement signals in a sequence of

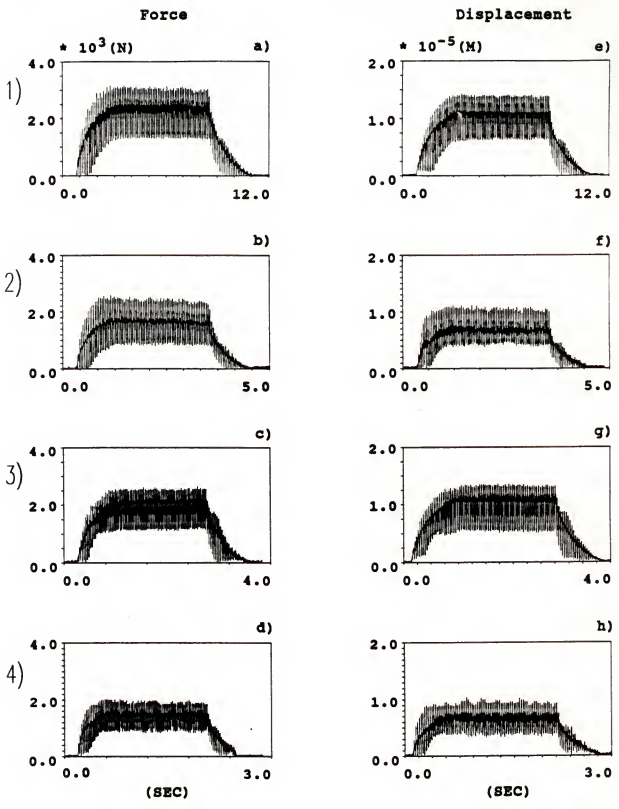


Figure 5.20 Average force and displacement signals obtained from different spindle speeds.

spindle speeds. The cutting parameters are listed in Table 5.5.

Table 5.5 Cutting parameters in up milling with force and displacement sensors active

| No | spindle speed | depth of cut | feed per tooth | radial immersion | workpiece material |
|---|---|---|---|---|---|
| | rpm | mm | mm | | |
| 1 | 600 | 2.54 | 0.254 | 1/2 | cast iron |
| 2 | 1500 | " | " | " | " |
| 3 | 1845 | " | " | " | " |
| 4 | 2250 | " | " | " | " |

Figure 5.21 shows the corresponding difference of the average force and displacement signals. It is shown that the average or the difference of the average displacement can be approximately treated as the average or the difference of the average force by multiplying a constant, K.

In the next chapter, numerous cutting test results will be presented to verify this detection algorithm under a variety of cutting conditions using the displacement signals.

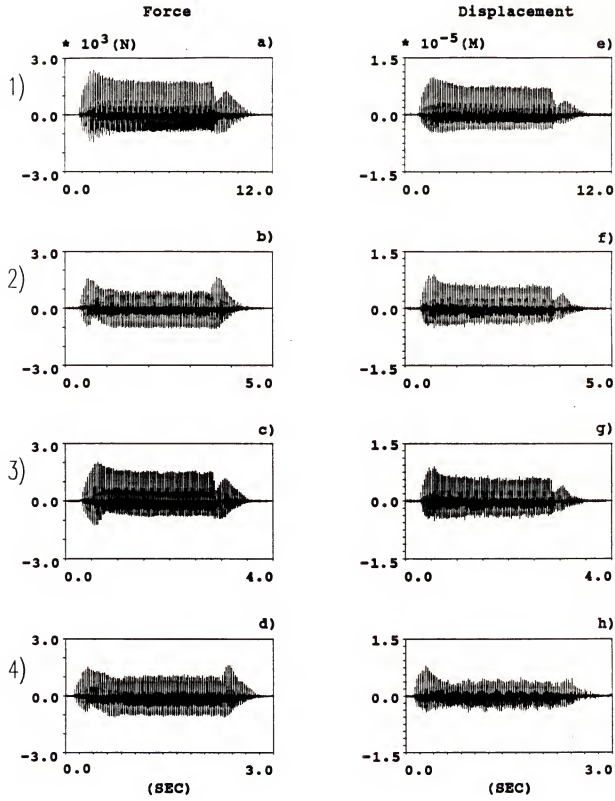


Figure 5.21 Difference of the average force and displacement signals obtained from different spindle speeds.

# CHAPTER 6
# DETECTION OF TOOL BREAKAGE USING DISPLACEMENT SIGNAL IN A VARIETY OF CUTTING CONDITIONS

The use of the difference per tooth average method to detect tool breakage in the displacement signal has been proven to be feasible. However, the applicability of this method needs to be verified to various cutting conditions. A lot of experimental results using different cutting parameters are shown in this chapter.

## 6.1 Spindle Speed

Figure 6.1 shows the transfer function between the force on the cutter and the displacement on the spindle in the Y and X directions in the experimental set-up as shown in Figure 5.12. There are several modes with resonant peaks in both directions. Within the range of interest, it contains two resonant peaks: at 262 Hz, 476 Hz in the Y direction and at 244 Hz, 450 Hz in the X direction. By experiments, the transfer function is changed little by the spindle motion of the Z axis.

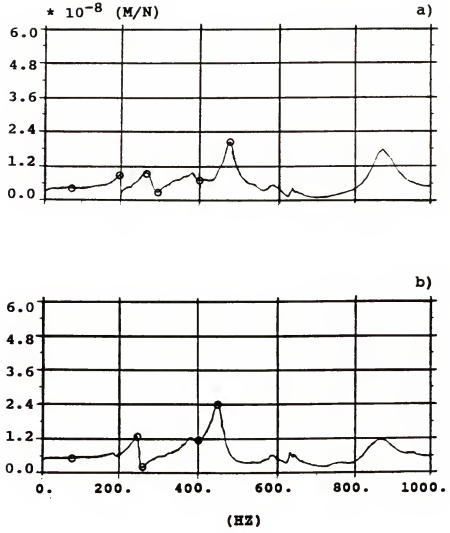


Figure 6.1 Transfer function between the force on the cutter and displacement of the spindle. a) Y direction; b) X direction.

Different spindle speeds have their tooth frequencies corresponding to the magnification ratios in Figure 6.1. In up milling of cast iron using the face milling cutter, the displacement signal in the Y direction is the major component in comparison to that in the X direction. Therefore, a sequence of cutting tests was done, and the locations of tooth frequencies corresponded to the marks in the transfer function of the Y direction. Figure 6.2 shows the average displacement signal, and the difference of the average displacement signal is shown in Figure 6.3. The cutting parameters are listed in Table 6.1.

Table 6.1 Cutting parameters in up milling with different spindle speeds

| No | spindle speed | depth of cut | feed per tooth | tooth frequency | radial immersion |
|---|---|---|---|---|---|
| | rpm | mm | mm | Hz | |
| 1 | 600 | 1.27 | 0.254 | 80 | 1/2 |
| 2 | 1425 | " | " | 190 | " |
| 3 | 1965 | " | " | 262 | " |
| 4 | 2160 | " | " | 290 | " |
| 5 | 3000 | " | " | 400 | " |
| 6 | 3570 | " | " | 476 | " |

In down milling, the displacement signal in the X direction is the major component. Therefore, another

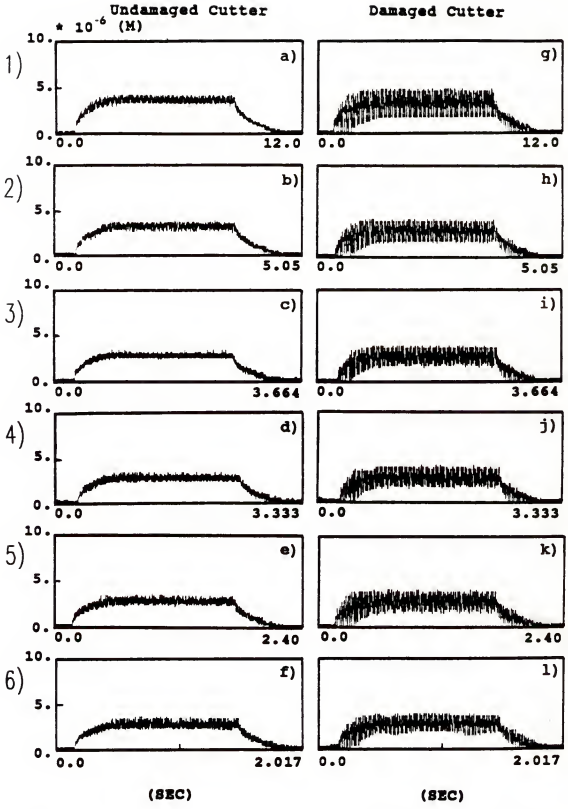


Figure 6.2 Average displacement signal in up milling with different spindle speeds.

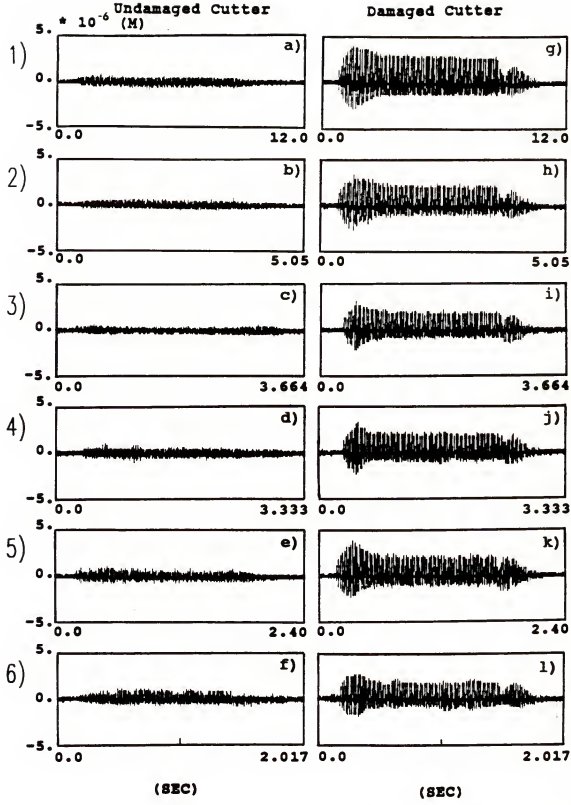


Figure 6.3 Difference of the average displacement signal in up milling with different spindle speeds.

sequence of cutting tests was done, see Figure 6.4 and Figure 6.5. The tooth frequencies correspond to the marks in the transfer function of the X direction. The cutting parameters are listed in Table 6.2.

Table 6.2 Cutting parameters in down milling with different spindle speeds.

| No | spindle speed | depth of cut | feed per tooth | tooth frequency | radial immersion |
|---|---|---|---|---|---|
| | rpm | mm | mm | Hz | |
| 1 | 600 | 1.27 | 0.254 | 80 | 1/2 |
| 2 | 1830 | " | " | 244 | " |
| 3 | 1920 | " | " | 256 | " |
| 4 | 3000 | " | " | 400 | " |
| 5 | 3375 | " | " | 450 | " |

It is seen that the displacement signal can detect tool breakage quite well, even at a tooth frequency equal to the most dominant resonant mode. As to the most dominant mode cases in up and down millings, the difference signal becomes a little bigger for the undamaged cutter due to the large vibration and high frequency noise (see Figure 6.2.f and Figure 6.4.e) Therefore, it may make the detection margin smaller between undamaged and damage cutters. However, experiments demonstrated that this could be further improved by using a high order anti-aliasing filter

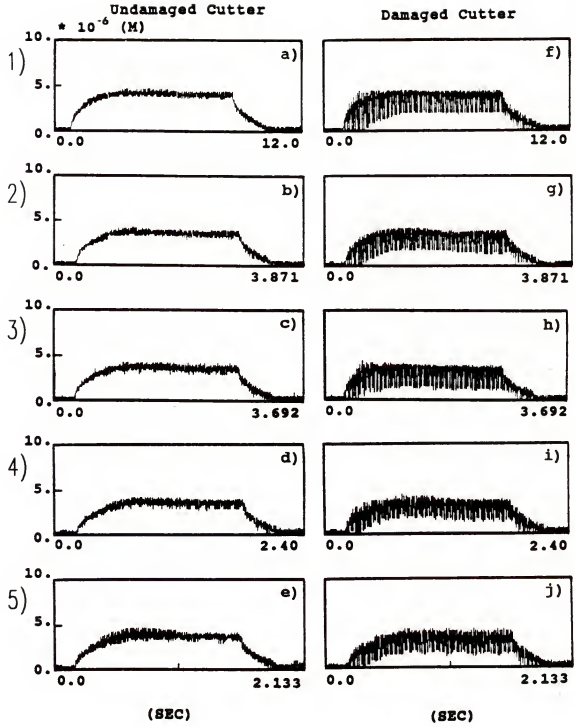


Figure 6.4 Average displacement signal in down milling with different spindle speeds.

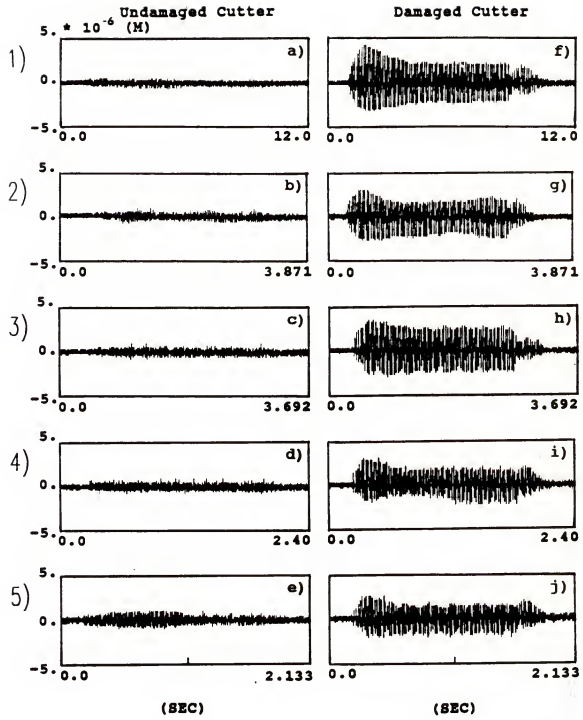


Figure 6.5 Difference of the average displacement signal in down milling with different spindle speeds.

so that the margin increases.

As a result, the tool breakage feature is almost independent of the change of spindle speeds as shown in the simulation results in Chapter 5. This is because the frequency response of the transfer function is reasonably flat up to half or over half of the dominant natural frequency (see the explanations in Sections 4.5 and 5.6).

## 6.2 Workpiece Material

In Equation (5.21), the average displacement signal is proportional to the cutting stiffness. Therefore, the different workpiece materials will have different levels of detection signal in the difference of the average displacement, even using the same other cutting parameters.

Figure 6.6 shows the average displacement signal obtained for three kinds of workpiece material in up milling. The cutting parameters are listed in Table 6.3. The first row displays the signal obtained from the steel workpiece. The second row displays the signal obtained from the cast iron workpiece and the third row, the aluminum workpiece. It is clearly shown that the order of cutting stiffness is steel, then cast iron, and then aluminum.

The corresponding difference of the average displacement signal is shown in Figure 6.7. This tells us that the tool breakage signal in the difference of the average displacement signal is proportional to the cutting

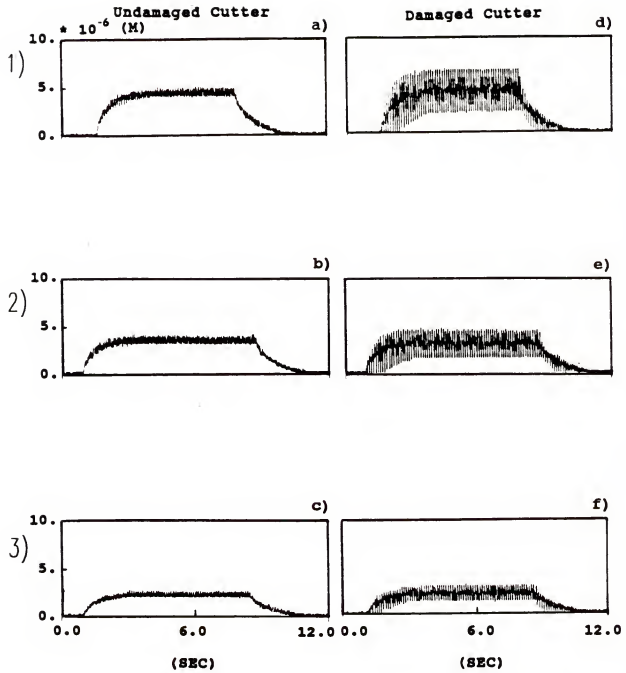


Figure 6.6 Average displacement signal obtained from the three kinds of workpiece material: steel, cast iron, aluminum.

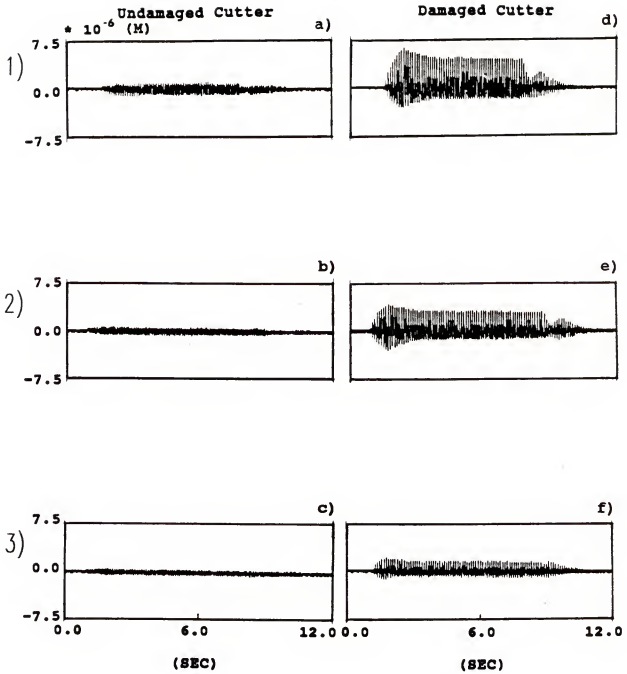


Figure 6.7 Difference of the average displacement signal obtained from the three kinds of workpiece material: steel, cast iron, aluminum.

stiffness of the workpiece material.

Table 6.3 Cutting parameters in the cutting tests using different workpiece materials

| No | spindle speed | depth of cut | feed per tooth | radial immersion | workpiece material |
|---|---|---|---|---|---|
| | rpm | mm | mm | | |
| 1 | 600 | 1.27 | 0.254 | 1/2 | steel |
| 2 | " | " | " | " | cast iron |
| 3 | " | " | " | " | aluminum |

## 6.3 Axial Depth of Cut

The changes of axial depth of cut (ADC) can be divided by two kinds: one is sudden change of ADC, and the other is gradual change of ADC. Figure 6.8 shows the geometries of sudden and gradual changes of ADC in the cutting tests. The cutting parameters are listed in Table 6.4. Figure 6.9 shows the average displacement signal, and Figure 6.10 shows the difference of the average displacement signal.

Except in the transient states, the changes of the average and the difference of the average signals are actually followed the changes in the axial depths of cut. This tells us that the tool breakage signal in the difference of the average displacement is proportional to the axial depth of cut.

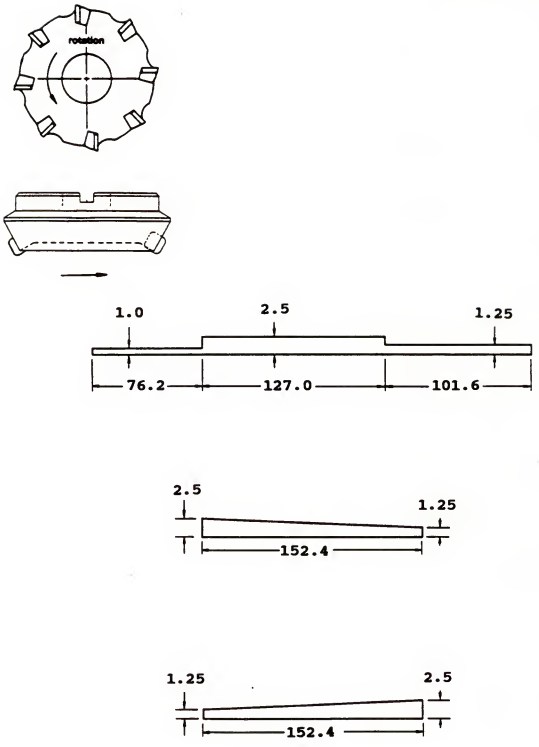


Figure 6.8 Cut geometry with the varying axial depths of cut.

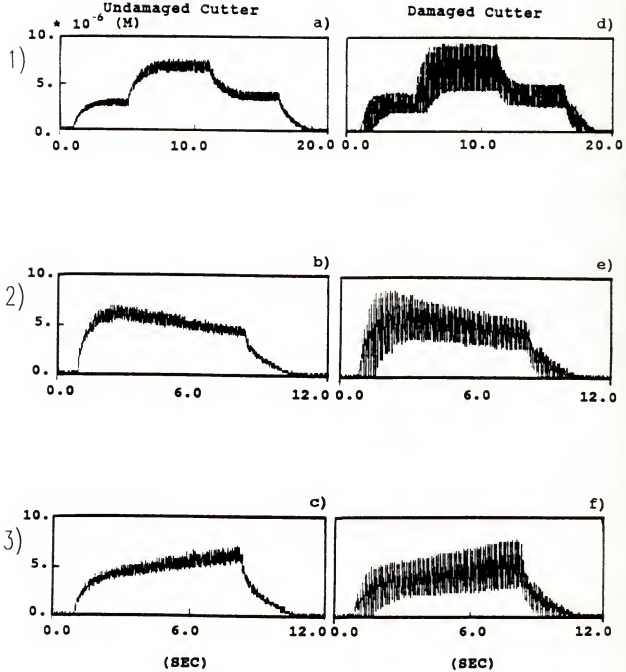


Figure 6.9 Average displacement signal with the changes of the axial depths of cut.

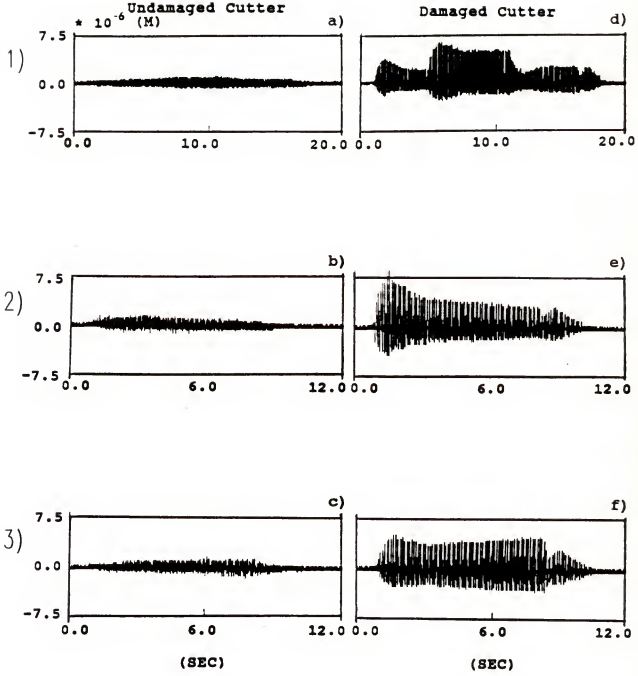


Figure 6.10 Difference of the average displacement signal with the changes of the axial depths of cut.

Table 6.4 Cutting parameters in the cutting tests with different axial depths of cut

| No | spindle speed | depth of cut | feed per tooth | radial immersion | workpiece material |
|---|---|---|---|---|---|
| | rpm | mm | mm | | |
| 1 | 600 | * | 0.254 | 1/2 | cast iron |
| 2 | " | * | " | " | " |
| 3 | " | * | " | " | " |

* see Figure 6.8

## 6.4 Feedrate

Feedrate is also a very important cutting parameter relating to tool life. Figure 6.11 shows the feedrate changes in the cutting tests. Figure 6.12 and Figure 6.13 show the average and the difference of the average signals in the varying feedrates. The cutting parameters are listed in Table 6.5.

Table 6.5 Cutting parameters in the cutting tests with different feedrates

| No | spindle speed | depth of cut | feed per tooth | radial immersion | workpiece material |
|---|---|---|---|---|---|
| | rpm | mm | mm | | |
| 1 | 600 | 1.27 | * | 1/2 | cast iron |
| 2 | " | " | * | " | " |
| 3 | " | " | * | " | " |

* see Figure 6.11

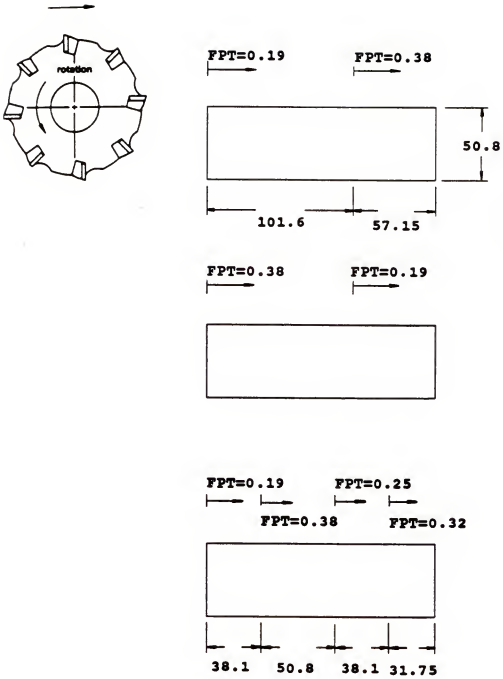


Figure 6.11 Cut geometry with the varying feedrates.

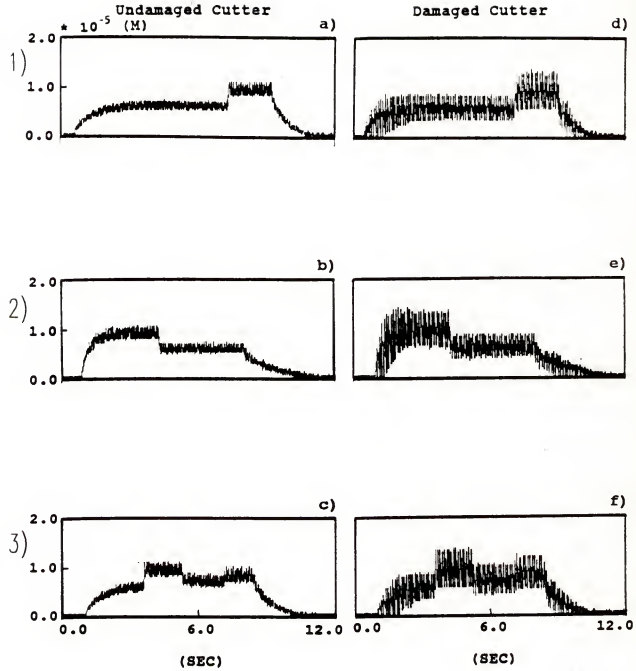


Figure 6.12 Average displacement signal with varying feedrates.

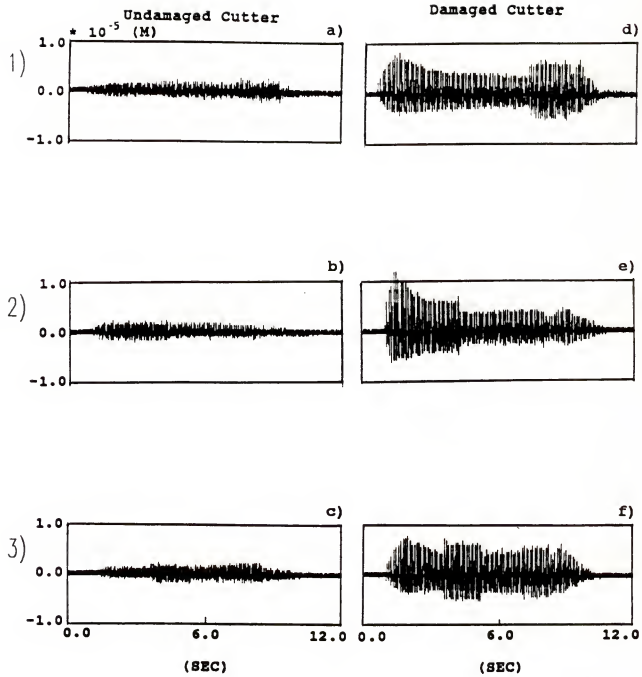


Figure 6.13 Difference of the average displacement signal with varying feedrates.

It is shown that the changes of feedrate affect the average and the difference of the average displacement signals proportionally.

## 6.5 Radial Immersion of Cut

In milling operations, the radial immersion of cut is changed only in the transient state because of the variation of the swept angle of cut. Figure 6.14 shows the average displacement signal in the 1/8, 1/4, 1/2, 3/4, 1/1 radial immersions up milling. The corresponding difference of the average signal is shown in Figure 6.15. The cutting parameters are listed in Table 6.6.

Table 6.6 Cutting parameters in the cutting tests with different radial immersions of cut

| No | spindle speed | depth of cut | feed per tooth | radial immersion | workpiece material |
|---|---|---|---|---|---|
| | rpm | mm | mm | | |
| 1 | 600 | 1.27 | 0.254 | 1/8 | steel |
| 2 | " | " | " | 1/4 | " |
| 3 | " | " | " | 1/2 | " |
| 4 | " | " | " | 3/4 | " |
| 5 | " | " | " | 1/1 | " |
| 6 | " | " | " | * | cast iron |
| 7 | " | " | " | * | " |

* see Figure 6.16

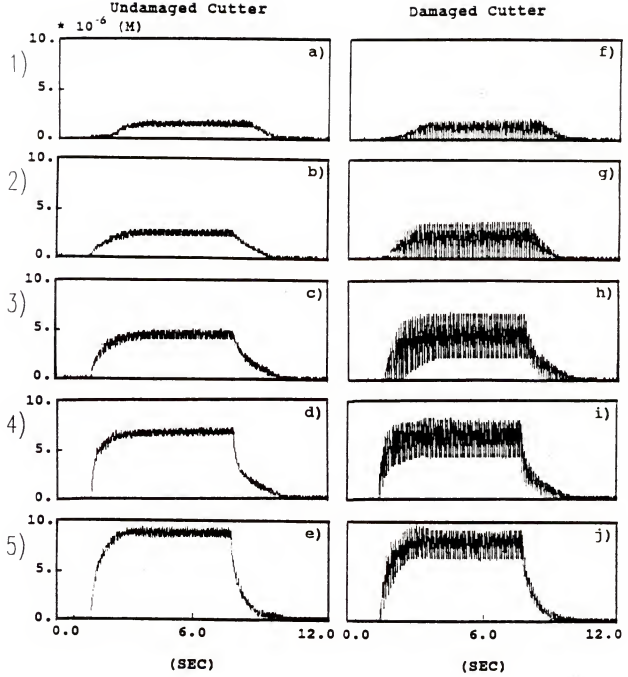


Figure 6.14 Average displacement signal in the 1/8, 1/4, 1/2, 3/4, and 1/1 immersions of cut.

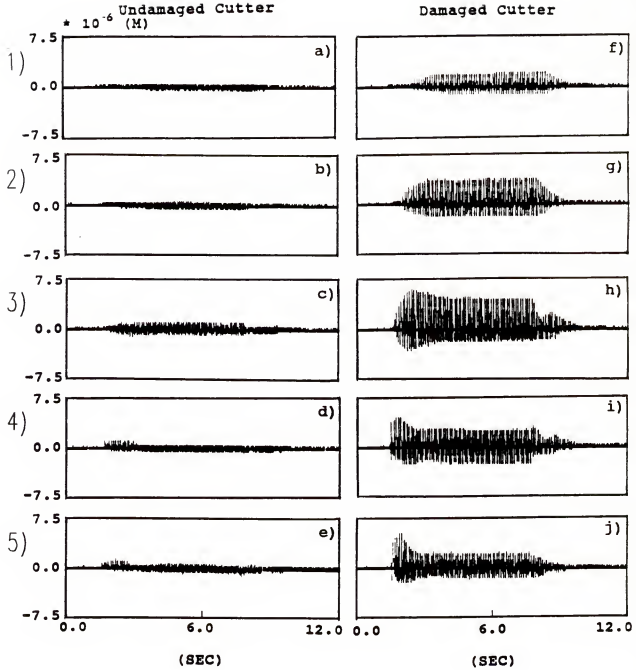


Figure 6.15 Difference of the average displacement signal in the 1/8, 1/4, 1/2, 3/4, and 1/1 immersions of cut.

It is shown that the DC component is almost proportional to the radial immersion of cut, but the AC component of the tool breakage signal in the difference of the average displacement is not. The tool breakage signal reaches the maximum value in the 1/2 immersion of cut. Then, it decreases as the radial immersion increases.

In addition to this, two special cut geometries with gradual change of radial immersion of cut are shown in Figure 6.16. Figure 6.17 shows the cutting test results. The cutting parameters are also listed in Table 6.6. It is shown that clear distinction of the tool breakage feature is available even in varying immersions of cut.

## 6.6 Interrupted Cuttings

In general, the boundary of the workpiece is a rectangle whose sides are parallel or perpendicular to the feed direction. As the cutter enters into the workpiece, there are three common cutting states: entry, steady, and exit. If the workpiece contains holes, bores, slots, pockets, or curvilinear boundaries interrupted cuttings happen, which change start and exit angles of cut dependent on the geometry of workpiece. As a result, the shape of the displacement signal may be different. Therefore, it is necessary to investigate the influence of interrupted cuttings in the average and the difference of the average displacement signals.

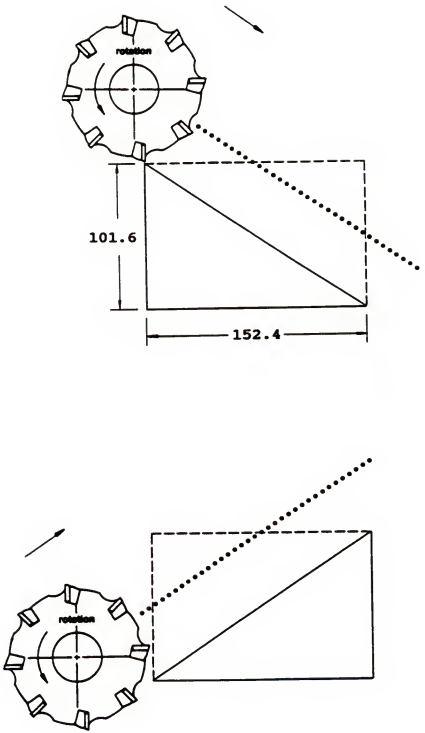


Figure 6.16 Cut Geometry for the gradual change of the radial immersion of cut.

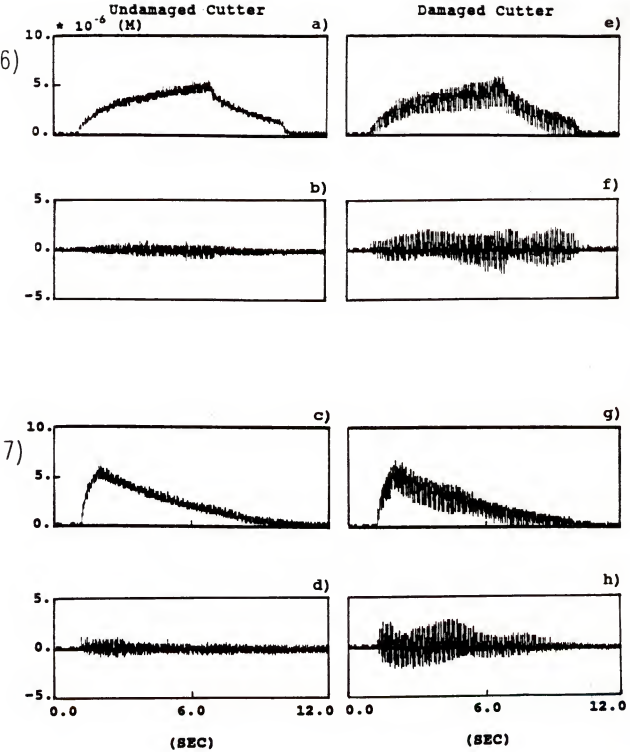


Figure 6.17 Average displacement and difference of the average displacement signals with the gradual change of radial immersion of cut.

Three special cases of interrupted cutting are represented in this section. The face milling cutter was used to mill over a slot, a hole, circular exit and entry boundaries. The cutting parameters are listed in Table 6.7.

Table 6.7 Cutting parameters in the interrupted cuttings

| No | spindle speed | depth of cut | feed per tooth | radial immersion | workpiece material |
|---|---|---|---|---|---|
| | rpm | mm | mm | | |
| 1 | 600 | 1.27 | 0.254 | 3/4 | cast iron |
| 2 | " | " | " | 1/2 | " |
| 3 | " | 2.54 | " | 1/2 | " |

### 6.6.1 Milling over a Slot

The geometry of the workpiece is shown in Figure 6.18. The cutting test results are shown in Figure 6.19. The first row displays the average displacement signal and the second row, the difference of average displacement signal. It is shown that the difference per tooth average method is able to remove the transient effect of milling over a slot.

### 6.6.2 Milling over a Hole

Figure 6.20 shows the geometry of the workpiece with a hole. The cutting test results are shown in Figure 6.21.

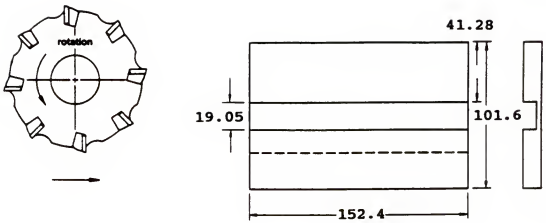


Figure 6.18 Cut geometry of the slot.

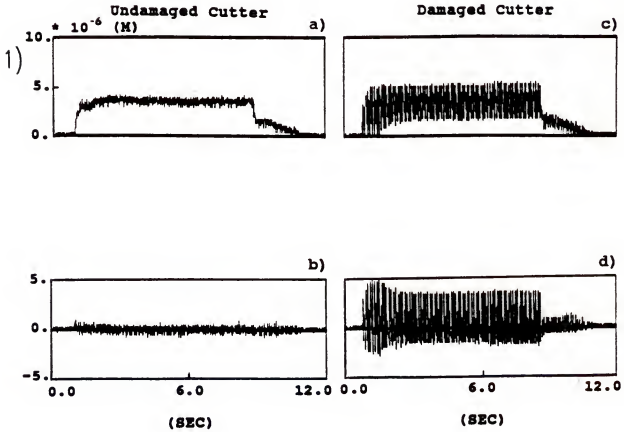


Figure 6.19 Average displacement and difference of the average displacement signals during milling over a slot.

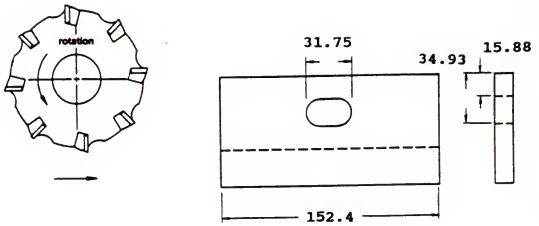


Figure 6.20 Cut geometry of the hole.

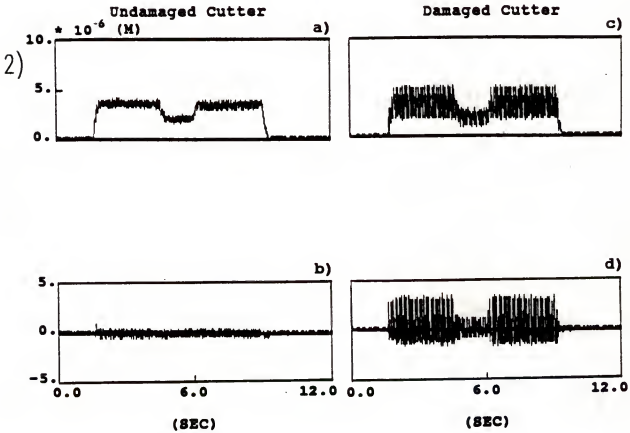


Figure 6.21 Average displacement and difference of the average displacement signals during milling over a hole.

Again, the first row displays the average displacement signal and the second row, the difference of the average displacement signal. In this case, the average displacement signal decreases when the cutter starts milling over the hole. Then, the signal gradually increases until the cutter has passed the hole. Nevertheless, it is efficient to remove the influence of this transient and keep the tool breakage feature by using the difference per tooth average method (see Figure 6.21.b and Figure 6.21.d).

### 6.6.3 Milling over Circular Exit and Entry Boundaries

Figure 6.22 shows circular exit and entry boundaries. The cutting test results are shown in Figure 6.23. Using the undamaged cutter, the average displacement signal is displayed in the first row and the difference of the average displacement is display in the second row.

Due to the sudden change of the workpiece boundary, a peak of the difference signal is generated even for the undamaged cutter, which may be higher than the tool breakage signal produced by the damaged cutter. However, this is only a one shot event. A special detection strategy (Section 7.1) is necessary to avoid a false alarm caused by these transients.

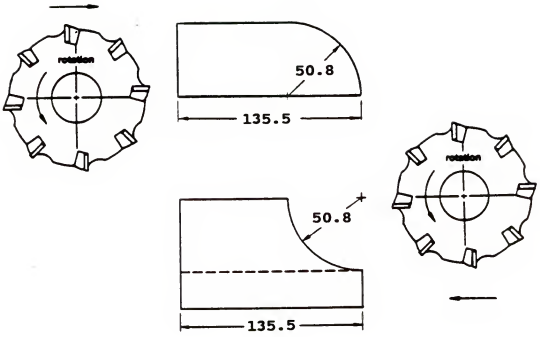


Figure 6.22 Cut geometry with the circular exit and entry boundaries.

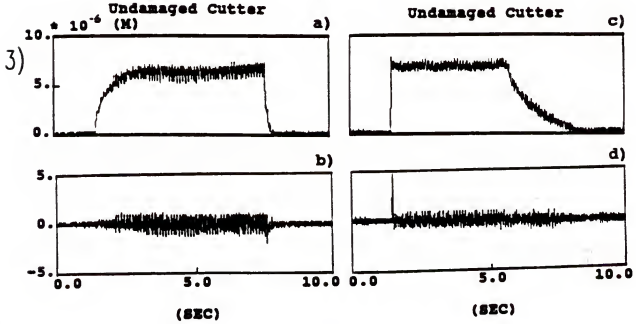


Figure 6.23 Average displacement and difference of the average displacement signals during milling over circular boundaries.

## 6.7 Corner Slotting

In milling operations, there are two common corner slottings, square corner slotting and corner slotting with a radius. The transient response is much stronger in the square corner slotting because the cutter switches from full immersion to half immersion at the corner, then the cutter reaches full immersion again, see Figure 6.24.

A three fluted undamaged end mill cutter (diameter = 19.05 mm) was used in the cutting test. The cutting parameters are listed in Table 6.8.

Table 6.8 Cutting parameters in the corner slotting

| spindle speed | depth of cut | feed per tooth | radial immersion | workpiece material |
|---|---|---|---|---|
| rpm | mm | mm | | |
| 600 | 2.54 | 0.254 | 1/1 | cast iron |

Figure 6.25.a shows the average signal and Figure 6.25.b, the difference of the average signal. Similar to the milling over circular boundaries, either a negative peak or a positive peak with a small time delay is generated during the sudden changes of immersions at the corner. However, this is still a one shot event, unlike the tool breakage event which repeats once per revolution after a broken tooth exists and has a minus-plus or plus-minus sequence of strong signal.

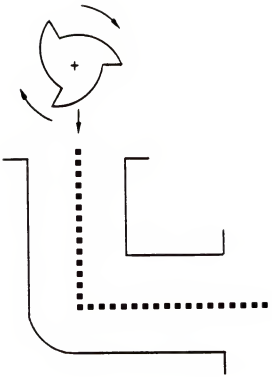

Figure 6.24 Cut geometry of the corner slotting.

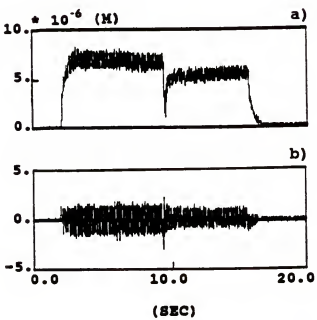


Figure 6.25 Average displacement and difference of the average displacement signals during slotting the square corner.

## 6.8 Different Flutes of Cutters

As shown in Equation (5.21), the average displacement signal is also proportional to the number of teeth on the cutter. Figure 6.26 shows slotting results using the undamaged end mill cutters with different flutes. The first row displays the signal obtained from a 4 fluted cutter. The second row displays the signal obtained from a 3 fluted cutter and the third row, a 2 fluted cutter. The cutting parameters are listed in Table 6.9.

Table 6.9 Cutting parameters in the cutting tests with different flutes of cutters

| No | spindle speed | depth of cut | feed per tooth | number of teeth | workpiece material |
|---|---|---|---|---|---|
| | rpm | mm | mm | | |
| 1 | 400 | 1.27 | 0.254 | 4 | cast iron |
| 2 | 600 | " | " | 3 | " |
| 3 | 800 | " | " | 2 | " |

The figures of the average signal are shown in the left-hand side, and the figures of the difference of the average signal are shown in the right-hand side. It is shown that the DC component of the average signal is proportional to the number of flutes on the cutter. The difference of the average signal varies depending not only

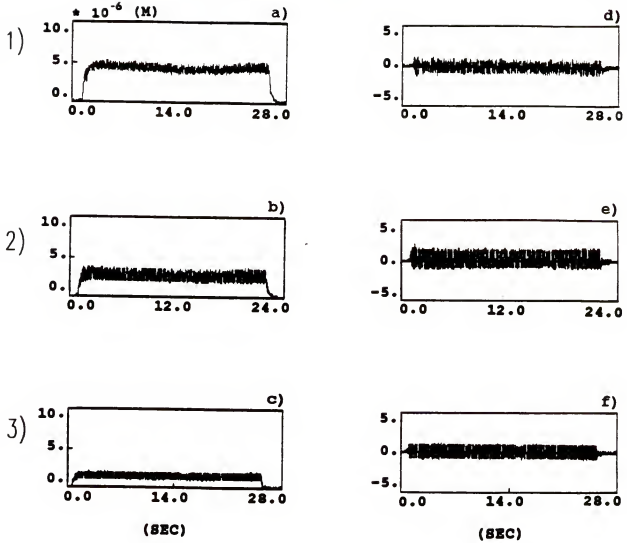


Figure 6.26 Average displacement and difference of the average displacement signals in the end milling with 4, 3, and 2 flutes of cutters.

on the magnitude of run-out on the end mill cutter but also on the number of teeth, which is not a linear relationship.

## 6.9 Percentage of Tool Breakage

Chipping occurs when the cutting edge is broken off only partly rather than being totally broken. This makes the cutting edge ragged and inefficient. As a result, the total breaking of cutting edge usually follows very quickly. Therefore, detection of chipping is also important.

Figure 6.27 shows the up milling cutting test results with different percentages of tool breakage. The cutting parameters are shown in Table 6.10.

Table 6.10 Cutting parameters in the cutting tests with different percentages of broken edge

| spindle speed | depth of cut | feed per tooth | radial immersion | workpiece material |
|---|---|---|---|---|
| rpm | mm | mm | | |
| 600 | 1.27 | 0.254 | 1/2 | cast iron |

A face milling cutter with eight unbroken inserts was used, see the first row. Then, one of the inserts was replaced with a chipped insert with about 60% of the

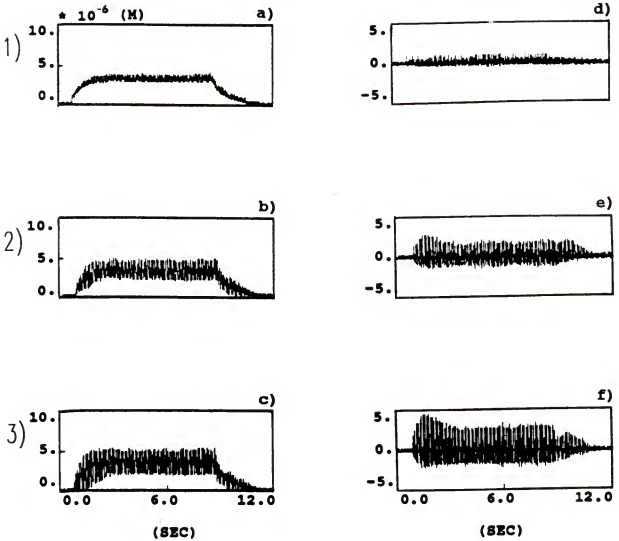


Figure 6.27 Average displacement and difference of the average displacement signals with different percentages of a broken cutting edge.

cutting edge broken off, see the second row. Finally, a totally broken insert was used, see the third row. Again, the figures of the left-hand side show the average signal; the figures of the right-hand side, the difference of the average signal.

It seems that the tool breakage signal in the difference of the average displacement is approximately proportional to the percentage of broken cutting edge. Therefore, the difference of the average displacement signal with a proper threshold value can also be used to detect chipping in milling.

# CHAPTER 7
# STRATEGIES FOR DETECTION OF TOOL BREAKAGE UNDER VARYING CUTTING CONDITIONS

In Chapter 6, it was clearly shown that the difference of the average displacement signal is effective in the recognition of tool breakage. However, a knowledge of allowable level of the difference of the average displacement is necessary to distinguish between the undamaged and damaged cutters. Furthermore, an algorithm is required to separate tool breakage from the sudden transient changes like corner slotting or milling over circular exit and entry boundaries.

## 7.1 Pattern Analysis

In Chapter 6, it was shown that the difference of the average displacement can easily remove the effect of slow varying transients. These slow varying transients include milling during entry, exit, slot, hole, or circular interpolation, etc. However, a problem occurs in the sudden transient changes. A sudden one shot of difference signal is generated. In order to avoid the occurrence of a false

alarm, a special algorithm to separate tool breakage from all kinds of transients has been developed [29]. This is possible because the pattern of sudden transient changes is different from that of tool breakage or chipping.

It is shown throughout that the difference of the average displacement signal decreases then immediately increases, or increases then immediately decreases, at the presence of tool breakage. However, the difference of the average displacement signal in transients without tool breakage is either positive or negative. That is, a one shot event.

In order to distinguish them, two threshold values are required. One is on the positive side; the other is on the negative side. If the difference signal is greater than the positive threshold value, the flag is equal to 1. When the difference signal is smaller than the negative threshold value, the flag is equal to -1. When the difference signal is within the band of the two threshold values, the flag is equal to 0. Tool breakage only occurs at the changes of the flag from -1 to 1 or from 1 to -1.

## 7.2 Threshold Setting

For a practical sensor system, a high sensitivity to tool breakage and a low sensitivity to the variation of cutting parameters such as speed, axial depth of cut, radial immersion of cut, feed, and workpiece material are

required. Therefore, how to set an alarm threshold on the positive and negative sides needs to be investigated.

In the processing of the displacement signal, the average displacement per tooth is calculated and differenced to remove the regular periodic and deterministic trends. Generally speaking, small residuals of the difference of the average displacement are left for the undamaged cutter. Hence, a minimum allowable level of this difference signal, which is called the threshold value, has to be determined.

This small residual signal is basically composed of two components. One is the component of process noise; the other is the component of cutter run-out. The amplitude of the noise signal can only be determined by experiments. In practice, the signal-to-noise ratio is large and therefore the residual signal can be mostly attributed to the cutter run-out. Run-out on the cutter, especially radial throw, also produces the same pattern in the difference signal as a broken tooth. If the radial throw becomes severe, it is as equally harmful as tool breakage because of the overload on the following tooth. It is then conceivable to set an alarm threshold equal to the summation of the noise signal and the difference signal produced by the tolerable amount of run-out on the cutter.

Using the run-out model developed in Chapter 3, the difference signal produced by the cutter run-out can be calculated. However, it is necessary to know the cutting

parameters first. In reality, the axial depth of cut and radial immersion of cut may vary in the cutting process. Therefore, the development of strategies for the real-time identification of the cutting geometry is required so that an analytical estimate of the expected threshold may be made.

Unfortunately, up to now, an efficient method for the identification of the axial depth of cut or radial immersion of cut is not available. A similar identification strategy using the average cutting force has been presented [51]. It has been shown that it is only possible to identify the axial and radial depths of cut in the steady state. Even though this strategy can be applied to the displacement signal, it is still not satisfactory due to the poor identification of transients.

An alternative way, which is a normalization of the difference of the average displacement signal, has been proposed [4]. It is proposed to obtain a ratio of the difference signal to a reference signal so that the ratio may be independent of cutting parameters. In addition, the tool breakage feature in the spectrum is also available for the calculation of the ratio, see Figure 4.24. Considerable efforts have been devoted to this approach. So far, it is still not fully developed.

The reference signals, either DC or AC, such as the moving average displacement signal or the tooth frequency signal in the instantaneous displacement signal, have been

considered either in the time or in the frequency domains. For example, the moving average displacement signal may be expressed as

$$D_{mavg}(j) = \frac{1}{2\omega+1} \sum_{i=-\omega}^{+\omega} D_{avg}(i) \qquad (7\text{-}1)$$

where

$D_{mavg}$ - moving average displacement

$2\omega+1$ - length of the window for moving average

$j$ - index for time increment per tooth period

The ratio eliminates the influence of the axial depth of cut, feedrate, workpiece material, and some cutter constants because the reference signal is also proportional to these cutting parameters. However, they all suffer the same problem, which is that the ratio is extremely dependent on the radial immersion of cut.

Figure 7.1 shows a simulation of the ratio of the peak difference signal to the moving average displacement signal per revolution versus the swept angle using a face milling cutter with eight teeth. The line of tool breakage represents a cutting edge totally broken; the line of run-out represents the radial throw amounting to one tenth of the feed per tooth. Using Equation (3-39), the two lines intersects at $h_{mc} = 0$. That is

$$r_{i-1} - r_i = 0.1f_t = f_t \sin\theta$$

and

$$\theta = \sin^{-1}0.1 = 5.74°$$

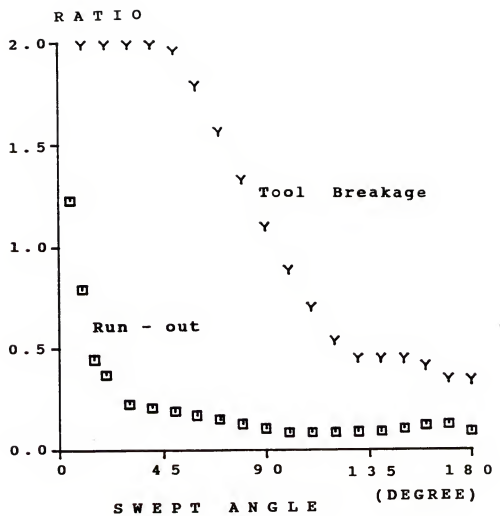


Figure 7.1 Simulation of the ratio of the difference displacement to the mean displacement.

That tells us that radial throw and tool breakage are indistinguishable when the swept angle is smaller than 5.74°. As shown in Figure 7.1, the ratio of run-out increases in the smaller radial immersion of cut for the undamaged cutter. However, the ratio of tool breakage decreases quickly in the larger radial immersion of cut, even for the damaged cutter. In Section 6.5, the experimental results also show the same conclusion. In other words, an on-line identification of the extent of the radial immersion of cut is still necessary so that the alarm threshold can be adaptively varied as the amount of immersion changes, see Figure 7.2. The solution of this approach still depends on the development of an identification strategy. Furthermore, the signal-to-noise ratio is decreased in small radial immersions of cut because the moving average displacement is relatively small. Therefore, the possibility of false alarm increases even, with the identification strategy, in small radial immersions of cut. This makes the scheme difficult to implement.

Figure 7.2 shows an example of the ratio calculated for the complete cycle of cutting tests. The cutting parameters are same as listed in Table 6.10. The first row displays the moving average displacement signal which is independent of tool breakage. The second row displays the difference signals per tooth; the third row, the ratio. It is seen that the ratio increases in the entry and more so

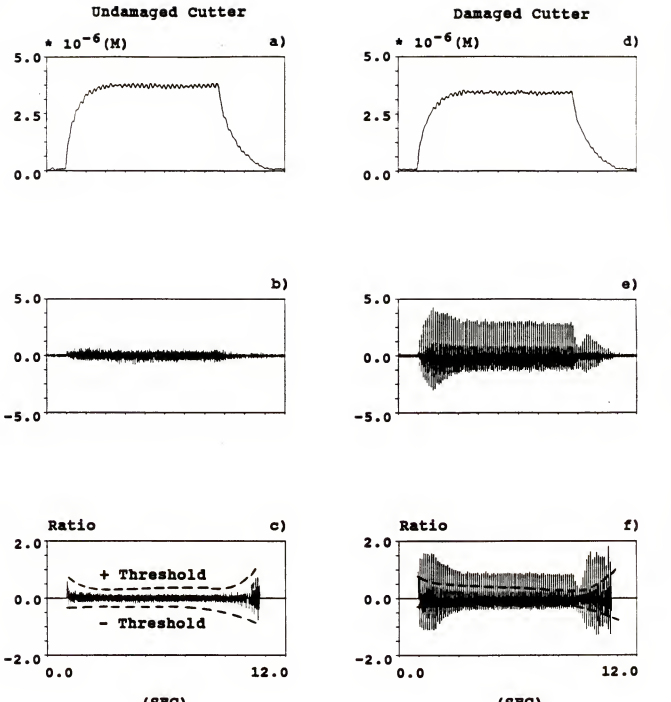


Figure 7.2 Moving average and difference of the average displacement signals with the normalization ratio of the difference of the average displacement signal.

in the exit, even for the undamaged cutter. This is because the entry swept angle of cut changes from 0° to 90° and the exit swept angle of cut changes from 90° to 0°.

Another promising way has been considered [52]. It utilizes a geometric modelling system to predict the cutting torque in face and end milling operations. In this system, a geometric simulation of the cut is made and then the cutting parameters may be estimated from the input data and the shape of the removed segment. Therefore, using the estimated cutting parameters, the proper threshold values could be set under varying cutting conditions. This should be dealt with in future research.

In recent years, commercial tool condition monitoring systems use a "teaching" method to obtain the threshold under varying cutting conditions, for instance Promess sensors [53], TCM sensors [54], and Feed Force Sensor [55]. Even though this teaching method has some disadvantages [56], these system are still widely accepted by the industry.

This teaching method can also be applied to the difference of the average displacement signal very well because the difference signal provides the distinct tool breakage feature. The teaching method applied to the displacement sensor can be explained as follows: at the beginning of the milling process, the system is set to a "teach in" mode, and a protection device is turned on. The monitoring system measures the whole cycle of the

difference signal and then calculates limit patterns for tool breakage at different time intervals. In the following cuts, the monitoring system is set to a "pattern matching" mode. The limit patterns which have controllable factors are compared with the new measurement of the difference signal. If it is over a certain level and the change of flag is also from -1 to 1 or 1 to -1, tool breakage is assumed.

This teaching method is free of modelling and easy to implement. However, a trial cut is required for initialization. Using this teaching methodology, a tool breakage monitoring system has been implemented at the Machine Tool Laboratory, University of Florida. It demonstrates a high sensitivity and reliability for the detection of tool breakage in milling.

# CHAPTER 8
# CONCLUSIONS AND FUTURE WORK

A tool diagnostic system has been developed to sense cutter breakage by monitoring the pattern changes of the cutting force. The variation per tooth is filtered out by averaging the cutting force per tooth. The pattern of tool breakage is extracted by differencing the average cutting force.

Because of the practical difficulties for measurement of the cutting force in milling, the use of vibration signals was explored. It was shown the displacement signal of the spindle maintains the same tool breakage pattern as the cutting force signal under all kinds of cutting conditions. Finally, the setting of threshold values was also investigated to make the system independent of changes in cutting conditions.

Further research should be focused on the development of a real-time strategy for the identification of cut geometry or solid modelling of the milling process, in order to obtain the cutting parameters. Hence, a reliable threshold for cutter breakage detection can be established using the estimated cutting parameters under varying

cutting conditions. In addition, it may be advantageous to integrate information from several sensors so that the best features of all the sensors are utilized. A multi-sensor scheme using artificial intelligence technologies through a knowledge-based (analytical and experimental) system is also considered. Then, the tool breakage sensor will be fully developed to achieve the final goal of unmanned milling.

# APPENDIX A

## LISTING OF SUBROUTINES FOR MODELLING OF MILLING PROCESS

```
C    SIMULATION PROGRAM FOR MODELLING OF MILLING PROCESS
C
C                          BY YEONG-SHIN TARNG
C
C
C    MILLIB.LIB IS A LIBRARY FILE CONTAINING 23 SUBROUTINES
C
C
C     1) ANGLE - CALCULATE ANGULAR POSITIONS OF THE TEETH IN THE
C                INITIAL CONDITION. P.168.
C     2) ROTAT - CALCULATE INCREMENTAL POSITIONS OF THE TEETH IN
C                THE CUTTING OPERATION. P.168.
C     3) FORTR - CALCULATE TANGENTIAL AND RADIAL FORCES ON EACH
C                TOOTH. (RIGID FORCE MODEL) P.169.
C     4) FXYS  - DECOMPOSE TANGENTIAL AND RADIAL FORCES INTO X
C                AND Y DIRECTIONS. P.169.
C     5) SUM   - SUM THE SIGNALS IN THE X AND Y DIRECTIONS.
C                P.170.
C     6) RESXY - CALCULATE THE RESULTANT AVERAGE SIGNAL. P.170.
C     7) BREAK - SIMULATE THE CHANGES OF TANGENTIAL AND RADIAL
C                FORCES DUE TO TOOL BREAKAGE. P.170.
C     8) VIBRA - SIMULATE THE VIBRATION SIGNALS IN THE X AND Y
C                DIRECTIONS. P.171.
C     9) THSE1 - CALCULATE STARTING AND EXIT ANGLES OF CUT IN
C                UP/DOWN MILLING. P.172.
C    10) THSE2 - CALCULATE STARTING AND EXIT ANGLES OF CUT IN
C                UP/DOWN MILLING. P.173.
C    11) THSE4 - CALCULATE STARTING AND EXIT ANGLES OF CUT IN
C                UP/DOWN MILLING. P.174.
C    12) THSE8 - CALCULATE STARTING AND EXIT ANGLES OF CUT IN
C                UP/DOWN MILLING. P.175.
C    13) LOFIL - SIMULATE THE SIGNALS PASSING THROUGH A 1ST ORDER
C                LOW-PASS FILTER. P.177.
C    14) HIFIL - SIMULATE THE SIGNALS PASSING THROUGH A 2ND ORDER
C                HIGH-PASS FILTER. P.177.
C    15) FORTR - CALCULATE TANGENTIAL AND RADIAL FORCES ON EACH
C                TOOTH. (END MILLING MODEL) P.177.
C    16) TRANS - CALCULATE INITIAL ANGULAR POSITIONS OF THE
C                FLUTES. P.178.
C    17) HELIX - CALCULATE INCREMENTAL POSITIONS OF THE FLUTES
C                IN END MILLING. P.178.
C    18) UNROL - CALCULATE THE COEFFICIENTS OF THE UNROLLED END
C                MILL CUTTER. P.179.
C    19) FORTR - CALCULATE TANGENTIAL AND RADIAL FORCES ON EACH
C                TOOTH. (RUN-OUT MODEL) P.179.
C    20) THROW - INPUT THE ARRAY OF RADIAL THROW. P.180.
C    21) FORTR - CALCULATE TANGENTIAL AND RADIAL FORCES ON EACH
C                TOOTH. (REGENERATIVE FORCE MODEL) P.180.
C    22) TEETH - CALCULATE THE FEED PER TOOTH FOR EACH TOOTH.
C                (REGENERATIVE FORCE MODEL) P.181.
C    23) DEFLE - SIMULATE THE VIBRATION OF CUTTER. P.182.
C
```

```
C
C
      SUBROUTINE ANGLE(THETA,THP,THO,NTEETH)
C
C     MILLING SUBROUTINE
C
C     ANGULAR POSITIONS OF THE TEETH
C
C     THETA  - ANGULAR POSITIONS OF THE TEETH
C     THP    - ANGLE OF THE TOOTH PERIOD
C     THO    - INITIAL SAMPLING ANGLE
C     NTEETH - NUMBER OF THE TEETH
C
      DIMENSION THETA(1)
C
      DO 10 I=1,NTEETH
   10 THETA(I)=(I-1)*THP+THO
C
       DO 20 I=1,NTEETH
         IF (THETA(I) .GE. 360.) THEN
            THETA(I)=THETA(I)-360.0
         ELSE
            IF (THETA(I) .LT. 0.) THEN
               THETA(I)=THETA(I)+360.0
            ENDIF
         ENDIF
   20  CONTINUE
C
      RETURN
      END
C
C
      SUBROUTINE ROTAT(THETA,THADD,THALL,NTEETH)
C
C     MILLING SUBROUTINE
C
C     INCREMENTAL POSITIONS FOR EACH TOOTH
C
C     THETA  - ANGULAR POSITIONS OF THE TEETH
C     THADD  - INCREMENTAL ANGLE IN THE SIMULATION
C     THALL  - TOTAL ROTATION ANGLE IN THE CUTTING
C     NTEETH - NUMBER OF THE TEETH
C
      DIMENSION THETA(1)
C
      DO 10 I=1,NTEETH
   10 THETA(I)=THETA(I)+THADD
C
      DO 20 I=1,NTEETH
      IF (THETA(I) .GE. 360.) THEN
         THETA(I)=THETA(I)-360.
      ENDIF
   20 CONTINUE
C
```

```
      THALL=THALL+THADD
C
      RETURN
      END
C
C
      SUBROUTINE FORTR(FT,FR,THETA,THS,THE,NTEETH)
C
C      MILLING SUBROUTINE (RIGID FORCE MODEL)
C
C     TANGENTIAL & RADIAL FORCES ON EACH TOOTH
C
C     FT      - ARRAY OF THE TANGENTIAL FORCES
C     FR      - ARRAY OF THE RADIAL FORCES
C     THETA   - ANGULAR POSITIONS OF THE TEETH
C     THS     - STARTING ANGLE OF CUT
C     THE     - EXIT ANGLE OF CUT
C     NTEETH - NUMBER OF THE TEETH
C
      COMMON /COEFF/ AXL,FEED,FK,RATIO,RAD
C
      DIMENSION FT(1),FR(1),THETA(1)
C
      DO 10 I=1,NTEETH
         IF (THETA(I) .GE. THS .AND. THETA(I) .LE. THE) THEN
            FT(I)=FK*AXL*FEED*SIND(THETA(I))
            FR(I)=FT(I)*RATIO
         ELSE
            FT(I)=0.0
            FR(I)=0.0
         ENDIF
   10 CONTINUE
C
      RETURN
      END
C
C
      SUBROUTINE FXYS(FX,FY,FT,FR,THETA,NTEETH)
C
C     MILLING SUBROUTINE
C
C     DECOMPOSE FORCES INTO THE X & Y DIRECTIONS
C
C     FX      - CUTTING FORCE IN THE X DIRECTION
C     FY      - CUTTING FORCE IN THE Y DIRECTION
C     FT      - ARRAY OF THE TANGENTIAL FORCES
C     FR      - ARRAY OF THE RADIAL FORCES
C     THETA   - ANGULAR POSITIONS OF THE TEETH
C     NTEETH - NUMBER OF THE TEETH
C
      DIMENSION FT(1),FR(1),THETA(1)
C
      FSX=0.0
```

```
      FSY=0.0
C
      DO 10 I=1,NTEETH
         FSX=FSX+FR(I)*SIND(THETA(I))+FT(I)*COSD(THETA(I))
   10    FSY=FSY-FR(I)*COSD(THETA(I))+FT(I)*SIND(THETA(I))
C
        FX=FSX
        FY=FSY
C
        RETURN
        END
C
C
      SUBROUTINE SUM(XCOM,YCOM,XAVG,YAVG)
C
C     MILLING SUBROUTINE
C
C     SUM THE SIGNALS IN THE X & Y DIRECTIONS
C
C     XCOM - COMPONENT IN THE X DIRECTION
C     YCOM - COMPONENT IN THE Y DIRECTION
C     XAVG - SUMMATION OF THE X DIRECTION COMPONENTS
C     YAVG - SUMMATION OF THE Y DIRECTION COMPONENTS
C
         XAVG=XAVG+DIMX
         YAVG=YAVG+DIMY
C
      RETURN
      END
C
C
      SUBROUTINE RESXY(RES,XCOM,YCOM,NUM)
C
C     MILLING SUBROUTINE
C
C     RESULTANT AVERAGE SIGNAL
C
C     RES  - RESULTANT SIGNAL
C     XCOM - SIGNAL IN THE X DIRECTION
C     YCOM - SIGNAL IN THE Y DIRECTION
C     NUM  - NUMBER OF SAMPLES
C
      RNUM=NUM
C
      RES=(XCOM**2.+YCOM**2.)**0.5/RNUM
C
      RETURN
      END
C
C
      SUBROUTINE BREAK(FT,FR,NTEETH,NBR,NP,PER,THETA)
C
C     MILLING SUBROUTINE
C
```

```
C     CHIPPED OR TOTALLY BROKEN ON THE CUTTING EDGE
C
C     FT      - ARRAY OF THE TANGENTIAL FORCES
C     FR      - ARRAY OF THE RADIAL FORCES
C     NTEETH - NUMBER OF THE TEETH
C     NBR     - TOOTH PERIOD AS THE OCCURRENCE OF TOOL BREAKAGE
C     NP      - CURRENT TOOTH PERIOD
C     PER     - PERCENTAGE OF THE BROKEN CUTTING EDGE
C     THETA   - ANGULAR POSITIONS THE TEETH
C
      COMMON /COEFF/ AXL,FEED,FK,RATIO,RAD
C
      DIMENSION FT(1),FR(1),THETA(1)
C
      PERCENT=PER/100.
      ERROR=FEED*PERCENT
      CHIPT=FEED*SIND(THETA(1))
C
      IF (NP .GE. NBR) THEN
         IF (CHIPT .LE. ERROR) THEN
            FT(1)=0.0
            FR(1)=0.0
            FT(NTEETH)=2.*FT(NTEETH)
            FR(NTEETH)=2.*FR(NTEETH)
         ELSE
            FT(1)=(1.-PERCENT)*FT(1)
            FR(1)=(1.-PERCENT)*FR(1)
            FT(NTEETH)=(1.+PERCENT)*FT(NTEETH)
            FR(NTEETH)=(1.+PERCENT)*FR(NTEETH)
         ENDIF
      ENDIF
C
      RETURN
      END
C
C
      SUBROUTINE VIBRA(FX,FY)
C
C     MILLING SUBROUTINE
C
C     VIBRATIONS IN THE X & Y DIRECTIONS
C
C     FX       - CUTTING FORCE IN THE X DIRECTION
C     FY       - CUTTING FORCE IN THE Y DIRECTION
C     DMASS    - MASS PARAMETER
C     ETA      - DAMPING RATIO
C     WN       - NATURAL FREQUENCY
C     DDX,DDY - ACCELERATIONS IN X AND Y DIRECTIONS
C     DX,DY    - VELOCITIES IN X AND Y DIRECTIONS
C     X,Y      - DISPLACEMENTS IN X AND Y DIRECTIONS
C     DT       - TIME INTERVAL
C
      COMMON /VIBPAR/ WN,ETA,DMASS,DX,DY,DT,X,Y,TS
C
```

```
      DDX=FX/DMASS-2.*ETA*WN*DX-(WN**2.)*X
      DDY=FY/DMASS-2.*ETA*WN*DY-(WN**2.)*Y
C
      DX=DX+DDX*DT
      DY=DY+DDY*DT
C
      X=X+DX*DT
      Y=Y+DY*DT
C
      RETURN
      END
C
C
      SUBROUTINE THSE1(THS,THE,THP,THALL,WSL,DELY)
C
C     1/1 IMMERSION MILLING
C
C     STARTING & EXIT ANGLES FOR CUTTING
C
C     THS   - STARTING ANGLE OF CUT
C     THE   - EXIT ANGLE OF CUT
C     THP   - ANGLE OF THE TOOTH PERIOD
C     THALL - TOTAL ROTATION ANGLE IN THE CUTTING
C     WSL   - LENGTH OF THE WORKPIECE
C     DELY  - DISTANCE BETWEEN THE CUTTER AND WORKPIECE
C
      COMMON /COEFF/ AXL,FEED,FK,RATIO,RAD
C
      DIMENSION THS(2),THE(2)
C
      FLEN=FEED*(THALL/THP)-DELY
      ELEN=WSL+RAD
C
      DO 10 I=1,2
         THS(I)=0.0
 10      THE(I)=0.0
C
      IF (FLEN .LT. 0.0) THEN
         THS(1)=0.0
         THE(1)=0.0
      ELSE
         IF (FLEN .LT. RAD) THEN
            THCUT=ACOSD(1.-(FLEN/RAD))
            THS(1)=90.-THCUT
            THE(1)=90.+THCUT
         ELSE
            IF (FLEN .LT. WSL) THEN
               THS(1)=0.0
               THE(1)=180.0
            ELSE
               THCUT=ACOSD(1.-(FLEN-WSL)/RAD)
               THS(1)=0.0
               THE(1)=90.-THCUT
               THS(2)=90.+THCUT
```

```
            THE(2)=180.0
          ENDIF
        ENDIF
      ENDIF
C
      RETURN
      END
C
C
      SUBROUTINE THSE2(THS,THE,THP,THALL,WSL,IUD,DELY)
C
C     1/2 IMMERSION UP AND DOWN MILLINGS
C
C     STARTING & EXIT ANGLES FOR CUTTING
C
C     THS    - STARTING ANGLE OF CUT
C     THE    - EXIT ANGLE OF CUT
C     THP    - ANGLE OF THE TOOTH PERIOD
C     THALL  - TOTAL ROTATION ANGLE IN THE CUTTING
C     WSL    - LENGTH OF THE WORKPIECE
C     IUD    - UP OR DOWN MILLING
C     DELY   - DISTANCE BETWEEN THE CUTTER AND WORKPIECE
C
      COMMON /COEFF/ AXL,FEED,FK,RATIO,RAD
C
      FLEN=FEED*(THALL/THP)-DELY
      ELEN=WSL+RAD
C
      IF (FLEN .LT. 0.0) THEN
         THS=0.0
         THE=0.0
      ELSE
         IF (IUD .EQ. 1) THEN
            IF (FLEN .LT. RAD) THEN
               THS=ASIND(1.-(FLEN/RAD))
               THE=90.
            ELSE
               IF (FLEN .LT. WSL) THEN
                  THS=0.0
                  THE=90.0
               ELSE
                  IF (FLEN .LT. ELEN) THEN
                     THS=0.0
                     THE=90.0-ACOSD(1.-(FLEN-WSL)/RAD)
                  ELSE
                     THS=0.0
                     THE=0.0
                  ENDIF
               ENDIF
            ENDIF
C
         ELSE
C
            IF (FLEN .LT. RAD) THEN
```

```
                THS=90.0
                THE=180.0-ASIND(1.-(FLEN/RAD))
             ELSE
                IF (FLEN .LT. WSL) THEN
                   THS=90.0
                   THE=180.0
                ELSE
                   IF (FLEN .LT. ELEN) THEN
                      THS=90.0+ACOSD(1.-(FLEN-WSL)/RAD)
                      THE=180.0
                   ELSE
                      THS=0.0
                      THE=0.0
                   ENDIF
                ENDIF
             ENDIF
          ENDIF
C
       ENDIF
C
       RETURN
       END
C
C
       SUBROUTINE THSE4(THS,THE,THP,THALL,WSL,IUD,DELY)
C
C      1/4 IMMERSION UP AND DOWN MILLINGS
C
C      STARTING & EXIT ANGLES FOR CUTTING
C
C      THS    - STARTING ANGLE OF CUT
C      THE    - EXIT ANGLE OF CUT
C      THP    - ANGLE OF THE TOOTH PERIOD
C      THALL  - TOTAL ROTATION ANGLE IN THE CUTTING
C      WSL    - LENGTH OF THE WORKPIECE
C      IUD    - UP OR DOWN MILLING
C      DELY   - DISTANCE BETWEEN THE CUTTER AND WORKPIECE
C
       COMMON /COEFF/ AXL,FEED,FK,RATIO,RAD
C
       FLEN=FEED*(THALL/THP)-DELY
       SLEN=(2.0-SQRT(3.0))/2.0*RAD
       BLEN=WSL+SLEN
       ELEN=WSL+RAD
C
       IF (FLEN .LT. SLEN) THEN
          THS=0.0
          THE=0.0
       ELSE
          IF (IUD .EQ. 1) THEN
             IF (FLEN .LT. RAD) THEN
                THS=ASIND(1.-FLEN/RAD)
                THE=ACOSD(1./2.)
             ELSE
```

```
            IF (FLEN .LT. BLEN) THEN
               THS=0.0
               THE=ACOSD(1./2.)
            ELSE
               IF (FLEN .LT. ELEN) THEN
                  THS=0.0
                  THE=ASIND(1.-(FLEN-WSL)/RAD)
               ELSE
                  THS=0.0
                  THE=0.0
               ENDIF
            ENDIF
         ENDIF
C
      ELSE
C
         IF (FLEN .LT. RAD) THEN
            THS=180.0-ACOSD(1./2.)
            THE=180.0-ASIND(1.-FLEN/RAD)
         ELSE
            IF (FLEN .LT. BLEN) THEN
               THS=180.0-ACOSD(1./2.)
               THE=180.0
            ELSE
               IF (FLEN .LT. ELEN) THEN
                  THS=180.0-ASIND(1.-(FLEN-WSL)/RAD)
                  THE=180.0
               ELSE
                  THS=0.0
                  THE=0.0
               ENDIF
            ENDIF
         ENDIF
      ENDIF
C
      ENDIF
C
      RETURN
      END
C
C
      SUBROUTINE THSE8(THS,THE,THP,THALL,WSL,IUD,DELY)
C
C     1/8 IMMERSION UP AND DOWN MILLINGS
C
C     STARTING & EXIT ANGLES FOR CUTTING
C
C     THS    - STARTING ANGLE OF CUT
C     THE    - EXIT ANGLE OF CUT
C     THP    - ANGLE OF THE TOOTH PERIOD
C     THALL  - TOTAL ROTATION ANGLE IN THE CUTTING
C     WSL    - LENGTH OF THE WORKPIECE
C     IUD    - UP OR DOWN MILLING
C     DELY   - DISTANCE BETWEEN THE CUTTER AND WORKPIECE
```

```
C
      COMMON /COEFF/ AXL,FEED,FK,RATIO,RAD
C
      FLEN=FEED*(THALL/THP)-DELY
      SLEN=(4.-SQRT(7.))/4.*RAD
      BLEN=WSL+SLEN
      ELEN=WSL+RAD
C
      IF (FLEN .LT. SLEN) THEN
         THS=0.0
         THE=0.0
      ELSE
         IF (IUD .EQ. 1) THEN
            IF (FLEN .LT. RAD) THEN
               THS=ASIND(1.-FLEN/RAD)
               THE=ACOSD(3./4.)
            ELSE
               IF (FLEN .LT. BLEN) THEN
                  THS=0.0
                  THE=ACOSD(3./4.)
               ELSE
                  IF (FLEN .LT. ELEN) THEN
                     THS=0.0
                     THE=ASIND(1.-(FLEN-WSL)/RAD)
                  ELSE
                     THS=0.0
                     THE=0.0
                  ENDIF
               ENDIF
            ENDIF
C
         ELSE
C
            IF (FLEN .LT. RAD) THEN
               THS=180.0-ACOSD(3./4.)
               THE=180.0-ASIND(1.-FLEN/RAD)
            ELSE
               IF (FLEN .LT. BLEN) THEN
                  THS=180.0-ACOSD(3./4.)
                  THE=180.0
               ELSE
                  IF (FLEN .LT. ELEN) THEN
                     THS=180.0-ASIND(1.-(FLEN-WSL)/RAD)
                     THE=180.0
                  ELSE
                     THS=0.0
                     THE=0.0
                  ENDIF
               ENDIF
            ENDIF
C
      ENDIF
C
```

```
      RETURN
      END
C
C
      SUBROUTINE LOFIL(XI,YO,X1,Y1,COEF1,COEF2)
C
C     MILLING SUBROUTINE
C
C     1ST ORDER BUTTERWORTH LOWPASS FILTER
C
C     XI  - INPUT SIGNAL
C     YO  - OUTPUT SIGNAL
C
      YO=COEF1*Y1+COEF2*XI
C
      X1=XI
      Y1=YO
C
      RETURN
      END
C
C
      SUBROUTINE HIFIL(XI,YO,X2,X1,Y2,Y1)
C
C     MILLING SUBROUTINE
C
C     2ND ORDER BUTTERWORTH HIPASS FILTER
C
C     XI - INPUT SIGNAL
C     YO - OUTPUT SIGNAL
C
      COMMON /HIPAS/ COEF1,COEF2,COEF3
C
      YO=(X2-2.*X1+XI-COEF1*Y2-COEF2*Y1)/COEF3
C
      X2=X1
      X1=XI
C
      Y2=Y1
      Y1=YO
C
      RETURN
      END
C
C
      SUBROUTINE FORTR(FT,FR,THETA,THS,THE,NTEETH,DAXL)
C
C     MILLING SUBROUTINE (END MILLING MODEL)
C
C     TANGENTIAL & RADIAL FORCES ON EACH TOOTH
C
C     FT      - ARRAY OF THE TANGENTIAL FORCES
C     FR      - ARRAY OF THE RADIAL FORCES
C     THETA   - ANGULAR POSITIONS THE TEETH
```

```
C     THS    - STARTING ANGLE OF CUT
C     THE    - EXIT ANGLE OF CUT
C     NTEETH - NUMBER OF THE TEETH
C     DAXL   - INCREMENTAL AXIAL DEPTH OF CUT
C
      COMMON /COEFF/ AXL,FEED,FK,RATIO,RAD
C
      DIMENSION FT(1),FR(1),THETA(1)
C
      DO 10 I=1,NTEETH
         IF (THETA(I) .GE. THS .AND. THETA(I) .LE. THE) THEN
            CHIPT=FEED*SIND(THETA(I))
            FT(I)=FK*DAXL*CHIPT
            FR(I)=FT(I)*RATIO
         ELSE
            FT(I)=0.0
            FR(I)=0.0
         ENDIF
   10 CONTINUE
C
      RETURN
      END
C
C
      SUBROUTINE TRANS(PHI,THETA,NTEETH)
C
C     MILLING SUBROUTINE (END MILLING)
C
C     ANGULAR POSITIONS OF END MILL CUTTING EDGES
C
C     PHI    - ANGULAR POSITIONS OF THE CUTTING EDGES
C     THETA  - STARTING ANGULAR POSITIONS OF THE TEETH
C     NTEETH - NUMBER OF THE TEETH
C
      DIMENSION PHI(1),THETA(1)
C
      DO 10 I=1,NTEETH
         PHI(I)=THETA(I)
   10 CONTINUE
C
      RETURN
      END
C
C
      SUBROUTINE HELIX(PHI,NTEETH,DPSI)
C
C     MILLING SUBROUTINE (END MILLING)
C
C     INCREMENTAL ANGULAR POSITIONS OF END MILL CUTTING EDGES
C
C     PHI    - ANGULAR POSITIONS OF THE CUTTING EDGES
C     NTEETH - NUMBER OF THE TEETH
C     DPSI   - INCREMENTAL ENGAGEMENT ANGLE
C
```

```
      DIMENSION PHI(1)
C
      DO 10 I=1,NTEETH
         PHI(I)=PHI(I)-DPSI
         IF (PHI(I) .LT. 0.0) THEN
            PHI(I)=PHI(I)+360.
         ENDIF
   10 CONTINUE
C
      RETURN
      END
C
C
      SUBROUTINE UNROL(BETA,PSI,DPSI,DAXL,NSTEP)
C
C     MILLING SUBROUTINE (END MILLING)
C
C     COEFFICIENTS OF END MILL CUTTER
C
C     BETA  - HELIX ANGLE
C     PSI   - ENGAGEMENT ANGLE
C     DPSI  - INCREMENTAL ENGAGEMENT ANGLE
C     DAXL  - INCREMENTAL AXIAL DEPTH OF CUT
C     NSTEP - NUMBER OF STEPS IN THE SIMULATION
C
      COMMON /COEFF/ AXL,FEED,FK,RATIO,RAD
C
      DIMENSION PHI(1),THETA(1)
C
      PSIRAD=AXL*TAND(BETA)/RAD
      PSI=PSIRAD*(180./3.14159)
      DPSI=PSI/NSTEP
      DAXL=AXL/NSTEP
C
      RETURN
      END
C
C
      SUBROUTINE FORTR(FT,FR,THETA,THS,THE,NTEETH,ERROR)
C
C     MILLING SUBROUTINE (RUN-OUT MODEL)
C
C     TANGENTIAL & RADIAL FORCES ON EACH TOOTH
C
C     FT     - ARRAY OF THE TANGENTIAL FORCES
C     FR     - ARRAY OF THE RADIAL FORCES
C     THETA  - ANGULAR POSITIONS OF THE TEETH
C     THS    - STARTING ANGLE OF CUT
C     THE    - EXIT ANGLE OF CUT
C     NTEETH - NUMBER OF THE TEETH
C     ERROR  - ARRAY OF THE RADIAL THROW
C
      COMMON /COEFF/ AXL,FEED,FK,RATIO,RAD
C
```

```
      DIMENSION FT(1),FR(1),THETA(1),ERROR(-16:16)
C
      DO 30 I=1,NTEETH
         IF (THETA(I) .GE. THS .AND. THETA(I) .LE. THE) THEN
            CHIP=FEED*SIND(THETA(I))
            CHIPT=CHIP+ERROR(I)-ERROR(I-1)
            RESUM=0.0
            IF (CHIPT .GT. 0.0) THEN
               DO 10 J=1,NTEETH-1
                  RESIDAL=CHIP+ERROR(I-J)-ERROR(I-J-1)
                  IF (RESIDAL .LT. 0.0) THEN
                     RESUM=RESUM+RESIDAL
                  ELSE
                     GOTO 20
                  ENDIF
   10          CONTINUE
            ELSE
               CHIPT=0.0
            ENDIF
   20       FT(I)=FK*AXL*(CHIPT+RESUM)
            FR(I)=FT(I)*RATIO
         ELSE
            FT(I)=0.0
            FR(I)=0.0
         ENDIF
   30 CONTINUE
C
      RETURN
      END
C
C
      SUBROUTINE THROW(ERROR,NTEETH)
C
C     MILLING SUBROUTINE
C
C     RESET THE ARRAY OF RADIAL THROW
C
C     ERROR  - ARRAY OF THE RADIAL THROW
C     NTEETH - NUMBER OF THE TEETH
C
      DIMENSION ERROR(-16:16)
C
      DO 10 I=1,NTEETH
   10    ERROR(-NTEETH+I)=ERROR(I)
C
      RETURN
      END
C
C
      SUBROUTINE FORTR(FT,FR,THETA,THS,THE,NTEETH,FPT,ZBACK)
C
C     MILLING SUBROUTINE (REGENERATIVE FORCE MODEL)
C
C     TANGENTIAL & RADIAL FORCES ON EACH TOOTH
```

```
C
C     FT      - ARRAY OF THE TANGENTIAL FORCES
C     FR      - ARRAY OF THE RADIAL FORCES
C     THETA   - ANGULAR POSITIONS OF THE TEETH
C     THS     - STARTING ANGLE OF CUT
C     THE     - EXIT ANGLE OF CUT
C     NTEETH  - NUMBER OF THE TEETH
C     FPT     - ARRAY OF THE FEED PER TOOTH
C     ZBACK   - SURFACE PRODUCED BY THE PRECEDING CUT
C
      COMMON /COEFF/ AXL,FEED,FK,RATIO,RAD
      COMMON /SURWA/ Z,VIBX,VIBY,NZPOS,THADD
C
      DIMENSION FT(1),FR(1),THETA(1),FPT(1),ZBACK(1)
C
      DO 10 I=1,NTEETH
C
         IF (THETA(I) .GE. THS .AND. THETA(I) .LE. THE) THEN
            NZPOS=THETA(I)/THADD
            Z     =VIBX*SIND(THETA(I))+VIBY*COSD(THETA(I))
            Z     =Z*1000.0
            CHIPM=FPT(I)*SIND(THETA(I))
            CHIPT=CHIPM-ZBACK(NZPOS)+Z
            IF (CHIPT .LT. 0.0) THEN
               CHIPT=0.0
               ZBACK(NZPOS)=ZBACK(NZPOS)-CHIPM
            ELSE
               ZBACK(NZPOS)=Z
            ENDIF
         ELSE
            CHIPT=0.0
         ENDIF
C
         FT(I)=FK*AXL*CHIPT
         FR(I)=FT(I)*RATIO
C
   10 CONTINUE
C
      RETURN
      END
C
C
      SUBROUTINE TEETH(FPT,NTEETH,NBR,NP,PER,THETA,ID)
C
C     UNDAMAGED OR DAMAGED CUTTER (REGENERATIVE FORCE MODEL)
C
C     FPT     - ARRAY OF THE FEED PER TOOTH
C     NTEETH  - NUMBER OF TEETH
C     NBR     - TOOTH PERIOD AS THE OCCURRENCE OF TOOL BREAKAGE
C     NP      - CURRENT TOOTH PERIOD
C     PER     - PERCENTAGE OF THE BROKEN CUTTING EDGE
C     THETA   - ANGULAR POSITIONS OF THE TEETH
C     ID      - UNDAMAGED OR DAMAGED CUTTER
C
```

```
      COMMON /COEFF/ AXL,FEED,FK,RATIO,RAD
C
      DIMENSION THETA(1),FPT(1)
C
         DO 10 I=1,NTEETH
   10       FPT(I)=FEED
C
      IF (ID .EQ. 2) THEN
         PERCENT=PER/100.
         ERROR=FEED*PERCENT
         CHIPT=FEED*SIND(THETA(1))
         IF (NP .GE. NBR) THEN
            IF (CHIPT .LE. ERROR) THEN
               FPT(1)      =0.0
               FPT(NTEETH)=2.*FEED
            ELSE
               FPT(1)      =(1.-PERCENT)*FEED
               FPT(NTEETH)=(1.+PERCENT)*FEED
            ENDIF
         ENDIF
      ENDIF
C
      RETURN
      END
C
C
      SUBROUTINE DEFLE(VIBX,VIBY,FX,FY,MODE,DT)
C
C     MILLING SUBROUTINE (REGENERATIVE FORCE MODEL)
C
C     VIBRATION OF THE CUTTER
C
C     VIBX     - VIBRATION IN THE X DIRECTION
C     VIBY     - VIBRATION IN THE Y DIRECTION
C     FX       - CUTTING FORCE IN THE X DIRECTION
C     FY       - CUTTING FORCE IN THE Y DIRECTION
C     MODE     - TOTAL MODES IN THE X AND Y DIRECTIONS
C     DT       - TIME INTERVAL
C     DMASS    - MASS PARAMETER
C     ETA      - DAMPING RATIO
C     WN       - NATURAL FREQUENCY
C     DDX,DDY - ACCELERATIONS IN THE X AND Y DIRECTIONS
C     DX,DY    - VELOCITIES IN THE X AND Y DIRECTIONS
C     X,Y      - DISPLACEMENTS IN THE X AND Y DIRECTIONS
C
      COMMON /SPINDL/ WN(10),ETA(10),DMASS(10)
      COMMON /EXCITX/ DDX(10),DX(10),X(10)
      COMMON /EXCITY/ DDY(10),DY(10),Y(10)
C
      VIBX=0.0
      VIBY=0.0
C
      DO 10 I=1,MODE
C
```

```
      DDX(I)=FX/DMASS(I)-2.*ETA(I)*WN(I)*DX(I)
     &          -(WN(I)**2.)*X(I)
      DDY(I)=FY/DMASS(I)-2.*ETA(I)*WN(I)*DY(I)
     &          -(WN(I)**2.)*Y(I)
C
      DX(I)=DX(I)+DDX(I)*DT
      DY(I)=DY(I)+DDY(I)*DT
C
      X(I)=X(I)+DX(I)*DT
      Y(I)=Y(I)+DY(I)*DT
C
      VIBX=VIBX+X(I)
   10 VIBY=VIBY+Y(I)
C
      RETURN
      END
```

# APPENDIX B

## EXAMPLE PROGRAM FOR SIMULATION OF DISPLACEMENT SIGNAL OF SPINDLE

```
C
C
C
C     AN EXAMPLE SHOWS HOW TO CALL < MILLIB.LIB > FOR
C
C      SIMULATION OF DISPLACEMENT SIGNAL OF SPINDLE
C
C
C
C
C     CUTTING PARAMETERS
C
      COMMON /COEFF/ AXL,FEED,FK,RATIO,RAD
C
C     VIBRATION PARAMETERS
C
      COMMON /VIBPAR/ WN,ETA,DMASS,DX,DY,DT,X,Y,TS
C
C     MAXIMUM TEETH ON THE CUTTER: 16
C
      DIMENSION FT(16),FR(16),THETA(16)
C
      PRINT*,'NUMBER OF THE TEETH ON THE CUTTER'
      READ(*,*) NTEETH
C
      PRINT*,'(1) UP OR (2) DOWN MILLING -> (1,2)'
      READ(*,*) IUD
C
      PRINT*,'SPINDLE SPEED(R. P. M.)'
      READ(*,*) RPM
C
      THP  =360./NTEETH
      DPS  =RPM*360./60.
      SPT  =THP/DPS
C
      PRINT*,'SEC PER TOOTH --> ',SPT
C
      PRINT*,'SIMULATION TIME INTERVAL (SEC)'
      READ(*,*) DT
      PRINT*,'SAMPLING TIME INTERVAL (SEC)'
      READ(*,*) TS
      PRINT*,'INITIAL SAMPLING ANGLE (DEG)'
      READ(*,*) THO
C
C     CALCULATE SIMULATION TIME COEFFICIENTS
C
      THADD=DT*DPS
      NPTS =THP/THADD+0.5
      INTVL=TS/DT+0.5
      ICOUNT=INTVL-1
      NSAMP=NPTS/INTVL
C
      PRINT*,'TOOL BROKEN ? -> (Y/N)'
```

```
      READ(*,10) TYPE
   10 FORMAT(A1)
C
      IF (TYPE .EQ. 'Y') THEN
         PRINT*,'INPUT FROM WHICH TOOTH PERIOD'
         READ(*,*) NBR
         PRINT*,'PERCENTAGE OF MISSING CUTTING EDGE (%)'
         READ(*,*) PER
      ENDIF
C
      PRINT*,'CLEARANCE BETWEEN THE WORKPIECE AND CUTTER'
      READ(*,*) DELY
      PRINT*,'TOTAL TOOTH PERIODS IN THE SIMULATION'
      READ(*,*) NPMAX
C
C     CUTTING PARAMETERS
C
      AXL  =2.54
      FEED =0.25
      FK   =1500.0
      RATIO=0.5263
      RAD  =50.8
      WSL  =100.0
C
C     VIBRATION COEFFICIENTS
C
      DMASS=1.0
      ETA  =0.04
      FN   =600.0
      WN   =2.*3.14159*FN
C
      TIME =0.0
C
C     OPEN A DATA FILE FOR OUTPUT
C
      OPEN(UNIT=5,FILE='STEP.DAT',STATUS='NEW')
C
C     CALCULATE ANGULAR POSITIONS OF THE TEETH
C
      CALL ANGLE(THETA,THP,THO,NTEETH)
C
C
C     * SIMULATION OF THE CUTTING PROCESS *
C
C
      DO 20 I=1,NPMAX
C
         DO 20 J=1,NPTS
C
C     CALCULATE STARTING AND EXIT ANGLES OF CUT
C        IN THE 1/2 IMMERSION MILLING
C
            CALL THSE2(THS,THE,THP,THALL,WSL,IUD,DELY)
C
```

```
C     CALCULATE TANGENTIAL AND RADIAL FORCES
C       (FACE MILLING, RIGID FORCE MODEL)
            CALL FORTR(FT,FR,THETA,THS,THE,NTEETH)
C
C     MONITOR TOOL BREAKAGE
C
            IF (TYPE .EQ. 'Y') THEN
               CALL BREAK(FT,FR,NTEETH,NBR,I,PER,THETA)
            ENDIF
C
C     DECOMPOSE FORCES INTO X AND Y DIRECTIONS
C
            CALL FXYS(FX,FY,FT,FR,THETA,NTEETH)
C
C     SIMULATE VIBRATION SIGNALS IN THE X AND Y DIRECTIONS
C
            CALL VIBRA(FX,FY)
C
            ICOUNT=ICOUNT+1
C
C     STORE SIMULATION DATA INTO THE DATA FILE
C
            IF (ICOUNT .EQ. INTVL) THEN
               ICOUNT=0
               WRITE(5,*) TIME,X,Y
            ENDIF
C
C     CALCULATE INCREMENTAL POSITIONS OF THE TEETH
C
          CALL ROTAT(THETA,THADD,THALL,NTEETH)
C
   20   TIME=TIME+DT
C
        STOP
        END
```

## REFERENCES


1. Kegg, R., "On-Line Machine and Process Diagnostics," Annals of the CIRP, vol. 32/2, 1984, pp. 469-473.

2. Sivakumaran, K., "Wear of Silicon Nitride Ceramic Tools in High Speed High Power Milling of Cast Iron," Research Report, 1986, Machine Tool Laboratory, Mechanical Engineering, University of Florida.

3. Matsushima, K., Kawabata, T., and Sata, T., "Recognition and Control of the Morphology of Tool Failures," Annals of the CIRP, vol. 28/1, 1979, pp. 43-47.

4. Tlusty, J., and Tarng, Y., "Sensing Cutter Breakage in Milling," Annals of the CIRP, vol. 37/1, 1988, pp. 45-51.

5. Micheletti, G., Koenig, W., and Victor, H., "In-process Tool Wear Sensors for Cutting Operations," Annals of the CIRP, vol. 25/2, 1976, pp. 483-496.

6. Yamazaki, K., and Yamada, A., and Sawai, N., "A study on Adaptive Control in a NC Machine," Annals of the CIRP, vol. 23/1, 1974, pp. 153-154.

7. Tlusty, J., and Andrew, G., "A Critical Review of Sensors for Unmanned Machining," Annals of the CIRP, vol. 32/2, 1983, pp. 563-577.

8. Kannatey-Asibu, E., and Dornfeld, D., "A Study of Tool Wear Using Statistical Analysis of Metal Cutting Acoustic Emission," Wear, vol. 76, 1982, pp. 247-261.

9. Kannatey-Asibu, E., "Acoustic Emission Sensing of Tool Wear in Metal Cutting--A General Overview and Problem Areas," 10th North American Metal Work Research Conference, May 1982.

10. Iwata, K., and Moriwaki, T., "An Application of Acoustic Emission Measurement to In-Process Sensing of Tool Wear," Annals of CIRP, vol. 25/1, 1977, pp. 21-26.

11. Kakino, Y., "In-Process Detection of Tool Breakage by Monitoring Acoustic Emission," Proceedings of International Conference on Cutting Tool Materials, 1980, pp. 25-39.

12. Grabec, I., and Leskovar, P., "Acoustic Emission of a Cutting Process," Ultrasonics, vol. 15/1, 1977, pp. 17-20.

13. Moriwaki, T., "Detection of Tool Fracture by Acoustic Emission Measurement," Annals of the CIRP, vol. 29/1, 1980, pp. 35-40.

14. Lee, M., Wildes, D., Hayashi, S., and Keramati, B., "Effects of Tool Geometry on Acoustic Emission Intensity," Annals of the CIRP, vol. 37/1, 1988, pp. 57-60.

15. Kannatey-Asibu, E., and Dornfeld, D., "Quantitative Relationships for Acoustic Emission from Orthogonal Metal Cutting," Journal of Engineering for Industry, ASME, vol. 103, 1981, pp. 330-340.

16. Liang, S., and Dornfeld, D., "Detection of Cutting Tool Wear Using Adaptive Time Series Modelling of Acoustic Emission Signal," Proceedings of ASME 1987 Winter Annual Meeting, vol. 26, pp. 27-38.

17. Rangwala, S., and Dornfeld, D., "Integration of Sensors via Neural Networks for Detection of Tool Wear States," Proceedings of ASME 1987 Winter Annual Meeting, pp. 109-117.

18. Ramalingam, S., Shi, T., Frohrib, D., and Moser, T., "Acoustic Emission Sensing with an Intelligent Insert and Tool Fracture Detection in Multi-Tooth milling," Proceedings of 16th North American Manufacturing Research Conference, 1988, pp. 245-255.

19. Diei, E., and Dornfeld, D., "Acoustic Emission from the Face Milling Process--The Effect of Process Variables," Proceedings of ASME 1985 Winter annual Meeting, vol. 18, pp. 75-84.

20. Altintas, Y., "In-Process Detection of Tool Breakage Using Time Series Monitoring of Cutting Forces," submitted for publication, International Journal of Machine Tools Manufact., 1987.

21. Box, G., and Jenkins, G., "Time Series Analysis: Forecasting and Control," San Francisco, California, Holden-Day Inc., 1976.

22. Matsushima, K., Bertok, P., and Sata, T., "In-Process Detection of Tool Breakage by Monitoring the Spindle Motor Current of a Machine Tool," Measurement and Control for Batch Manufacturing, Winter Annual Meeting, ASME, 1982, pp. 145-153.

23. Lan, M., and Naerheim, Y., "In-Process Detection of Tool Breakage in Milling," Proceedings of ASME 1985 Winter Annual Meetings, vol. 18, 1985, pp. 49-56.

24. Tarn, M., and Tomizuka, M., "On-Line Monitoring of Tool and Cutting Conditions in Milling," Proceedings of ASME 1987 Winter Annual Meeting, vol. 26, pp. 17-25.

25. Ishikawa, T., and Yamada, Y., "Fracture Detection of Cutting Edge in Multi-point Tools," Proceedings of 16th North American Manufacturing Research Conference, 1988, pp. 256-263.

26. Takata, S., Nakajima, T., Ahn, J., and Sata, T., "Tool Breakage Monitoring by Means of Fluctuations in Spindle Rotational Speed," Annals of CIRP, vol. 36/1, 1987, pp. 49-52.

27. Altintas, Y., Yellowley, I., and Tlusty, J., "Detection of Tool Breakage in Milling," Proceedings of ASME 1985 Winter Annual Meetings, vol. 18, 1985, pp. 41-48.

28. Tlusty, J., Smith, S., Hernandez, I., and Tarng, Y., "Unmanned Machining, High Speed Milling," Proceedings of NSF Manufacturing System Research Conference, 1986, pp. 131-139.

29. Tarng, Y., "Sensing of Tool Breakage in Milling," Master Thesis, 1986, Mechanical Engineering, University of Florida.

30. Tlusty, J., Jang, D., and Tarng, Y., "Measurements of the Milling Force over a Wide Frequency Range," Proceedings of 14th North American Manufacturing Research Conference, 1986, pp. 273-280.

31. Tarng, Y., "Studies of Spindle Vibrations Applied to the Detection of Tool Breakage in Milling," Research Report, 1987, Machine Tool Laboratory, Mechanical Engineering, University of Florida.

32. Yoon, T., "A Knowledge-Based System to Monitor Cutter Damage of Machine Tool," Proposal for PhD Research, 1988, Electrical Engineering, University of Florida.

33. Martellotti, M., "An Analysis of the Milling Process," Transactions of the ASME, vol. 63, 1941, pp. 677-700.

34. Martellotti, M., "An Analysis of the Milling Process --Down Milling," Transactions of the ASME, vol. 67, 1945, pp. 233-251.

35. Koenigsberger, F., and Sabberwal, A., "Chip Section and Cutting Force during the Milling Operation," Annals of the CIRP, 1960.

36. Koenigsberger, F., and Sabberwal, A., "An Investigation into the Cutting Force Pulsations during Milling Operations," International Journal of Machine Tool Design and Research, vol. 1, 1961.

37. DeVor, R., Kapoor, S., and Fu, H., "Effect of Variable Chip Load on Machining Performance in Face Milling," Proceedings of 11th North American Manufacturing Research Conference, 1983, pp. 348-355.

38. Tlusty, J., and Ismail, F., "Special Aspects of Chatter in Milling," Journal of Vibration, Stress, and Reliability in Design, ASME, vol. 105, 1983, pp. 24-32.

39. Fu, H., DeVor, R., and Kapoor, S., "A Mechanistic Model for the Prediction of the Force System in Face Milling Operations," Journal of Engineering for Industry, ASME, vol. 106, 1984, pp. 81-88.

40. Tlusty, J., and MacNeil, P., "Dynamics of Cutting Forces in End Milling," Annals of the CIRP, vol. 24/1, 1975, pp. 21-25.

41. Kline, W., and DeVor, R., "The Effect of Runout on Cutting Geometry and Forces in End Milling," International Journal of Machine Tool Design and Research, vol. 23, 1983, pp. 123-140.

42. Kennamental Inc., "Kennamental Milling/87 Manual," Latrobe, PA, Kennamental Inc., 1987, pp. 148.

43. Smith, S., "Automatic Selection of the Optimum Spindle Speed in High-Speed Milling," PhD Dissertation, 1987, Mechanical Engineering, University of Florida.

44. Ber, A., and Feldman, D., "The Influence of Radial location on the Wear Behavior of Multi-Tooth Face Milling Cutter," Annals of the CIRP, vol. 26/1, 1977, pp. 1-4.

45. Smith, S, "Chatter, Forced Vibrations, and Accuracy in High Speed Milling," Masters Thesis, 1985, Mechanical Engineering, University of Florida.

46. Tarng, Y., "Sensing Cutter Breakage in Milling," Proposal for PhD Dissertation, 1988, Mechanical Engineering, University of Florida.

47. White-Sundstrand Machine Tool Company, "Machine Operations," Belvidere, Illinois, White-Sundstrand Machine Tool Company, June 1984.

48. Smith, S., and Tlusty, J., "Update on High-Speed Milling Dynamics," Symposium on Intelligent Integrated Manufacturing Analysis and Synthesis, vol. 25, ASME, 1987, Winter Annual Meetings.

49. Oppenheim, A., and Schafer, R., "Digital Signal Processing," Englewood Cliffs, New Jersey, Prentice-Hall Inc., 1975.

50. Tlusty, J., Livingston, R., and Teng, Y., "Nonlinearities in Spindle Bearings and Their Effects," Annals of CIRP, vol. 35/1, 1986, pp. 269-273.

51. Altintas, Y., and Yellowley, I., "The Identification of Radial Width and Axial Depth of Cut in Peripheral Milling," International Journal of Machine Tools Manufact., vol. 27/3, pp. 367-381, 1987.

52. Bertok, P., Takata, S., Matsushima, K., Ootsuka, J., and Sata, T., "A System for Monitoring the Machining Operation by Referring to a Predicted Cutting Torque Pattern," Annals of CIRP, vol. 32/1, 1983, pp. 439-444.

53. Promess Inc., "Promess Tool Condition Monitoring EPR 2.0 Technical Manual," Brighton, Michigan, Promess Inc., 1983.

54. Uhlman, W., and Schmenk, M., "Torque Controlled Machining for Numerical Control Machining Centers," IEEE Paper CH1707-9/81/0000-0055, 1981.

55. Wolf, W., and Magadanz, P., "Feed Force Monitoring for Operation Security and Reliability," International Tool and Manufacturing Conference, Detroit, Michigan, 1981, SME Paper IQ81-161.

56. Altintas, Y., and Yellowley, I., "In-Process Detection of Tool Failure in Milling Using Cutting Force Models," Proceedings of ASME 1987 Winter Annual Meeting, vol. 26, pp. 1-16.

## BIOGRAPHICAL SKETCH

Yeong-shin Tarng was born on July 28th, 1959. In July 1981, he received his Bachelor's degree from the Department of Mechanical Engineering, National Central University, Chungli, Taiwan. In December 1988, he completed his whole graduate study in the Department of Mechanical Engineering, University of Florida, Gainesville, Florida.

I certify that I have read this study and that in my opinion it conforms to acceptable standards of scholarly presentation and is fully adequate, in scope and quality, as a dissertation for the degree of Doctor of Philosophy.

Dr. Jiri Tlusty, Chairman
Graduate Research Professor
of Mechanical Engineering

I certify that I have read this study and that in my opinion it conforms to acceptable standards of scholarly presentation and is fully adequate, in scope and quality, as a dissertation for the degree of Doctor of Philosophy.

Dr. Donald W. Dareing
Professor
of Mechanical Engineering

I certify that I have read this study and that in my opinion it conforms to acceptable standards of scholarly presentation and is fully adequate, in scope and quality, as a dissertation for the degree of Doctor of Philosophy.

Dr. Jose C. Principe
Associate Professor
of Electrical Engineering

I certify that I have read this study and that in my opinion it conforms to acceptable standards of scholarly presentation and is fully adequate, in scope and quality, as a dissertation for the degree of Doctor of Philosophy.

Dr. John K. Schueller
Assistant Professor
of Mechanical Engineering

I certify that I have read this study and that in my opinion it conforms to acceptable standards of scholarly presentation and is fully adequate, in scope and quality, as a dissertation for the degree of Doctor of Philosophy.

Dr. Carl D. Crane
Assistant Professor
of Mechanical Engineering

This dissertation was submitted to the Graduate Faculty of the College of Engineering and to the Graduate School and was accepted as partial fulfillment of the requirements for the degree of Doctor of Philosophy.

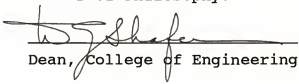

December 1988

Dean, College of Engineering

Dean, Graduate School